University of Nairobi

School of Engineering

DEPARTMENT OF MECHANICAL AND MANUFACTURING ENGINEERING

Tensile and Flexural Strength Properties of Surface-Modified Sisal Fibre Composites

BY

WILLIAM KITHIIA MENGO

F56/81975/2015

A thesis submitted in partial fulfilment of the requirements for the degree of Master of Science in Mechanical Engineering, in the Department of Mechanical and Manufacturing Engineering, of the University of Nairobi

August 2022

DECLARATION

This thesis is my original work and has not been presented for a degree in any other university.

07/08/2022

William K. Mengo — Date

This thesis has been submitted for examination with our approval as university supervisor(s).

08/08/2022

Prof. Stephen M. Mutuli — Date

University of Nairobi

08/08/2022

Eng. Dr David M. Munyasi — Date

University of Nairobi

11/08/2022

Dr Sipula W. Mumenya — Date

University of Nairobi

DEDICATION

To my loving parents Joseph and Justina, my lovely wife Dr Salome and my adorable daughters Annie-Ella, Lisa-Marie and Olivia-Albertina.

DIE WIDMUNG

Diesen Leute widmen sich die nachfolgenden seiten:

An meine lieben Eltern Josef und Justina, ihr seid die besten Eltern der Welt.

An meiner lieben Frau Salome, und meine schönen und anbetungswürdig Töchter Annie-Ella, Lisa-Marie und Olivia-Albertina,

Ihr seid meine Welt, ihr seid meinen grünen, ihr seid meinen Blau, ihr seid meine Essenz.

ACKNOWLEDGEMENTS

I would like to appreciate the following people for the pivotal roles they played in this study.

1) My lead supervisor, Professor Stephen Mutuli who has been like a father to me who consistently, continuously and tirelessly guided and held my hand throughout the course of this study. My other supervisors; the late Professor Moses Frank Oduori, Eng. Dr David Munyasi and Dr Siphila Mumenya for their encouragement, guidance and support throughout the study. Professor Moses Frank Oduori was my second supervisor for a good part of this study and he unfortunately fell sick and passed on.
2) The Managing Director of Rea Vipingo Sisal Estate Ltd, Mr Neil Cuthbert, for generously providing all the sisal fibre used in this study.
3) Mr John Muchina of the Concrete Workshop, Department of Civil and Construction Engineering at the University of Nairobi for helping with the mortar specimens.
4) Mr Fredrick Nakhale and Mr Solomon Sitati of the Timber Workshop, Department of Civil and Construction Engineering at the University of Nairobi for helping with the construction of the wooden moulds.
5) Mr Anyona Oduya, Ms Jackline Amondi, Mr Kimani Kamau, Mr Kipyegon Kigen and Mr Macharia Mwangi of the Mechanical Engineering workshops and Laboratories, Department of Mechanical and Manufacturing Engineering, the University of Nairobi for their assistance in the steel tensile rig fabrication and sisal fibre cornification.
6) Ms' Margaret Wambui and Joyce Nyawira of the Public Health Laboratory, Department of Civil and Construction Engineering, the University of Nairobi for assisting me in the safe handling and dilution of the concentrated glacial acetic acid in the fume chamber.

7) Mr. Ephantus Mwangi of the Chemistry Laboratory, Department of chemistry, the University of Nairobi for assisting me in the safe handling and dilution of the concentrated hydrochloric acid, and in the testing of the sand/cement ratio in my specimens.
8) My friends Philemon Kipkemoi, Jasper Ochieng', Nicholas Wandera, Dr Josey Chako, Douglas Ndonga, Swaleh Mohammed and Abdul Wanjohi for the encouragement and support they offered throughout the study.

Finally, I would like to thank my father, Eng. Joseph M. Mengo, for continually checking on my progress every so often and for being the great dad that he has always been to me.

Anti-Plagiarism Statement

I confirm that I have written this thesis in my own words, except where otherwise explicitly acknowledged. I am aware that the incorporation of material from other works or paraphrase of such material without acknowledgement will be treated as plagiarism, subject to the custom and usage of the subject, according to the University Regulations on the Conduct of Examinations.

SIGNATURE:…… 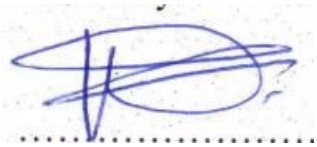 ……..

DATE: 07/08/2022

ABSTRACT

Over the last five decades, extensive research has been done to investigate the strengthening effect of several fibre surface-modification techniques on ligno-cellulosic fibres. This has been necessitated by the need to find eco-friendly, sustainable, low-cost alternatives to synthetic, mineral and man-made fibres that are otherwise known to cause serious environmental degradation due to their non-biodegradability. Despite there being large amounts of data on strengthening effect of various fibre surface-modification methods on ligno-cellulosic fibres, no known studies have been carried out to compare the strengthening effect of alkali and thermal fibre surface-modification on high lignin content UG grade Kenyan sisal fibres. This study aimed at determining and comparing the strength properties of mercerised (alkali-treated) and cornified (thermally treated) UG grade Kenyan sisal fibres.

The fibres strength properties were determined and analysed using the Weibull Cumulative Distribution function. The untreated, mercerised and cornified fibres, in different volume fractions, were then used to make composites in hydrophilic (Portland cement) and hydrophobic (polyester resin) matrices. Tensile and flexural strength tests were carried out on these composites, and comparisons of the results obtained done. Mercerised sisal fibres displayed the most significant improvement in tensile strength properties with mean fracture strength of 271 MN/m^2, which showed a 68.30% increase in tensile strength compared to untreated sisal fibres. Cornified sisal fibres had a mean fracture stress value of 198.57 MN/m^2, which was a 23.32% increase compared to untreated sisal fibres. OPC mortar composites of mercerised sisal in uniaxial orientation had a peak Modulus of Rupture of 9.39 MN/m^2 at 2.3% fibre volume fraction, which was a 151.07% increase in flexural strength compared to the unreinforced mortar specimens. Chopped, randomly oriented mercerised sisal fibre mortar composites had a peak Modulus of Rupture value of 9.8 MN/m^2 at a 4.2% fibre volume

fraction, which showed a 36.11% increase in flexural strength when compared to the unreinforced mortar specimens. In polyester resin, the untreated, mercerised and cornified fibre reinforcements all exhibited a negative reinforcement, with the composite tensile strength decreasing with increasing fibre volume fractions. The negative reinforcement was attributed to the exothermic curing temperature (about 113°C) of the polyester resin. Upon controlling the curing temperature to some degree, untreated sisal fibre-reinforced polyester resin displayed the most significant gain in flexural strength with a Modulus of Rupture that was 66.93% higher than that of the unreinforced polyester specimens. Finally, in order to ascertain whether the negative reinforcement of the polyester resin was due to the resin's exothermic curing temperature, the fibres were used as reinforcement in a non-exothermic curing polymeric matrix (epoxy resin) where mercerised sisal fibre-reinforced epoxy resin composites displayed the most significant gain in tensile strength with an ultimate tensile stress value that was 118.52% higher than that of the unreinforced epoxy resin. These findings were in agreement with the results reported in earlier studies.

SYMBOLS

τ – Interfacial shear stress

P – Load

E –Modulus of Elasticity

ν – Poisson's ratio

ε- Strain

σ –Tensile/Compressive stress

$U\gamma$ – Total fracture energy of a composite

ACRONYMS

A – Area

b – Breadth (Bending test specimens)

d – Depth (Bending test specimens)

CDF – Cumulative Density Function

CFRC – Continuous Fibre-reinforced Composite

CH_3COOH – Glacial Acetic Acid

DFRC – Discontinuous Fibre-reinforced Composite

FRI – Fibre Reinforcement Index

HABRI – Housing and Building Research Institute

HCL – Hydrochloric Acid

KOH – Potassium Hydroxide

L – Length (Bending test specimens)

l_c– Critical fibre length

LiOH – Lithium Hydroxide

m – Mass

MOR – Modulus of Rupture

NaOH – Sodium Hydroxide

OPC – Ordinary Portland cement

r – Fibre radius

ROM – Rule of Mixtures

UoN – University of Nairobi

v – Volume

V_f – Fibre Volume fraction

w/c – water to cement ratio

TABLE OF CONTENTS

DECLARATION ii

DEDICATION iii

ACKNOWLEDGEMENTS iv

Anti-Plagiarism Statement vi

ABSTRACT vii

SYMBOLS ix

ACRONYMS x

TABLE OF CONTENTS xii

LIST OF FIGURES xix

LIST OF TABLES xxiii

CHAPTER ONE 1

1.0 INTRODUCTION 1

1.1 Background Information 1

1.2 Problem Statement 5

1.3 Main Objective 8

1.3.1 Specific Objectives 8

1.4 Justification 8

1.5 Scope of the Research 9

2.0 LITERATURE REVIEW 11

2.1 Sisal Fibres 11

2.1.1 Historical Background 11

2.1.2 Sisal Fibre Morphology 16

2.1.3 Fibre Surface Behaviour and Modification 21

2.1.4 Mercerisation 27

2.1.5 Cornification 28

2.2 Matrices 30

2.2.1 Ordinary Portland Cement 30

2.2.2 Unsaturated Polyester Resin 32

2.2.3 Epoxy Resin 34

2.3 Fibre-Reinforced Composites 34

2.3.1 Stress Distribution in Fibre-Reinforced Composites 35

2.3.1.1 Unidirectional CFRC 35

2.3.1.2 Unidirectional DFRC 37

2.3.2 Interfacial Bond Strength 42

2.4 Summary of Literature Review 44

CHAPTER THREE 45

3.0 MATERIALS AND METHODS 45

3.1 Experimental Procedures 46

3.1.1 Experimental Procedure I - Sisal Fibres 46

3.1.1.1 Fibre Surface-Modification 46

3.1.1.2 Mercerisation of Sisal Fibres 48

3.1.1.3 Cornification 49

3.1.1.4 Fibre Morphology 50

3.1.1.5 Fibre Absorbency 51

3.1.1.6 Fibre Diameter 52

3.1.1.7 Fibre Density 53

3.1.1.8 Fibre Tensile Test 54

3.1.2 Experimental Procedure II - Mortar Composites 60

3.1.2.1 Preparation of Sisal Fibre Specimens for Mortar Reinforcement 60

3.1.2.2 Preparation of Wooden Moulds for Mortar Composite Specimen..... 60

3.1.2.3 Sand Particle Size Distribution..... 63

3.1.2.4 Mortar Specimens..... 63

3.1.2.5 Composite Void Volume Fraction 66

3.1.2.6 Gravimetric Method of Determination of Sand/Cement Ratio in Mortar 67

3.1.2.7 Determination of Moisture Content in Mortar 68

3.1.3 Experimental Procedure III - Unsaturated Polyester and Epoxy Resin Composites 70

3.1.3.1 Preparation of Sisal Fibre Specimens for Polyester Resin Reinforcement 70

3.1.3.2 Preparation of Moulds for Polyester Resin Composite Specimen 71

3.1.3.3 Polyester and Epoxy Resin Specimens 72

3.1.3.4 Unreinforced Polyester and Epoxy – Resin Specimens 73

3.1.3.5 Sisal Fibre-Reinforced Polyester and Epoxy – Resin Composites..... 73

3.2 Mechanical Testing 75

3.2.1 Sisal Fibre-Reinforced Mortar Specimens 75

3.2.1.1 Tensile Test 75

3.2.1.2 Flexural Test 78

3.2.2 Polyester and Epoxy Resin Specimens 80

3.2.2.1 Tensile Test 80

3.2.2.2 Three-Point Bending Test 81

3.3 Data Analysis and Interpretation 83

CHAPTER FOUR 84

4.0 RESULTS AND DISCUSSION 84

4.1 Sisal Fibres 84

4.1.1 Sisal Fibre Surface Morphology 84

4.1.2 Absorbency 86

4.1.3 Sisal Fibre Diameter 88

4.1.4 Fibre Density 89

4.1.5 Fibre Tensile Test 89

4.2 Cement Mortar Composites 94

4.2.1 Sand Particle Size Distribution 94

4.2.2 OPC Mortar Specimens 95

4.2.2.1 Flexural Rigidity 95

4.2.2.1.1 Uniaxially Aligned Continuous Fibre-Reinforced Mortar (Untreated Sisal Fibres) 95

4.2.2.1.2 Randomly Oriented Discontinuous Fibre-Reinforced Mortar (Untreated Sisal Fibres) 101

4.2.2.2 Tensile and Interfacial Bond Strength 105

4.3 Sisal Fibre-reinforced Polyester Resin Composites 111

4.3.1 Tensile Strength 111

4.3.2 Flexural Strength 114

4.4 Sisal Fibre-reinforced Epoxy Resin Composites 116

4.4.1 Tensile Strength 116

CHAPTER FIVE 119

5.0 CONCLUSIONS AND RECOMMENDATIONS FOR FURTHER WORK 119

5.1 Conclusions 119

5.2 Recommendations 122

REFERENCES 124

APPENDICES 144

APPENDIX A – SISAL FIBRE 144

Untreated, Mercerised and Cornified Sisal Fibres Fracture Stress Analysis 147

APPENDIX B – SISAL FIBRE-REINFORCED COMPOSITE RESULTS AND DATA ANALYSIS 151

Untreated Sisal CFRC of Mortar 154

Mercerised Sisal CFRC of Mortar 158

Cornified Sisal CFRC of Mortar 161

Untreated Sisal DFRC of Mortar 164

Mercerised Sisal DFRC of Mortar 166

Cornified Sisal DFRC of Mortar 168

Tensile Test Results - Sisal CFRC of Polyester Resin 170

Flexural Test Results - Sisal CFRC of Polyester Resin 174

Tensile Test Results - Sisal CFRC of Epoxy Resin 178

Temperature Variation during Curing of Polyester Resin 182

APPENDIX C – LIST OF PUBLICATIONS FROM THE STUDY 184

LIST OF FIGURES

Figure 2.1: Image showing harvesting of mature Agave sisalana plant leaves in Kitui County, Kenya [148] *17*

Figure 2.2: Image showing different fibres in sisal leaf cross-section [149] *17*

Figure 2.3: Structural constitution of a ligno-cellulosic fibre [152] *18*

Figure 2.4: Ultimate cells in a sisal leaf cross-section [152] *19*

Figure 2.5 Vector representation of vapour-liquid-solid equilibrium on planar surface *22*

Figure 2.6: Cellubiose molecule [171] *24*

Figure 2.7: Alder's structural model of a lignin molecule [168] *25*

Figure 2.8: Hemicellulose molecule [175] *26*

Figure 2.9: Mercerisation mechanism as given by Okano and Sarko [183] *28*

Figure 2.10: Schematic diagram showing untreated and cornified fibre cross-sections [185]. *29*

Figure 2.11: Dimension changes during hardening of Portland cement [189]. *31*

Figure 2.12: Polyesterification reaction between isophthalic acid (dibasic), maleic anhydride and propylene glycol to form an unsaturated polyester resin molecule [195] *33*

Figure 2.13: Unsaturated polyester resin/styrene copolymerisation network [192] *34*

Figure 3.1: Image showing sisal fibres mercerising in a 0.06M NaOH solution. 49

Figure 3. 2: Image showing (a) sisal fibres cornifying in an electric oven (b) combed cornified sisal fibres ready for use as fibre reinforcement. 50

Figure 3.3: Image showing Vickers hardness testing machine at the Materials Laboratory, UoN, used in this research 51

Figure 3.4: Image showing absorbency specimens in (a) convection oven and (b) desiccator jar before weighing. 52

Figure 3.5: Image showing (a) A 30 fibre strand tensile test in progress on a Hounsfield tensile testing machine at the Timber Laboratory, UoN. (b) Specimen after failure..... 56

Figure 3.6: Wooden mould design for mortar flexural specimen (dimensions in mm)..... 61

Figure 3.7: Wooden mould design for mortar tensile specimen (dimensions in mm)..... 62

Figure 3.8: Image showing well-oiled flexural specimen wooden moulds at the Concrete Laboratory, Mechanical Engineering building, UoN 64

Figure 3.9: Image showing 30 mm chopped sisal fibre mixing with OPC mortar in the cement mixer at the Concrete Laboratory, UoN. 66

Figure 3.10: Images showing a pulverised mortar specimen in a crucible drying at 1000°C in a scientific furnace at the Mechanical Engineering Laboratory and Workshop, UoN..... 69

Figure 3.11: Wooden mould for polyester and epoxy resin specimens (dimensions are in mm) 71

Figure 3.12: Image showing cured polyester resin specimens in mould ready for demoulding 72

Figure 3.13: Assembly drawing of tensile test rig showing two square side plates [46] (dimensions are in mm) 76

Figure 3.14: Image showing KAPCI polyester putty and dibenzyl peroxide hardener used in the study..... 76

Figure 3.15: Image showing (a)50x50x300mm tensile test specimen with affixed rig during a tensile test (b) Specimen after tensile test displaying MMF and (c) Kerosene blow torch being used to de-bond rig from polyester putty on specimen..... 77

Figure 3.16: ASTM C 293-02 Diagrammatic view of 3-point bending arrangement used in this research [229] 78

Figure 3.17: Image showing 3-point bending test on a fibre-reinforced OPC mortar specimen in progress on a bending and transverse testing machine at the Timber Laboratory, UoN.... 79

Figure 3.18: Image showing failure mechanism for a dog bone-shaped composite specimen [17] 81

Figure 3.19: Image showing sisal fibre-reinforced polyester resin specimen after failure during a tensile test on a Hounsfield tensometer at the Concrete Laboratory, UoN..... 81

Figure 3.20: Image showing sisal fibre-reinforced polyester resin specimen undergoing a 3-point bending test on a Hounsfield tensometer. 82

Figure 4.1(a, b & c): Optical microscopy image showing surface-modified and untreated sisal fibres *84*

Figure 4.2: Bar graph showing change in mass of untreated, mercerised and cornified sisal fibres with time during drying *87*

Figure 4.3: Weibull Plot of untreated, mercerised and cornified sisal fibres fracture stress (with plotlines extended for clarity) *92*

Figure 4.4: River sand sieve analysis grading curve *95*

Figure 4.5: Graph showing MOR of uniaxially aligned continuous fibre-reinforced mortar (untreated, mercerised and cornified sisal fibres) against fibre V_f *%* *96*

Figure 4.6: A uniaxially aligned, 2% V_f *continuous fibre-reinforced mortar specimen showing single crack failure mode and fibre pull-out during a flexural test.* *98*

Figure 4.7: A uniaxially aligned, 5% V_f *continuous fibre-reinforced mortar specimen showing multiple cracking during a flexural test.* *99*

Figure 4.8: Column graph comparing the variation of void volume fraction with the fibre volume fraction of sisal fibre-reinforced mortar. *100*

Figure 4.9: Column comparing mortar composite density with the fibre volume fraction of sisal fibre-reinforced mortar *101*

Figure 4.10: Graph showing MOR of randomly aligned, discontinuous fibre-reinforced mortar (untreated, mercerised and cornified sisal fibres) against fibre V_f *%* *102*

Figure 4.11: Image showing (a) single crack with fibre pull-out and (b) fracture surface with fibres jutting out of a 3% V_f discontinuous, randomly aligned fibre-reinforced mortar 104

Figure 4.12: Image showing fibre clumps on a 7% randomly oriented discontinuous fibre-reinforced mortar surface. 105

Figure 4.13: Graph showing tensile test results for untreated, mercerised and cornified sisal fibre-reinforced mortar. 106

Figure 4.14: Graph showing interfacial bond strength (IBS) results for untreated, mercerised and cornified sisal fibre-reinforced mortar (@≈ 0.5% V_f). 108

Figure 4.15: Graph showing tensile test results for untreated, mercerised and cornified sisal fibre-reinforced unsaturated polyester resin. 111

Figure 4.16: Temperature variation within the mould during curing of unreinforced and fibre-reinforced polyester resin (See Appendix B, Tables B8(a, b &c)) 113

Figure 4.17: Graph showing flexural test results for untreated, mercerised and cornified sisal fibre-reinforced unsaturated polyester resin. 114

Figure 4.18: Graph showing tensile test results for untreated, mercerised and cornified sisal fibre-reinforced epoxy resin. 116

LIST OF TABLES

Table 2.1: Increase in value of exports (in £/tonne), East Africa Protectorate [113] 12

Table 2.2: Sisal fibre chemical composition 20

Table 2.3: Chemical composition of Portland cement (Blanks and Kennedy [188]) 30

Table 4.1: Tensile test results summary for untreated, mercerised and cornified sisal fibres 90

CHAPTER ONE

1.0 INTRODUCTION

1.1 Background Information

Sisal (Botanical name *Agave Sisalana*) is named after the port of Sisal in Yucatan, Mexico [1–3]. For thousands of years, man has cultivated it for use as a vegetable, fruit, fodder, medicine, hallucinogen[1] (used in religious rites), and fibre. The ancient Aztecs and the Mayans are the earliest known sisal farmers who cultivated it for clothing and papermaking [4, 5].

German agronomist, Dr Richard Hindorf, who imported the bulbils from a trading company in Florida, USA, is credited with the introduction of sisal to German East Africa (Tanganyika) in 1893 [6, 7]. Commercial farming of sisal began a decade later, and the first plantations were set up at Punda Milia by R. Swift and E.A Rutherford in 1907 [7]. Since then, sisal farming has continued to contribute to the economic development of communities within the East African Region.

Currently, Rea Vipingo group headquartered in Nairobi, Kenya, is the single largest producer of sisal fibre in Africa at 19,000 tonnes per annum. Ninety (90) per cent of this production is exported to the Middle East where it is mainly used in the reinforcement of domed roofing characteristic of the Persian architecture typical in that part of the world [8, 9].

By definition, a composite is a material that, on a macroscopic level, comprises of two or more uniquely distinct phases that possesses bulk qualities that are different from any of its constituent phases [10–14].

---

[1] A drug that causes profound distortions in a person's perception of reality

A strong material (known as reinforcement or the secondary phase) is usually embedded in a relatively weaker material (known as a matrix or the primary phase) resulting in a composite. The reinforcement confers upon the composite strength and rigidity, while the matrix maintains the orientation of the reinforcement [10, 12, 13, 15, 16]. This effectively arrests any variation in mechanical properties that would otherwise result from a realignment of the reinforcement especially when under load. The reinforcement is sometimes referred to as the dispersed phase. All materials in use, with the exception of elemental ones can in a broader 'augmented' definition be defined as composites, with impurities and/or additives serving as the dispersed phase [10, 17]. Examples of naturally occurring composites include bones, ligno-cellulosic plant fibres (with the hemicellulose-lignin functioning as the matrix), and, wood [10, 18, 19].

The use of fibre-reinforced composites dates back thousands of years in the Neolithic era where mud-mortars were reinforced with either herbs, roots or reeds with the aim being to increase the stability and durability of the mortars [17, 20–23]. Ancient civilizations such as the Egyptian, Inca and Mayans have been recorded as having used natural wood and straw fibre-reinforced traditional mortars [21]. In order to enhance bonding and arrest cracks in the walls of houses, it is reported in literature that ancient indo-Muslim architects incorporated jute and straw fibres into the mortar [21, 24, 25].

Like many other natural fibres, sisal has the potential of being utilised as fibre-reinforcement (dispersed phase) in natural fibre-reinforced composites. It has the advantage of being a low-cost fibre, both in production and processing terms and having a high strength to weight ratio when compared to other fibre reinforcements of synthetic origin such as carbon, asbestos and Kevlar [2, 23, 26–32]. Natural fibre-reinforced composites, due to the non-abrasive nature of the fibres, result in less tool wear in the workshop during machining operations [16, 30, 33,

34]. According to Khalil *et al.* [31], Mokhtar *et al.* [34], Brahmakumar *et al.* [35] and Biagiotti *et al.* [19], most natural fibres also have the added advantage of being less irritating to workers dermal and respiratory systems as compared to synthetic and mineral fibres.

Many researchers have investigated the potential of using sisal fibre as reinforcement in cement-based matrix. Research work by Savastano *et al.* [36] on the flexural behaviour of sisal fibre-reinforced cement-based composites confirmed theoretical predictions by reporting a two-fold gain in flexural strength of fibre-reinforced mortar. More recently, in the year 2020, these results have been confirmed by Bernard *et al.* [37] while analysing the mechanical behaviour of sisal fibre-reinforced Interpenetrating Polymer Networks (IPN) matrix.

Tonoli *et al.* [38] investigating on the mechanical properties of sisal pulp reinforced cement mortar found that inclusion of sisal pulp resulted in a doubling of flexural strength and a significant increase in fracture toughness of the pulp-reinforced mortar.

In Brazil, research work on cornified vegetable fibre-reinforced building materials by Ballesteros *et al.* [39] has reported a greater dimensional stability of the composite and a stronger fibre-matrix interfacial bond strength. Other researchers in the Americas, such as Yu *et al.* [40] and Hestiawan *et al.* [41] are recommending fibre pre-treatment as a possible way of improving the fibre matrix adhesion.

Fujiyama [42] and Angiolilli [43] later showed that inclusion of sisal fibres in cement mortar effectively transformed the failure mode from brittle to a more ductile mode of failure. Later work by Wu *et al.* [44] on sisal fibre-reinforced silty clay (which is relatively comparable to a cementitious matrix) has shown that discrete, randomly distributed sisal fibre-reinforced silty clay is 20% stronger than non-reinforced silty clay.

In Kenya, Mutuli *et al.* [45] have investigated the potential that sisal fibre has for use as reinforcement in cement-based matrices. Research work by Bessel and Mutuli [46] into the interfacial bond strength of sisal fibre-reinforced cement paste resulted in the development of a special rig that is nowadays used to test fibre-reinforced cementitious matrices in tension. Aruna [47], while testing sisal fibre-reinforced ordinary Portland cement mortar in tension, has reported a high energy absorption capacity of the sisal fibre-reinforced cement composites.

Further work in Kenya by Mutua [48], researching on the mechanical properties of sisal fibre-reinforced concrete recommended that water absorption properties of fibre-reinforced cementitious composites to be an area of interest for further research work. The water absorption properties of sisal fibres have been shown to play a key role in the fibre reinforcement of silty clay by Wu *et al.* [44].

The main disadvantage of using natural fibres as reinforcement in hydrophobic matrices (e.g. epoxy resin, polyester resin) is the incompatibility between the fibres and the matrix [16, 18, 28, 49–53]. Natural fibres can have their surface morphology modified by physical or chemical means to improve the fibre-matrix compatibility. Physically, fibres can be modified via stretching [54], cornification [39], grafting with polymers or calendaring [50, 55–59]. However, these physical methods only affect the superficial and anatomical characteristics of the fibre. Chemical modification treatments include but are not limited to, mercerisation, acylation, acetyl treatment and peroxide treatment [28, 53, 60, 61].

Mercerisation is defined as the chemical treatment of cellulose-based natural fibres with an alkaline solution effecting morphological changes on the fibre surface and structural changes in the fibres cellular structure [27, 28, 50, 62].

Cornification, on the other hand, is the irreversible stiffening of ligno-cellulosic fibre polymer structure that occurs as a result of repeated drying and rewetting using distilled water [61, 63, 64]. The repeated drying and rewetting of ligno-cellulosic fibres leads to an eventual and irreversible loss of fibre swellability and flexibility. This 'stiffening' of the fibres is what gives them dimensional stability making them better candidates for fibrous reinforcement of matrices than their native/untreated counterpart. The drying can be accelerated in the laboratory by heating the fibres to 80°C with the temperature set to increase at a rate of 1°C per minute to avoid thermal shock.

In this study, mercerisation and cornification are the methods of sisal fibre morphology modification adopted. The modified sisal fibres were then tested to establish their strength properties and after that, used as reinforcement in cementitious and polymeric matrices.

1.2 Problem Statement

Fibre reinforcement of cementitious and polymeric matrices is primarily done to improve on the matrices strength, stiffness, abrasion resistance and to reduce thermal expansion [42, 53, 65]. Several fibres, such as glass, carbon and asbestos have traditionally been used to reinforce cement and mortar. These fibres are non-biodegradable, expensive and- in the case of asbestos- been linked to over 80% of all pleural mesothelioma[2] cases and bronchogenic cancers[3] [66–70].

In recent years, nylon, glass and carbon fibre-reinforced resins have found use in aircraft and aerospace application [16, 29, 71–73]. Fibre-reinforced resins are also used in prosthetic

[2] A rare and malignant type of cancer caused by asbestos

[3] A malignant neoplasm of the lung occurring in the epithelium of the bronchus or bronchiole

dentistry in the manufacture of the Composipost[4]dowel for tooth restoration following root canal procedures [74–76]. Natural fibre-reinforced resin-based bio-composites have also found use in the biomedical field where studies have shown that the fibres are more compatible with human tissue than their synthetic counterparts. In particular, Pineapple leaf fibre nanocomposites have recently found use in the tissue engineering repair of human articulate cartilage, urethral catheters, penile prosthesis and vascular grafts [16, 77].

Unsaturated polyester resins are generally used in reactive processing manufacturing techniques such as compression moulding, resin transfer moulding, hand lay-up and resin casting processes [78–80]. According to Sreekumar *et al.* [78], fibre-reinforced thermosetting resin composites possess high tensile and flexural strength compared to unreinforced resin. This assertion has further been confirmed by Idicula *et al.* [81] in their dynamic mechanical analysis of randomly oriented fibre-reinforced polyester resin.

Processes employed in the production of synthetic fibres are expensive and exert a toll on the environment in terms of the energy required to produce the fibres from their precursors industrially [16, 50, 82–85]. Annually, mining of mineral fibres alone pumps 970 million tons of CO_2 into the atmosphere, which translates to approximately 2.7% of the world's global CO_2 emissions [24, 86]. Conversely, ligno-cellulosic fibre sources such as sisal capture more CO_2 over their lifetime than they produce, contributing to an overall reduction in global CO_2 levels [87]. Research work on natural fibre alternatives is an ongoing global endeavour. Addition of natural fibres into polymeric matrices has been shown by Milosevic *et al.* [24] to result in improved wear resistance properties of the natural fibre-reinforced composites

[4] A post made of a non-metallic material used for retaining the core of teeth having little coronal tissue

compared to the 'neat' unreinforced polymer. Kumar *et al.* [88] by measuring the coefficient of friction of sisal/glass fibre-reinforced epoxy resin reported increased frictional coefficient of the hybrid composite compared to the 'neat' epoxy resin. Dwivedi and Chand [89] investigated tribological behaviour of jute fibre-reinforced polyester matrix and reported improved wear resistance of the fibre-reinforced polyester specimens. Sisal fibre-reinforcement have also been shown by Xin *et al.* [90] to be a viable alternative to asbestos resin brake composites. Later studies by Fávaro *et al.* [65] focused on the effect of both fibre and matrix modification on mechanical properties of sisal-high density polyethene composites, reporting significant gains in tensile, flexural and impact strength of the fibre-reinforced polymeric composites.

In Kenya, studies by Mutuli [91] investigated the mechanical properties sisal fibre-reinforced cement paste and demonstrated that sisal fibres have the exploitable potential for use as reinforcement in corrugated roofing sheets. Later studies by Mutuli and Bessel [46] on the interfacial bond strength of sisal/cement composites found that moisture absorption by the fibre affected the interfacial bond strength. Li *et al.* [92] studied the sisal fibre and concluded that its ligneous waxy covering made it unsuitable for use as reinforcement in polymer matrices. Bassyouni [93] investigated dynamic mechanical properties of chemically treated sisal fibre-reinforced polypropylene composites and suggested dewaxing of sisal fibres as a possible way of improving the bonding of sisal fibre with the matrix.

With this aim in view, there is, therefore, need to find a suitable, sustainable, eco-friendly, low-cost alternative fibre reinforcement to be used as reinforcement in cement and polyester resin matrices with the fibres strength properties improved to equal or exceed those of synthetic fibres.

1.3 Main Objective

The main objective of this research was to carry out surface-modification (mercerisation and cornification) of Kenyan sisal fibre, carry out strength tests and ultimately compare the strength properties of sisal fibre-reinforced mortar, polyester and epoxy resins with the sisal fibres in their untreated, mercerised and cornified states.

1.3.1 Specific Objectives

The specific objectives were:

1. To determine the tensile strength properties of sisal fibre in its untreated, mercerised and cornified states.
2. To determine the tensile strength properties of uniaxially aligned continuous fibre-reinforced composites of mortar, polyester and epoxy resins with sisal fibre in its untreated, cornified and mercerised states.
3. To determine the flexural strength properties of randomly oriented discontinuous fibre-reinforced composites of mortar made with sisal fibre in its untreated, cornified and mercerised states.

1.4 Justification

According to Dunne *et al.* [83], the invention of synthetic fibres has reduced the use of sisal and other natural fibres in many applications. Biagiotti *et al.* [19] goes on further to show that low-wage developing economies in East Africa and Brazil that have traditionally relied on sisal fibre export for foreign exchange earnings have been most affected by this reduction, since, synthetic fibre production is mostly done in Europe and the Far East.

Increasing socio-economic pressure to conserve non-renewable petroleum reserves, coupled with the need to use eco-friendly materials has led to a renewed interest in natural fibres [29,

31, 34, 51, 52, 83, 94, 95]. Cooke and Johnson [96] and Mborah *et al.* [97] have linked the mining of mineral fibres to environmental degradation and the creation of derelict landscapes. These landscapes are of low agronomic and economic value and in some instances hazardous to communities living nearby as was concluded by Fields' [98] in his aptly titled article "The Earth's Open Wounds; Abandoned and Orphaned Mines."

According to Ramamoorthy *et al.* [29], Dris *et al.* [99] and Carney Almroth *et al.* [100], synthetic fibres are flammable, and, produce noxious, toxic gases upon combustion. They also present a unique disposal problem due to their non-biodegradability [101]. Mwasha [102] investigated the use of limited life geotextiles (LLG's) in the built environment and found that polyvinyl chloride (PVC) used in construction was a potential source of toxic and carcinogenic dioxins. Natural fibres of cellulosic origins, such as sisal fibres, have been shown to be an eco-friendly, non-toxic and sustainable alternative to these mineral and synthetic fibres in the production of LLG's [103].

Kenya's vision 2030 [104] underscores value addition of agricultural commodities as a priority area under the economic pillar. Researching ways of improving the mechanical properties of sisal is in line with the republic of Kenya's vision. It promises to rejuvenate the sisal industry, increase foreign exchange earnings from exports and ultimately benefit the rural community.

1.5 Scope of the Research

This study focused on the strength properties of untreated and surface modified sisal fibres and their mortar and polyester resin composites. Modification of the sisal fibre cellulose structure was via mercerisation and cornification. The study was conducted from October 2016 to March 2021 at the following laboratories and workshops:

1) Concrete Workshop, Department of Civil and Construction Engineering, University of Nairobi.
2) Timber Workshop, Department of Civil and Construction Engineering, University of Nairobi.
3) Department of Mechanical and Manufacturing Engineering Workshops and Laboratories, University of Nairobi.
4) Public Health Laboratory, Department of Civil and Construction Engineering, University of Nairobi.
5) Chemistry Laboratory, Department of Chemistry, University of Nairobi.

Rea Vipingo Sisal Estate Ltd supplied the sisal fibres used in this research while the river sand and Ordinary Portland Cement were procured locally. In this study, 129 fibre-reinforced mortar beams of dimensions 100 mm x 100 mm x 500 mm were tested for flexural strength, density and void volume fraction, 57 fibre-reinforced mortar beams of dimensions 50 mm x 50 mm x 400 mm were tested for tensile and interfacial bond strength, 48 fibre-reinforced polyester resin specimens measuring 5 mm x 20 mm x 160 mm were tested for tensile strength, 48 fibre-reinforced epoxy resin specimens measuring 5 mm x 20 mm x 160 mm were tested for tensile strength, and, 30 fibre-reinforced polyester resin beams measuring 20 mm x 8 mm x 300 mm were tested for flexural strength. Statistical analysis of the data was carried out using polynomial regression and the Weibull Cumulative Density Function (CDF). The mechanical properties of these fibre-reinforced cementitious and polymeric specimens were evaluated in accordance with the British Standard (BS) and the American Society for Testing and Materials (ASTM) standard.

CHAPTER TWO

2.0 LITERATURE REVIEW

2.1 Sisal Fibres

2.1.1 Historical Background

Agavaceae, are a family of monocotyledonous plants of the order *Asparagales* which possess antimicrobial properties and are commonly associated with the production of alcoholic beverages such as tequila (produced from *Agave Tequilana*) and mescal (produced from *Agave Salmiana*) [3, 105, 106].

There are 57 species of the *Agavaceae* family growing in the tropics and subtropics [106]. Several of these species are associated with fibre production. These include *Agave Sisalana, Agave Vera-cruz, Agave Ameniensis, Agave fourcroydes* and *Agave Angustifolia* [3, 107, 108]. Of these, *Agave Sisalana,* commonly known as sisal, has the highest fibre yield [107]. Sisal has its roots in the Americas where the ancient civilisations of the Mayans, Aztecs and Incas cultivated it for food, fodder, medicine, hallucinogenic power (for religious rites) and also for its fibrous leaves [5]. Over the millennia, sisal fibre found more uses in making of ropes, twine, upholstery, hammocks, padding, nets, baskets, dart boards, blankets, carpet padding, jewellery, sandals, musical instruments, clothing and construction material [1, 32, 106, 109, 110].

Sisal farming in the East African Protectorate was introduced in 1893 by German Agronomist Dr Richard Hindorff who imported 62 bulbils as seed stock from Florida, in the USA via Germany [6, 7, 106, 111]. Within five years, these plants had multiplied into 63,000 starter plants and formed the foundation stock for plantations in British and German East Africa [6, 7]. Being a colonial commodity and requiring expensive machine processing (such as

mechanical decorticators and combing machines) before marketing, sisal evolved as a cash crop and sisal plantations were considered markers of *kulturland* (civilized land) as opposed to *urproduktion* (aboriginal agriculture) in both British and German East Africa [7, 112]. The Department of Agriculture introduced sisal in Kenya in 1903 with trial plots near Nairobi, the Coast and around Lake Victoria.

The first commercial sisal plantations were put up in 1907 between Thika and Muranga by R. Swift and E.A. Rutherford. These large sisal estates soon began capitalisation, and between 1912 and 1914, individuals, companies and co-operatives embarked on the importation of sisal decorticators and power plants resulting in increased sisal processing capacity [7]. The disruption occasioned by the First World War in 1914 and subsequent cutting off of Belgium and Russia as Britain's principal source of fibre imports saw a considerable increase in value and demand of East African sisal [7]. Table 2.1 shows the increase in East Africa's sisal, flax and coffee prices at the height of the First World War.

Table 2.1: Increase in value of exports (in £/tonne), East Africa Protectorate [113]

	1912-13	**1913-14**	**1914-15**	**1915-16**	**1916-17**	**1917-18**
Sisal	17.61	11.67	21.52	32.18	40.66	43.72
Flax	exports negligible			11.91	9.52	42.44
Coffee	73.03	67.27	55.85	57.39	55.59	42.04

With the expansion of the railways line, sisal estates emerged throughout Kenya. By 1969, there were 54 active sisal estates in Kenya [111].

The annual production of sisal in Kenya was 30,000 tonnes between 1930 and 1950 [114]. In 1937, a high-level sisal research station was set up in Thika mandated with the development of superior varieties of sisal, improved agronomic management and processing practices [1].

Soon after the Second World War broke out in 1939, colonial market structures were dealt a blow. In an attempt to centralise purchases of essential commodities from overseas, the British government set up what came to be known as the Combined Food Board and the Raw Materials Board [115]. These boards were tasked with bulk purchases of essential commodities from overseas for the British economy. The essentials included but were not limited to; cotton, coffee, pyrethrum, tea and sisal [115]. Coupled with the subsequent capture of Java and the Philippines (both critical suppliers of natural fibre to Britain) by the Japanese, high demand was created for Kenyan sisal. Given the vital role that sisal had then assumed in the country's economic landscape, the colonial government decided to form a body to oversee the industry. The Kenya Sisal Industry Act Cap 341 of the Laws of Kenya was consequently enacted in 1946 [116]. By the mid-fifties, Kenya's annual sisal production peaked at 70,522 tonnes. The increased production led to the opening of Kenya's first sisal spinning factory in Juja in 1954.

This increased annual production was, however, short-lived when the low production costs of Abaca in the Philippines and Henequen[5] in Mexico led to Brazil, the world's largest sisal producer to lower its prices to remain competitive [117]. This, coupled with the influx of cheaper synthetic fibres such as polyester and acrylic, saw the annual production of sisal in Kenya drop by half to 40,000 tonnes [108, 118–120]. By 1970, only 28 of the first 54 sisal estates were producing [121].

The low production levels persisted throughout the 1980s until the early 1990s when a renaissance in the uses of sisal reversed the trend. Owing to sisal fibre's relatively low

[5] Botanical name: *Agave fourcroydes* is a 'fibre producing' plant native to Mexico and Guatemala.

specific gravity of about 1.25 – 1.5 gcm^{-3} compared to say, glass fibre's 2.6 gcm^{-3}, automobile manufacturers have begun using a flax-sisal fibre (in place of glass fibre) epoxy resin composite to manufacture door panels, door handles, fenders and dashboards [15, 29–32, 94, 122–126]. The use of natural fibre-reinforced polymeric matrices has the advantage of resulting in an overall reduction in the mass of the automobile, and, reduction in the fuel consumption of the vehicle [14, 15, 71, 94, 124, 127]. Leading automobile manufacturer Audi, currently uses sisal fibre-reinforced polyurethane composite to make the door trim panel of its A2 mid-range series of vehicles [94]. Canadian automobile manufacturers are also using flax fibre-reinforced polypropylene to make the rear-shelf panel of the Chevrolet *Impala* and the 1953 Chevrolet *Corvette* [17, 128]. German automobile manufacturer DaimlerChrysler currently uses flax fibre-reinforced polyester resin to fabricate the engine and transmission enclosures of the Mercedes-Benz *Travego* travel coach for insulation against sound [94, 129]. Already, there are plans to develop a Mercedes-Benz-K class series whose entire body is to be made using natural fibre-reinforced composite just like the Trabant[6] [128, 130]. In 2003, Wambua *et al.* [131] established that some specific properties of compression moulded natural fibre-reinforced composites of polypropylene are comparable to those of glass fibre-reinforced polypropylene composites.

Sisal waste, which consists of plant tissue (lignocelluloses), metabolites and water has also found new uses as a pesticide [132], as an antimicrobial agent [105], as an anthelmintic[7] in ovine and caprine flocks [133], in lactic acid production [134], biogas [87] and bioethanol production [135, 136]. New markets have also opened up, and East Africa sisal producers

[6] An old fashioned East German automobile with a body made using a cotton waste/phenol resin composite.

[7] An anti-parasitic drug that expels parasitic worms (helminths) without harming the host.

export sisal to North America and Japan where it is used for making sacks, carpets and paper [1, 137].

An increased socio-economic burden to safeguard petroleum resources and the need to use eco-friendly materials in light of the environmental pollution correlated with synthetic fibre use has led to renewed interest in natural fibres [34, 83, 118, 127, 138]. Since the early ’70s, the United Nations researched the potential of using sisal and coir waste in the manufacture of low-cost building boards [139]. More recently, sisal fibre has been used to reinforce mortar in building construction [42, 140, 141]. Ngala [142] by investigating the mechanical properties of sisal fibre-reinforced rice husk ash pozzolanic cement has also shown that sisal fibre has the potential to be used as reinforcement in special types of cement.

Sisal fibre has also been used to reinforce gypsum boards for use in construction as ceiling panelling and partition boards [15, 143, 144]. Civil works, especially bituminous road construction with textile reinforcement have been done, with sisal fibre being the base fibre [145]. In the United Kingdom, Danso *et al.* [146], research on the behaviour of soil reinforced with natural fibres, concluded that vegetable fibres could be successfully used together with soil to make composite load-bearing members such as soil blocks. Sisal fibre in particular, has been shown by Namango [147] as being a suitable fibre for stabilizing earthen building materials especially when used alongside cassava powder. A conclusion that was also drawn by Eichhorn *et al.* [56] in their review of current international research into cellulosic fibres and composites.

2.1.2 Sisal Fibre Morphology

Sisal fibre is harvested from the leaves of the *Agave Sisalana* plant. The leaves are typically arranged around the meristem[8] in whorls. A mature sisal plant produces between 200-250 leaves before flowering [3, 18, 29, 32, 106, 108].

Mature leaves attain a length of 1.2-2 meters, a width of 4.5-12 centimetres and a mass of 0.27 – 0.75 kilograms with fibres running the entire length of the leaf [3, 106]. The fibres are embedded in the parenchyma[9] tissue of the mesophyll[10]. A meter-long mature leaf contains approximately 1100 individual fibre strands and a dry fibre content of 3 – 4% by weight [3, 18, 32, 107]. A leaf is deemed mature either when it makes an angle of 45˚ with the central spike or when it attains a length of 0.6 – 1 meter [107]. Figure 2.1 shows a mature *Agave Sisalana* plant, with some of the mature leaves harvested.

[8] The tissue in most plants containing undifferentiated cells where growth takes place.

[9] Soft cellular tissue found in the soft parts of leaves, fruit pulp and pith of plants

[10] Parenchyma containing many chloroplasts

Figure 2.1: Image showing harvesting of mature Agave sisalana plant leaves in Kitui County, Kenya [148]

A sisal leaf contains three different fibres: Structural, arch and xylem fibres. Structural fibres are found on the edge of the leaf and give the sisal leaf its characteristic 'stiffness.' The arch fibres grow in the middle of the leaf running from the base to the pointed tip [149]. The xylem fibres grow obverse to the arch fibres and are composed of thin-walled cells [29, 149]. These different fibres are shown in Figures 2.2-2.3

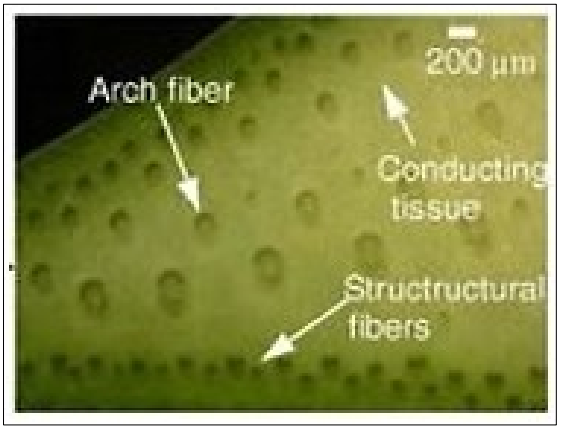

Figure 2.2: Image showing different fibres in sisal leaf cross-section [149]

Each of these three types of fibres comprises of elongated fusion cells that taper at both ends known as ultimates [150, 151]. Ultimates are composites made of rigid cellulose microfibrils[11] embedded in a lignin – hemicellulose matrix [52, 152]. They are usually hexagonal in cross-section and are hollow with the lumen/cell cavity being cylindrical [152].

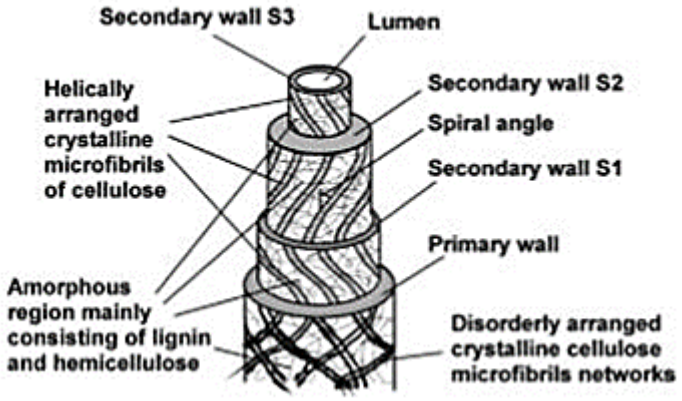

Figure 2.3: Structural constitution of a ligno-cellulosic fibre [152]

Sisal fibre has an irregular cross-section which tapers from butt end to tip end. The fibre has three distinct parts: butt end, neck and fibre tip. Ultimates have a relatively broad cross-section and a large lumen. The fibre cross-section narrows at the neck area where the corresponding ultimate cross-sectional area is smaller, and the fibre then proceeds to taper from the neck to the tip. In fully developed ultimates, secondary thickening takes place between the neck and the fibre tip. Figure 2.4 shows a cross-sectional view of a mature sisal leaf.

[11] A fine fibre like strand consisting of glycoproteins and cellulose

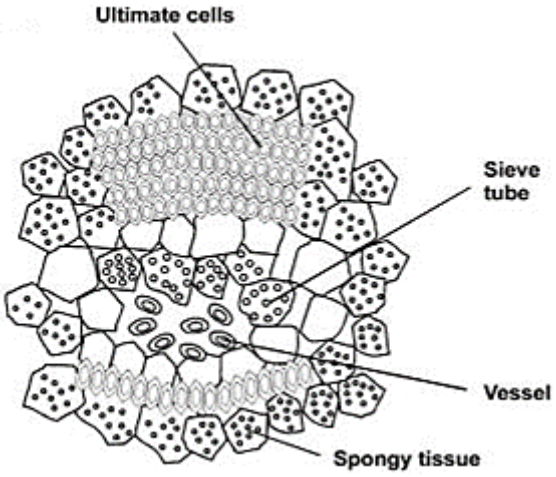

Figure 2.4: Ultimate cells in a sisal leaf cross-section [152]

Sisal fibre is harvested by mechanically scraping the leaves followed by drying, brushing and cleaning of the fibres—this decortication process yields 2 – 4% of fibre by weight [29, 153]. Alternatively, extraction can be done via water retting or by using chemicals such as NaOH and HCl at elevated temperatures [13, 124]. Sisal fibre extraction can also be accomplished via enzymatic bioprocessing using either cellulase, pectinase or lipidase in place of NaOH and HCl [50, 154].

Once the fibres have been extracted from the leaf, they are then air dried, which is a traditional microbial deterioration processing technique [71]. A more modern processing technique that is currently under investigation in Germany that can partially replace air drying is the steam explosion method. In this method, steam under pressure is driven into the spaces between the fibre bundles. This softens the lamella[12], which can then be washed off [19, 149, 155, 156].

[12] A membranous fold in a chloroplast

Several researchers have investigated the chemical composition of sisal fibres. Wilson [157] reported that sisal fibre contains 78% cellulose, 8% lignin, 10% hemicellulose, 2% wax and 1% ash. However, Kuruvilla *et al.* [158] indicated that sisal contains 85-88% cellulose. More recently, Wu *et al.* [44] gave sisal fibres chemical constitution as 64.9% cellulose, 13.7% hemicellulose, 10.4% Lignin, 8.8% water, 1.3% water-soluble matter, 0.7% pectin, 0.2% Lipids and waxes. These results are summarised in Table 2.2

Table 2.2: Sisal fibre chemical composition

	RESEARCHER			
	Wilson [156]	Kuruvilla et al. [157]	Wu et al. [42]	Ramamoorthy et al. [28]
Cellulose (%)	78	85-88	64.9	67-78
Hemicellulose (%)	10		13.7	10-14.2
Lignin (%)	8		10.4	08-11.1
Water (%)			8.8	
Water-soluble matter (%)			1.3	
Pectin (%)			0.7	
Lipids and Wax (%)	2		0.2	2

Several researchers, such as Namvara *et al.* [16], Ramamoorthy *et al.* [29], Khalil *et al.* [31], Li *et al.* [92], Koronis *et al.* [94] and Saxena [124] all attribute this variance in chemical composition to plant genetics, plant age, growth environment (geography), fibre extraction method, handling, and, storage conditions. Rao and Rao [159] report that even the density of natural fibres is dependent on plant age and growth environment.

Studies by Phologolo *et al.* [118] on the chemical characterisation of sisal have established that Kenyan sisal contains a higher proportion of wax, hemicelluloses and lignin than sisal from other parts of the world. This effectively places Kenyan sisal in the lower end of the sisal tensile strength spectrum compared to sisal from different parts of the world [118].

2.1.3 Fibre Surface Behaviour and Modification

Li *et al.* [92] attribute the mechanical properties of natural fibre-reinforced composites to the interfacial bond strength between the fibre and the matrix. Ligno-cellulosic fibre reinforcements, however, generally exhibit poor bonding behaviour with hydrophobic matrices. This behaviour can be explained by considering the equilibrium conditions at the boundary of a drop of liquid in contact with a solid surface such as a fibre surface.

The Young's equilibrium equation is given by [160]:

$$\gamma_{SV} - \gamma_{SL} = \gamma_{LV} \cos\theta \quad \textit{(2. 1)}$$

where:

γ_{SV} – Solid surface tension in equilibrium with the saturated liquid vapour

γ_{LV} – Liquid surface tension in equilibrium with the saturated liquid vapour

γ_{SL} – Interfacial tension between the liquid and solid surface

θ – Angle of contact between the liquid and the solid surface

Figure 2.5 is a vector representation of the vapour-liquid-solid equilibrium condition on a planar surface.

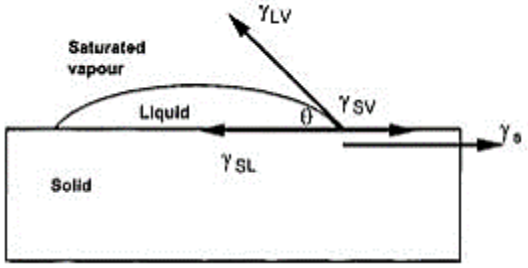

Figure 2.5 Vector representation of vapour-liquid-solid equilibrium on planar surface

Dupré [161] defines work of adhesion W_a as:

$$W_a = \gamma_S + \gamma_{LV} - \gamma_{SL} \quad \text{(2. 2)}$$

Where γ_S is the surface tension of the solid in a vacuum.

Combining Equations (1) and (2) gives the Young's – Dupré equation:

$$W_a = (\gamma_S - \gamma_{SV}) + \gamma_{LV}(1 + \cos\theta) \quad \text{(2. 3)}$$

This equation holds for an ideal smooth surface. When the surface is rough, the surface roughness is defined as:

$$r = \frac{\cos\theta_x}{\cos\theta} \quad \text{(2. 4)}$$

where

θ – Contact angle for a rough surface

θ_x – Contact angle for a rough surface

Wenzel [162] showed that the surface roughness is actually the ratio of the true surface area to the apparent surface area.

Substituting equation (4) into equation (1) and equation (5) yields:

$$(\gamma_{SL})r = r\gamma_{SL} \text{......} \quad (2.\ 5)$$

$$(\gamma_S)r = r\gamma_S \text{......} \quad (2.\ 6)$$

$$(W_a)r = W_a + (r-1)(\gamma_S - \gamma_{SL}) \text{......} \quad (2.\ 7)$$

Equations 2.5 – 2.7 are referred to as the Wenzel equations. From these equations, it becomes apparent that the work of adhesion, 'W_a,' can only be increased by increasing the surface roughness 'r' and the surface tension of the solid 'γ_S.'

Natural fibres have a surface that is coated with a waxy substance. The waxy cover makes the fibre surface smooth and 'lowers the surface tension of the solid,' γ_S. A low surface tension makes the fibre unsuitable for adhesion with polymer matrices. According to Li *et al.* [92], removal of this waxy layer via fibre surface-modification, can leave the fibre surface rougher, increase wettability, and, increase the interfacial bond strength between the fibre and a suitable matrix.

The mechanical properties of fibre-reinforced composites are dependent on the interfacial bond strength between the fibre and the matrix [23, 30, 34, 101, 163, 164]. Merlini *et al.* [164] and Peng *et al.* [165] in their studies of surface lignin and its influences on cellulosic fibre surface properties, concluded that, it is the interfacial bond that determines the strength of fibre-reinforced composites. Several researchers such as Khalil *et al.* [31], Koronis *et al.* [94], Bisanda and Ansell [166] and Zhou *et al.* [167] have postulated that low interfacial adhesion properties, coupled with poor moisture uptake properties, are the main reasons why cellulosic fibre have found limited use as reinforcement in polymeric matrices.

Cellulose ($C_6H_{10}O_5$), discovered by the French chemist Anselme Payene in the year 1838 is the most abundant naturally occurring biopolymer on earth [19, 51, 168, 169]. It is estimated that on earth, plants biosynthesise approximately 10^{11} tonnes of cellulose per annum [77]. Cellulose is defined by Brancato [170] and Huber *et al.* [171] as a cellobiose polymer forming a long polymer chain consisting of many hydrogen bonds. Figure 2.6 shows the molecular structure of a cellulose molecule.

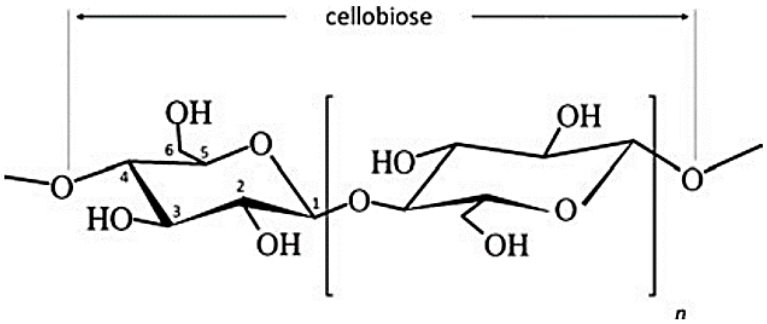

Figure 2.6: Cellubiose molecule [171]

Lignin is amongst the most abundant of all biopolymers on earth, second only to cellulose [168]. It is defined as a polymer of multiple phenyl propane units that generally exhibits hydrophobic properties [172]. Sergio *et al.* [173] describes its function in ligno-cellulosic fibres as being that of an amorphous binder consisting of both aliphatic and aromatic constituents that binds the cellulose and hemicellulose together. It also serves to protect the plant cellulose component from microbial attack [19, 29, 124]. The lignin composition in plants is largely dependent on the plant species. As a general rule, woods have a lignin content of between 20 – 30% while herbaceous plants such as sisal have a much lower lignin content of between 5 – 11% [168]. Figure 2.7 shows the molecular structure of a lignin molecule as given by Alder [168]

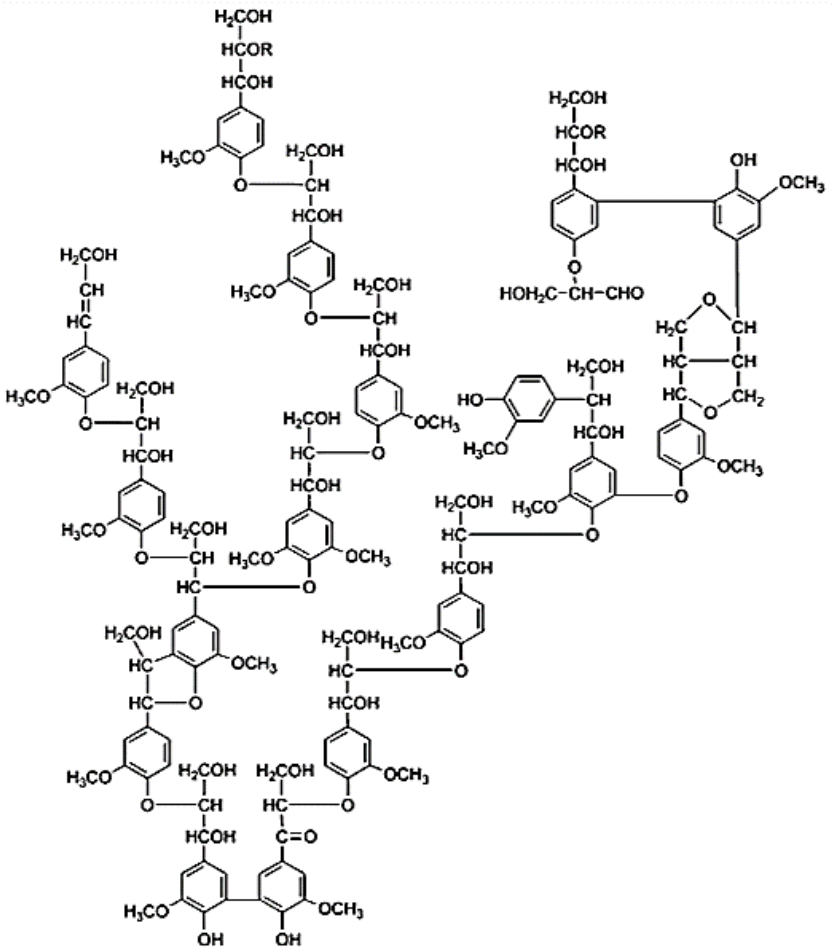

Figure 2.7: Alder's structural model of a lignin molecule [168]

Hemicellulose is the amorphous group of polysaccharides that remain attached to cellulose even in the absence of lignin. It contains hydroxide and acetyl groups making it hygroscopic [174]. The wax, together with the fibre cuticle, covers the fibre surface, making it smooth. Figure 2.8 shows the molecular structure of a hemicellulose molecule.

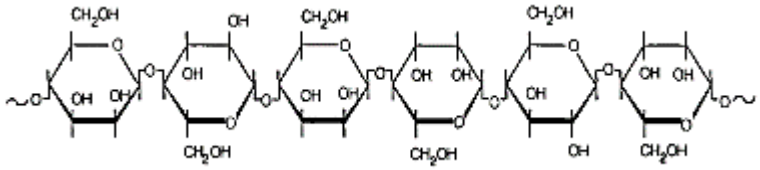

Figure 2.8: Hemicellulose molecule [175]

Removal of this waxy cover can be achieved through physical or chemical methods. Physically, modification of fibres can be done via stretching [54], thermo-treatment [39], grafting the fibre surface with polymers [50, 55, 56], or calendaring [56–59]. These techniques only affect the superficial and anatomical properties of the fibre, leaving the chemical composition intact.

Chemical treatment of ligno-cellulosic fibres involves the removal of wax, lignin, hemicelluloses and other impurities from the fibre surface [176]. This reduces the natural hydrophilic nature of cellulosic fibres by reducing the total number of hydroxyl groups within the cellulose molecule. Chemical modification of natural fibre morphology can be achieved using several different chemical treatments. These include but are not limited to mercerisation, acrylation, acetyl treatment, and peroxide treatment [28, 34, 53, 60, 61]. Ballesteros *et al.* [39] and Claramunt *et al.* [177] investigated the effect of cornification on the structural and physicochemical characteristics of softwood fibres. It was observed that cornified fibres exhibited improved dimensional stability, making them suitable candidates for composite reinforcement. Zhang *et al.* [101] also report improved thermal stability of silane and peroxide treated ramie fibres. In this study, mercerisation and cornification were the methods of modification of sisal fibre morphology that were employed. The choice of these two fibre-modification techniques was based on the low cost associated with each of the

processes, and, from other fibre surface-modification studies carried out on ligno-cellulosic leaf fibres similar to sisal fibre by previous researchers [34, 60, 64, 177].

2.1.4 Mercerisation

Mercerisation was discovered in the year 1844 by John Harwood in Lancashire, England. It is the treatment of cellulose-based natural fibres with a sodium hydroxide solution to effect morphological changes on the fibre surface and structural changes in the fibres cellular structure [27, 50, 52]. Mercerized natural fibres are observed to have more elastic microfibrils in the cellulose structure as compared to untreated cellulose [178]. Untreated cellulose is made of two distinct crystalline phases; cellulose I_α and I_β [179]. Following mercerisation, the structure of the fibre changes from an I_α and I_β cellulose mixture to a thermally stable cellulose II polymorph [180]. The surface-modification is achieved by the removal of wax, lignin and hemicelluloses from the fibre surface. This increases the fibre surface area available for adhesion with a suitable matrix [52]. The removal of these impurities leaves the fibre surface with a rough finish which can result in a better interlock between the fibre and matrix in a composite [181]. Chemical treatment also reduces the number of free hydroxyl groups of the cellulose molecule. This, in turn, reduces the polarity of the cellulose molecules and increases compatibility with hydrophobic polymer matrices [18, 182].

The chemical reaction takes place, as highlighted in equation 2.8 and Figure 2.9:

$$C_6H_7O_2(OH)_3 + NaOH \rightarrow C_6H_7O_2(OH)_2(ONa) \rightarrow C_6H_7O_2(OH)_3 + NaOH \ldots\ldots (2.8)$$

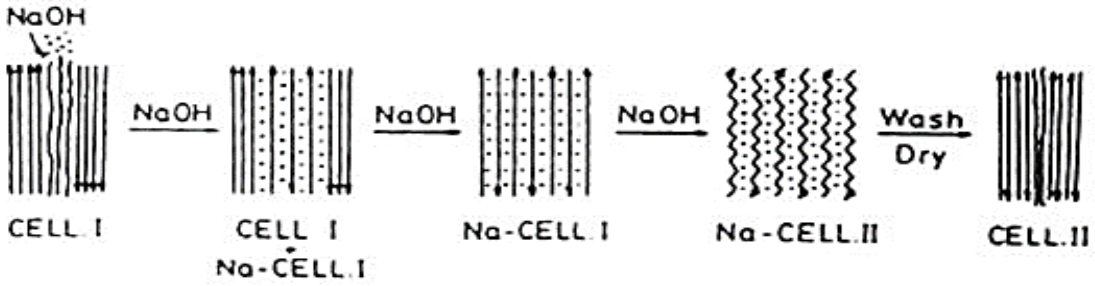

Figure 2.9: Mercerisation mechanism as given by Okano and Sarko [183]

In the textile industry, it is common to use NaOH solution for mercerisation of cellulosic fibres. Other alkali solutions can also be used to achieve mercerisation. These include KOH and LiOH. Chen *et al.* [184] investigated the cross-linking cotton fabrics mercerised with different alkali solutions. They established that these three alkalis, as mercerising agents, can be ranked in order of effectiveness as LiOH, NaOH and then KOH, the most effective being LiOH followed by NaOH. In terms of cost, NaOH treatment is considered to be one of the 'technologically' cheapest and cleanest fibre surface-modification methods [128, 184]. Mercerised lingo-cellulosic fibres have also been shown to be more absorbent than their untreated counterparts, and thus more suitable fibre reinforcements in hydrophilic matrices such as cement mortar [65]. This makes mercerisation a viable, affordable and environmentally friendly option for the surface-modification of UG-grade sisal fibres.

2.1.5 Cornification

Cornification also referred to as hornification, was discovered in 1944 by G. Jayme. Diniz *et al.* [63] define cornification as the irreversible stiffening of ligno-cellulosic fibres polymer structure that occurs as a result of repeated drying and rewetting. According to Ballestero *et al.* [39] and Claramunt *et al.* [177] repeated drying and rewetting of ligno-cellulosic fibres result in an eventual and irreversible loss of fibre swellability and flexibility. On the micro-scale, with each successive drying and rewetting cycle, the microfibrils become more tightly

packed and gradually, the capillary voids become completely closed. This translates into an increased degree of cross-linking within the fibre microstructure. The degree of cornification is measured as the attrition in water retention values (WRV) expressed as a percentage of the original value [64].

According to Ballesteros *et al.* [39] and Claramunt *et al.* [177], cornified fibres possess higher dimensional stability which makes them better suited for matrix reinforcement compared to their untreated counterparts. Figure 2.10 is a schematic drawing showing the cross-sections of an untreated and cornified ligno-cellulosic fibre.

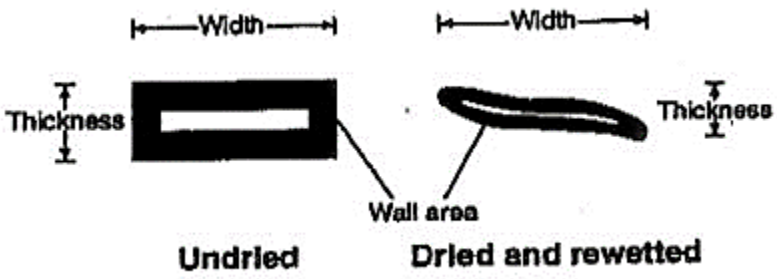

Figure 2.10: Schematic diagram showing untreated and cornified fibre cross-sections [185].

Stevulova *et al.* [186] study into the thermal degradation of natural hemp concluded that during the drying phase of the fibres, amorphous components such as lignin and hemicellulose are degraded resulting in improved crystallinity of the fibres.

Santos *et al.* [187] have also shown that under special conditions, cornification of wood pulp and non-wood cellulosic fibres can be achieved at room temperature by repeated pressing and drying. Repeated wetting and drying of ligno-cellulosic fibres also happens naturally in nature as is the case with mooring cleats for boats and ships and also in anvil rope ties that are made of sisal fibres [177]. These fibres, over time, due to the repeated wetting and drying in the sea, cornify and become 'tougher' than they initially were in their unused state. Cornified fibres

have also been shown to be more dimensionally stable than other surface-modified fibres [28,177]. The ease at which the process can be replicated in the laboratory makes cornification a suitable fibre surface-modification method for sisal fibres.

2.2 Matrices

2.2.1 Ordinary Portland Cement

Ordinary Portland cement (OPC) consists of clinker[13] that is ground to a particle size of 10-30 microns with a small percentage of gypsum. The chemical composition of Portland cement is given in Table 2.3.

Table 2.3: Chemical composition of Portland cement (Blanks and Kennedy [188])

Tricalcium Silicate	$3CaO.SiO_2$	54%
Dicalcium Silicate	$2CaO.SiO_2$	16%
Tricalcium Aluminate	$3CaO.Al_2O_3$	11%
Tetra-calcium Aluminoferrite	$4CaO.Fe_2O_3$	10%
Magnesia, Gypsum & Lime		9%

When water is added to cement, the gypsum forms a complex calcium sulphoaluminate with the lime and the alumina that is released from the clinker. The hydrated compounds then coagulate into a gel. It is this gel that lends cement its bonding properties by binding to untreated cement or any other aggregate material present (including the fibre reinforcement) [189, 190]. OPC cement gets most of its strength from hydrated calcium silicate.

During the hydration process, calcium hydroxide is precipitated and usually forms crystals in the pores. If it is allowed to set, Portland cement expands when exposed to an aqueous

[13] Lumps usually 3 - 25mm in diameter produced by sintering limestone and alumina-silicate substances like clay

environment. Upon drying, it undergoes a partially reversible shrinkage. This relationship is shown diagrammatically in Figure 2.11.

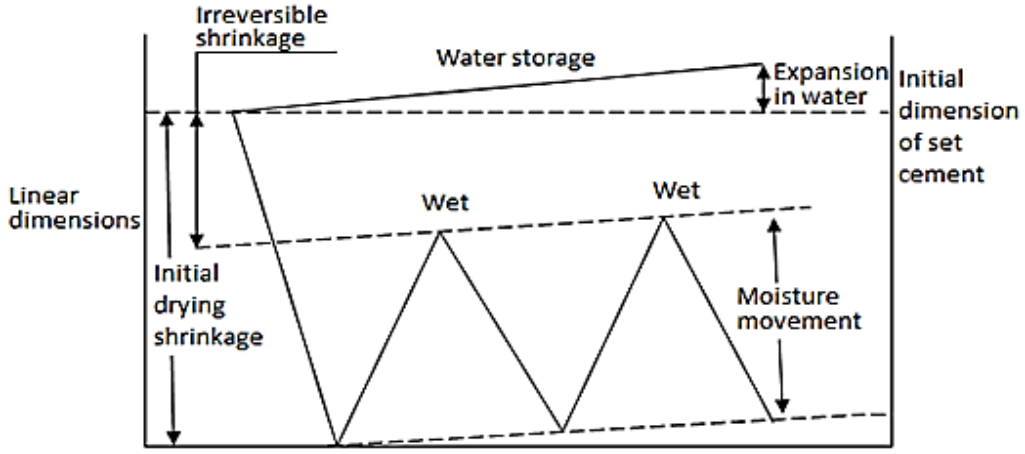

Figure 2.11: Dimension changes during hardening of Portland cement [189].

The expansion of cement immersed in water is dependent upon the composition of the cement and is of the order 0.3% change in linear dimension per annum [189].

The porosity of compacted Portland cement and consequently most of its mechanical properties depend on the Water: Cement *(w/c)* ratio used in the preparation of the mortar and also on the age of the mortar. If this ratio is below 0.4, then unhydrated cement remains in the cement paste indefinitely. Portland cement paste is made up of a porous gel, unhydrated cement, calcium hydroxide crystals and capillary pores. The pores of the gel average 15-30 Angstroms[14] in diameter while the capillary pores vary in size up to several hundred angstroms in diameter. Interconnected capillary pores are responsible for the porosity of the hardened cement paste.

[14] A unit of length equal to one hundredth-millionth of a centimetre or 10^{-10} metre

2.2.2 Unsaturated Polyester Resin

Polyesters are produced naturally by some animals, specifically by the lac insect (*Keria Lacca*) which it exudes onto Croton[15] tree barks. Bioactive polyesters are also produced naturally in the world's oceans by certain species of marine fungi [191, 192]. Researchers such as Zhang *et al.* [101] have further shown that bio-renewable polyesters can also be derived from vegetable oils using chemical techniques such as olefin metathesis.

Unsaturated polyester resins were first documented in the year 1894 by Vorlander [193]. The resin was compounded for use as a fibre-reinforcement using styrene, peroxides and fillers. The earliest documented commercial polyester production is by General Electric company laboratories between 1910 and 1915 with the patent being filed in 1912 [191].

Currently, fibre-reinforced polyester resins are widely used in the marine industries in the making of Yachts, workboats and dinghies and in the construction industry in formulation of polymer concrete [163, 192, 194].

By definition, an unsaturated polyester resin is a thermosetting condensation polymer formed by polymerising of low molar mass reactants such as monomers to form cross-linked network polymers [191, 192, 194]. The polyesterification reaction is shown in Figure 2.12

[15] A flowering plant in the spurge family, *Euphorbiaceae* native to the tropics of the Americas and East Africa. It has local names such as mũkindũri in gĩkũyũ, mũthũlũ in kamba and Ortuet in Tugen.

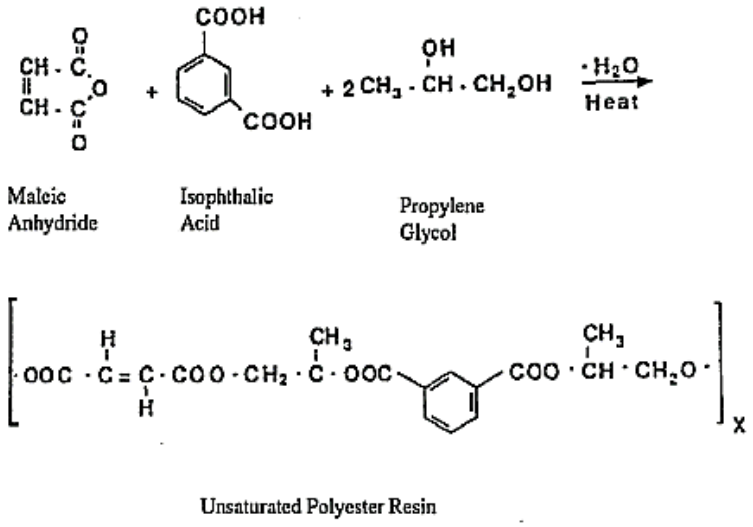

Figure 2.12: Polyesterification reaction between isophthalic acid (dibasic), maleic anhydride and propylene glycol to form an unsaturated polyester resin molecule [195]

The resulting pre-polymer has numerous unsaturated carbon bonds (C=C), and it is these unsaturated carbon bonds that crosslink with styrene to form the thermosetting polymer. Other chemicals that can be used in place of styrene include (but are not limited to) vinyl toluene, vinyl acetate and divinylbenzene methacrylate [192].

To initiate the cross-linking, a substance referred to as an initiator is added to the unsaturated polyester resin decomposing to provide two free radicals. The free radicals attack the unsaturated polyester C=C bonds and initiate an exothermic chain reaction. The final cross-linked chemical structure is shown in Figure 2.13. Most commonly used initiators are organic peroxides, although, in some specialized applications, dibenzyls and azos are employed [191, 192]. In the current work, Methyl ethyl ketone peroxide ($C_8H_{18}O_6$) was used as the initiator.

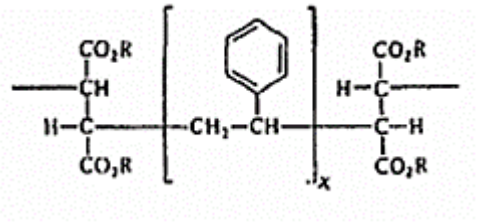

Figure 2.13: Unsaturated polyester resin/styrene copolymerisation network [192]

According to Saleh [192], metal salts can be used as catalysts to induce or catalyse initiator decomposition into free radicals. These catalysts include vanadium salts, cobalt salts, hydroperoxides and amines. Despite the apparent advantages of using catalysts to speed up the polymerisation, these metal salts, at high concentrations, react violently with the peroxide initiator [191, 192] and can potentially pose a risk to personal safety.

2.2.3 Epoxy Resin

Like polyester resins, epoxy resins are a group of thermoplastic resins that are isotropic, brittle and upon curing, cannot be melted back to their initial liquid state [142]. They are generally sold in a 4:1 or a 2:1 resin to hardener mixing ratio.

The main advantage that epoxies have over other resins such as polyester resins is that they generate less heat during curing. They also exhibit better thermal symmetry making suitable candidates for ligno-cellulosic fibre reinforcement.

2.3 Fibre-Reinforced Composites

Composites that are reinforced with long fibres are referred to as continuous fibre-reinforced composites (CFRC) while those that are reinforced with short fibres are referred to as discontinuous fibre-reinforced composites (DFRC) [10]. If the fibres are aligned in one direction, the composite is defined as being unidirectional. Unidirectional fibre-reinforced

composites are anisotropic, with high strength in the fibre direction, but, low strength in the direction perpendicular to the fibre reinforcement [12, 71]. Discontinuous fibre-reinforced composites on the other hand usually have randomly oriented fibres dispersed within the matrix. Such matrices are considered to be quasi isotropic [10, 11, 71]. In the current study, strength properties of both CFRC and DFRC of Ordinary Portland cement mortar and CFRC of polyester resin were determined using tensile and flexural tests.

2.3.1 Stress Distribution in Fibre-Reinforced Composites

2.3.1.1 Unidirectional CFRC

The strength properties of fibre-reinforced composites can be illustrated by considering a matrix reinforced with uniaxially oriented fibres. In order to derive the expressions governing the stress distribution in such composites, the following assumptions need to be made:

- The dispersed phase is aligned parallel to the direction of stress.
- Before cracking, the dispersed phase is fully bonded to the matrix, i.e. equal strain in both the fibre and the matrix also aptly referred to as iso-strain [10, 196].
- The Poisson's ratio in the fibre and the matrix is zero.

Assuming that the second assumption holds,

then:

$$\varepsilon_f = \varepsilon_m = \varepsilon_c \qquad (2.9)$$

where $\varepsilon_f, \varepsilon_m$ and ε_c are longitudinal strains of the fibres, matrix and the composite respectively.

Since both the fibres and matrix are elastic, their respective longitudinal stresses can be calculated as

$$\sigma_f = E_f \varepsilon_f = E_f \varepsilon_c \ldots\ldots(2.\ 10)$$

$$\sigma_m = E_m \varepsilon_m = E_m \varepsilon_c \ldots\ldots(2.\ 11)$$

Comparing equation 2.10 and 2.11 and noting that for effective fibre reinforcement, $E_f \gg E_m$, we can conclude that the fibre stress σ_f is always greater than the matrix stress σ_m.

Also, the load P_c is shared by the matrix and the dispersed phase as given in the equation below.

$$P_c = P_f + P_m \ldots\ldots(2.\ 12)$$

Since force = stress x area, equation 2.12 can be written as:

$$\sigma_c A_c = \sigma_f A_f + \sigma_m A_m$$

or

$$\sigma_c = \sigma_f \frac{A_f}{A_c} + \sigma_m \frac{A_m}{A_c} \ldots\ldots(2.\ 13$$

where

σ_c – average tensile stress in the composite

A_f – net cross-sectional area of the fibres

A_m – net cross-sectional area of the matrix

Due to the difficulty involved in the measurement of the areas A_f and A_m, fibre fraction is preferred.

Since

$$V_f = \frac{A_f}{A_c}\ and\ V_m = \left(1 - V_f\right) = \frac{A_m}{A_c}$$

Equation 2.13 becomes:

$$\sigma_c = \sigma_f V_f + \sigma_m V_m = \sigma_f V_f + \sigma_m (1 - V_f) \ldots\ldots\ldots\ldots\ldots\ldots\ldots\ldots\ldots\ldots (2.\ 14)$$

Dividing both sides of equation 2.14 by ε_c and using equations 2.10 and 2.11, we can thus write the longitudinal modulus for the composite as

$$E_L = E_f V_f + E_m V_m = E_f V_f \left(1 - V_f\right) = E_m + V_f \left(E_f - E_m\right) \ldots\ldots\ldots\ldots (2.\ 15)$$

Equation 2.15 is called the *rule of mixtures* [73, 125, 196, 197]. The equation shows that the longitudinal modulus of unidirectional CFRC is intermediate between the fibre modulus and the matrix modulus and that it increases linearly with increasing fibre volume fraction [12].

The assumptions made with the *rule of mixtures* are:

1) Uniform distribution of fibres within the matrix.
2) Perfect bonding at the fibre-matrix interface.
3) A void free matrix.
4) Applied loads are parallel to the fibre direction.
5) Fibre and matrix are linearly elastic materials.
6) There are no residual stresses in the lamina.

2.3.1.2 Unidirectional DFRC

A tensile load, when applied to a discontinuous fibre-reinforced composite, is transferred to the fibres via a shearing mechanism [73]. Since for reinforcement to occur, the matrix has a lower modulus than the fibres, the longitudinal strain in the matrix is higher than that in the

fibres. Assuming a perfect fibre-matrix bond, and ignoring stress transfer at the fibre end cross-sections, the normal stress distribution can be calculated using a force equilibrium analysis by considering an infinitesimal length *dx* at a distance *x* from one of the fibre ends. The force equilibrium equation becomes:

$$\left(\frac{\pi}{4}d_f^2\right)\left(\sigma_f + d\sigma_f\right) - \left(\frac{\pi}{4}d_f^2\right)\sigma_f - \left(\pi\sigma_f dx\right)\tau = 0 \quad \text{(2. 16)}$$

Which simplifies to

$$\frac{d\sigma_f}{dx} = \frac{4\tau}{d_f} \quad \text{(2. 17)}$$

where

σ_f – longitudinal stress in the fibre at a distance *x* from one of its ends

τ – shear stress at the fibre-matrix interface

d_f – fibre diameter

Now, assuming that there is no stress transfer at the fibre ends, i.e. σ_f = 0 at *x* = 0, by integrating equation 2.17, the longitudinal stress in the fibre becomes

$$\sigma_f = \frac{4}{d_f}\int_0^x \tau\, dx \quad \text{(2. 18)}$$

To simplify the analysis, assuming that the interfacial stress is constant and equal to τ_i integrating equation 2.18 yields

$$\sigma_f = \frac{4\tau_i}{d_f}x \quad \text{(2. 19)}$$

From equation 2.19, it can be observed that for a composite containing discontinuous fibres, the fibre stress is not uniformly distributed. According to equation 2.19, it is equal to zero at either of the fibre ends (i.e. at $x = 0$) and it increases linearly with increasing values of x. The maximum stress occurs at the central part of the fibre when $x = {}^{l_t}/_{2}$. The maximum stress that can be achieved at a given load thus becomes

$$\sigma_{f\,max} = 2\tau_i \frac{l_t}{d_f} \qquad \textit{(2. 20)}$$

where $x = {}^{l_t}/_{2}$ is the load transfer length from each fibre end. ${}^{l_t}/_{2}$ is thus the minimum fibre length where the maximum fibre stress is obtained.

For a given fibre diameter and fibre-matrix interfacial condition, the critical fibre length calculated from equation 2.20 becomes

$$l_c = \frac{\sigma_{fu}}{2\tau_i} d_f \qquad \textit{(2. 21)}$$

where

σ_{fu} – ultimate tensile strength of the fibre.

l_c – minimum fibre length required for the maximum fibre stress to be equal to the ultimate tensile stress of the fibre at mid-length.

τ_i – shear strength of the fibre-matrix interface or the shear strength of the matrix at the interface, whichever is less of the two.

From equations 2.20 and 2.21, the following observations can be made:

1) For $l_f < l_c$, the maximum fibre stress may never reach the fibres ultimate tensile strength. In this case, either the fibre-matrix interfacial bond, or, the matrix itself may fail before the fibres achieve their ultimate tensile strength.
2) For $l_f > l_c$, the maximum fibre stress may reach the ultimate fibre strength over much of the fibre length. However, over a distance equal to $l_c/2$ from either fibre end, the fibre remains less effective.
3) For effective fibre reinforcement. $l_f \gg l_c$.
4) For a given fibre diameter and strength, l_c can be controlled by increasing or decreasing τ_i. This can be achieved by using a matrix-compatible coupling agent or by fibre surface-modification.

While the discontinuous fibres can in theory, be unidirectional, in practice, it is not possible to control the orientation of the fibres. The discontinuous fibres may therefore accurately be considered as being randomly oriented within the matrix [10]. Uniform stress distribution in a discontinuous fibre-reinforced composites is dependent on the volume fraction of the fibres and the orientation of the fibres [198, 199]. Accounting for fibre disorientation is pretty much straightforward. If we let 'V_{ef}' represent the effective fibre volume fraction, then equation 2.14 becomes:

$$\sigma_c = \sigma_{uf} V_{ef} + \sigma_m V_m = \sigma_f n V_f + \sigma_m (1 - V_f) \ldots\ldots\ldots\ldots\ldots\ldots\ldots\ldots\ldots\ldots (2.\ 22)$$

where V_{ef} represents the real contribution of the fibres to the tensile strength of the composite taking into account the disorientation of the fibres in the composite.

Generally,

$$V_{ef} = V_f(1 - P) \ldots\ldots\ldots\ldots\ldots\ldots\ldots\ldots\ldots\ldots\ldots\ldots\ldots\ldots\ldots\ldots\ldots\ldots\ldots\ldots \quad (2.\ 23)$$

where *'p'* is the degradation factor and assumes the value $0 < p < 1$.

The orientation factor has been shown by researchers to have an effect on the dielectric properties of natural fibre-reinforced polymeric composites [200, 201]. Scheirs and Long [191] and Saleh [192] also point out that the reinforcing effect of the fibres is more significant when the composite is loaded in bending than when it is loaded in tension.

The effectiveness of stress distribution in both continuous and discontinuous fibre-reinforced composites is also dependent on the fibres surface-properties. Peng *et al.* [165] in their investigation of surface lignin and its influence on fibre surface properties concluded that the reduced lignin content in ligno-cellulosic fibres following laccasse[16] treatment led to an improved fibre-matrix bond in short sisal fibre/phenolic resin composites. Other enzyme-based fibre pre-treatments have also been recommended and successfully utilized by Islam *et al.* [50] and also by Foulk et al [154] in effecting fibre surface-modification prior to incorporation into a matrix. Li *et al.* [92] researching on developments in both continuous and discontinuous sisal fibre-reinforced composites found that by having more interlocking sites on the fibre surface, better interfacial bond strengths and load transfer were attained between the fibre reinforcement and the matrix. Ligno-cellulosic NaOH treated fibres having been shown by Favaro *et al.* [65] to be more absorbent than the untreated fibres. Cornification on the other hand, has been shown by Naidu and Kumar [28] and Claramunt *et al.* [177] to result in fibres that are dimensionally stable and suitable for use as matrix reinforcement This makes

---

[16] An Enzymatic catalysis treatment of cellulosic fibres also referred to as *Laccasse Doga* that results in fibres with reduced lignin content.

these two fibre surface-modification methods suitable choices for the surface-modification of UG-grade sisal fibres and subsequent incorporation as reinforcement in hydrophilic (mortar) and hydrophobic matrices (polyester and epoxy resins).

2.3.2 Interfacial Bond Strength

Interfacial bond strength refers to the strength of the bond between the fibre and matrix. The strength of a composite greatly depends on the fibre-matrix bond strength [30, 34, 164, 165, 202, 203]. Several researchers such as Srinivasa *et al.* [30], Hestiawan *et al.* [41], Dyczeck and Petri [204], and Azeez *et al.* [205] report that the strength of a fibre-matrix bond is a quality which determines to a considerable degree such properties as strength, Modulus of rupture (MOR) and fracture energy of the resulting composite.

A low bond strength is associated with poor tensile strength of the composite [128]. Different researchers have each proposed different methods of determining the fibre-matrix bond strength. These include;

1) Oakley and Proctor [206] proposed a method used in frictional fibre-matrix bonds where the shear stress along the fibre in a pull-out is constant and equal to the bond strength. The bond strength is given by:

$$\tau_b = \frac{F}{tp} \quad \text{(2. 24)}$$

where τ_b is the interfacial bond strength, F is the pull-out load, t is the embedded length or disk thickness and p the strand perimeter. This method of determining the fibre-matrix bond strength was employed by Atiqah *et al.* [202] while investigating interfacial bonding strength of sugar palm fibres with polyurethane.

2) Laws and Ali [207] gave the average fibre-matrix interfacial bond strength when very thin high strength fibres are used as reinforcements as:

$$\tau_b = \frac{\sigma_{fu} d_f}{4 l_c} \quad \text{(2. 25)}$$

where σfu is the fibre fracture strength, d_f is the fibre diameter, and l_c the critical fibre length

3) Laws and Ali [207] and later Gray [208] also proposed a method to be used when the critical fibre length is greater than the thickness of the specimen bond strength given as:

$$\tau_b = \frac{F}{\pi d_f l} \quad \text{(2. 26)}$$

where, l is the embedded fibre length.

4) Dyczek and Petri [204] developed a method which is applicable when a fibre that is fastened to a matrix along a length X is being pulled out by a force F and is given as:

$$\tau_b = \frac{\sigma_f d_f}{4X} \quad \text{(2. 27)}$$

where, $d_f = \frac{4A_f}{p_f}$, is the fibre diameter, A_f is the cross-sectional area, p_f is the fibre perimeter and X is the length of fibre embedment in the matrix. This method of determining the fibre-matrix bond strength has been successfully employed by [41] in determining the interfacial shear strength of unsaturated polyester/palm fibre composites.

5) Aveston [209] proposed a method that measures the bond by use of crack spacing. According to his theory, during multiple cracking, the cement matrix is broken into a

series of blocks of lengths X' and $2X'$ and is given by:

$$\tau_b = \frac{V_m \sigma_{mu} r}{V_f 2X'} \quad \text{.....(2. 28)}$$

where, σ_{mu} is the ultimate strength of matrix, r is the fibre radius and X' is the length of the inter-crack spacing.

The equation 2.28 proposed by Aveston [209] uses parameters that can be directly measured and therefore becomes more practical in most common applications.

2.4 Summary of Literature Review

Fibre surface-modification has been found to be a valuable method for improving the strength properties of ligno-cellulosic fibres [34, 60, 61, 177]. It has also been shown to greatly improve the interfacial-bond strength between the fibres and matrices [94, 151, 166, 167]. The effect of fibre surface-modification (specifically mercerisation and cornification) on the strength properties of UG-grade Kenyan sisal fibres, with their characteristic high lignin and hemicellulose content [118], is yet to be studied. The current study set out to investigate just that, and, to subsequently test the tensile and flexural properties of hydrophilic and hydrophobic matrices reinforced with the UG-grade sisal fibres in both their untreated and surface-modified states.

CHAPTER THREE

3.0 MATERIALS AND METHODS

The sisal fibre used in this research, supplied by Rea Vipingo Sisal Estate Limited, was wet-decorticated[17], UG grade sisal. The Kenya Sisal industry act [116] defines UG grade sisal as 'sisal fibre with a minimum length of 2 ft. that does not conform to grades 1, 2 and 3L as regards length, colour and cleaning.' The sisal was divided into three batches. The first batch was mercerised; the second batch was cornified while the third batch was left in its untreated state. Various tests were carried out on randomly picked fibre samples taken from these three batches to establish the fibre diameter, surface characteristics and absorbency, tensile strength, tensile Modulus of Elasticity and fibre density. Three sets of OPC mortar, Polyester and Epoxy resin composites were prepared using these three batches of fibres (untreated, mercerised and cornified) with the fibres in two different orientations: (i) uniaxially oriented and (ii) randomly oriented. Tensile and flexural strength properties of these composites were then determined in the laboratory.

[17] Estate sisal that has been extracted by crushing while simultaneously being washed with running water.

3.1 Experimental Procedures

3.1.1 Experimental Procedure I - Sisal Fibres

3.1.1.1 Fibre Surface-Modification

Mercerisation of sisal fibres was done using 0.06M NaOH in line with Mwaikambo and Ansell's [210] conclusion that a 6% NaOH solution treatment results in the highest crystallinity index of sisal fibres.

One mole NaOH is equal to 39.997 grams. One Molar (M) is defined as one mole of a substance in one litre of solvent (water in this case). In this research, one Molar was equal to 100%.

3.1.1.1.1 Preparation of 0.06M Sodium Hydroxide Solution.

The Sodium Hydroxide used in the current work was 98% LR grade NaOH pellets supplied by Griffchem™. Forty litres of 0.06M NaOH solution was prepared by dissolving 97.95 grams of 98% LR grade NaOH pellets in 20 litres of regular tap water. The solution was then diluted to the 40-litre mark by addition regular tap water. The method used to determine the mass of NaOH pellets to be dissolved was as follows:

$$100\% = 1\ Molar = \ Molecular\ mass\ x\ \frac{100\%}{Solute\ Purity\ \%}\ gl^{-1} \ldots\ldots\ldots\ldots\ldots \quad (3.\ 1)$$

$$= 39.997\ x\ \frac{100\%}{98\%}\ gl^{-1} = 40.81326531\ gl^{-1} \cong 40.81\ gl^{-1}.$$

$$6\% = 0.06Molar = \frac{6}{100}\ x\ 1Molar = \frac{6}{100}\ x\ 40.81gl^{-1} = 2.4486gl^{-1} \approx\ 2.45gl^{-1}\ .$$

$$Therefore\ to\ make\ 40\ litres\ of\ 0.06M\ NaO:$$

$$2.45 grams\ x\ 40 = 98\ grams\ of\ NaOH\ pellets\ in\ 40\ litres\ of\ Water.$$

The number of Sodium ions *(Na^+)* available for mercerisation was then calculated using the formula:

$$No.of\ ions\ in\ solution =$$
$$Molarity\ x\ N_A x\ No.of\ ions\ per\ molecule\ x\ Volume\ of\ soln\ \ldots\ldots\ldots \quad (3.\ 2)$$

where:

N_A- Avogadro's number = $6.0221409\ x\ 10^{23}$

The 40 litres of 0.06M NaOH had:

$$\{{}^{6}/_{100}\ x\ N_A\ x\ 1\ x\ 40\}Na^+ = (0.06\ x\ 6.0221409\ x\ 10^{23}\ x\ 40)Na^+$$
$$= 1.440531382\ x\ 10^{24}Na^+$$

3.1.1.1.2 Preparation of 0.01M Glacial Acetic Acid Solution

Preparation of the glacial acetic acid solution required the use of a fume chamber and was done at the Highways laboratory, Hyslop building, UoN.

A 1M CH_3COOH solution was prepared by diluting 58ml of 98.4% pure laboratory grade glacial acetic acid in 500ml of distilled water in a fume chamber. The solution was then topped up to the 1-litre mark by addition of 442 ml distilled water and the resulting 1M CH_3COOH stored in a calibrated Pyrex bottle. Fifty (50) litres of 0.01M CH_3COOH was then prepared by diluting 0.5 litres of the 1M CH_3COOH in 49.5 litres of regular tap water. The method used to calculate the volume of glacial acetic acid to use was as follows:

$$100\% = 1\ Molar = \frac{Acid\ Molecular\ mass\ (in\ grams)}{Acid\ Density\ (in\ grams.cm^{-3})}\ x\ \frac{100\%}{Acid\ Purity\ \%}\ cm^3 l^{-1} \ldots \quad (3.\ 3)$$

$$= \frac{60.05g}{1.05g.cm^{-3}}\ x\ \frac{100\%}{98.4\%} = 58.1204026\ ml\ \approx 58ml$$

$$\cong 58ml\ CH_3COOH\ diluted\ in\ 942\ ml\ of\ distilled\ Water$$

$$\cong 1\ litre\ of\ 1Molar\ CH_3COOH\ solution$$

$$Therefore\ to\ make\ 50\ litres\ of\ 0.01\ Molar\ CH_3COOH,$$

$$Dilute\ 0.5\ litres\ 1M\ CH_3COOH\ in\ 49.5\ Litres\ H_20.$$

3.1.1.2 Mercerisation of Sisal Fibres

Fifteen (15) Kg of combed sisal fibres were immersed in forty (40) litres of 0.06M NaOH solution in a plastic tank and maintained at room temperature for a period of 48 hrs. From equation 3.15, mercerisation took place at an ionic concentration of 9.603542547 x 10^{21} Na^+/Kg of sisal fibre. The fibres were then removed from the NaOH solution, rinsed thoroughly in the 0.01M glacial acetic acid solution (CH_3COOH) to neutralise any residual NaOH and then rinsed several times using tap water. They were then air-dried in the laboratory for five days. The purpose of this treatment was to reduce the percentage of lignin and hemicellulose present in the fibre, increase the fibre tensile strength and roughen the fibre surface. This allows for better bonding at the fibre matrix interface in the composites. The mercerised fibres were then combed to disentangle any knots and then cut into 500mm, 400mm, 300 mm and 30mm lengths to be used as OPC mortar and polyester resin composite reinforcements. Figure 3.1 shows mercerisation being carried out on sisal fibres.

Figure 3.1: Image showing sisal fibres mercerising in a 0.06M NaOH solution.

3.1.1.3 Cornification

The procedure employed in this study was based on one performed by Claramunt *et al.* [177] and more recently by Ballesteros *et al.* [39]. Combed sisal fibres were immersed in tap water at room temperature (20°C) for 12 hrs. The fibres were then removed from the water and put in an electric oven with the temperature set at 100 °C. The oven was programmed to heat at a heating rate of 1°C/min and to maintain the maximum temperature (100°C) for 6 hrs. The oven was then switched off, and the fibres cooled to room temperature in the oven (to prevent thermal shock.) The procedure was repeated six times. The fibres were then cut into 500mm, 400mm, 300 mm and 30mm lengths to be used as OPC mortar and polyester resin composite

reinforcements. Figure 3.2 (a) shows sisal fibre cornification in a Daihan FX programmable scientific furnace and (b) Cornified sisal fibres.

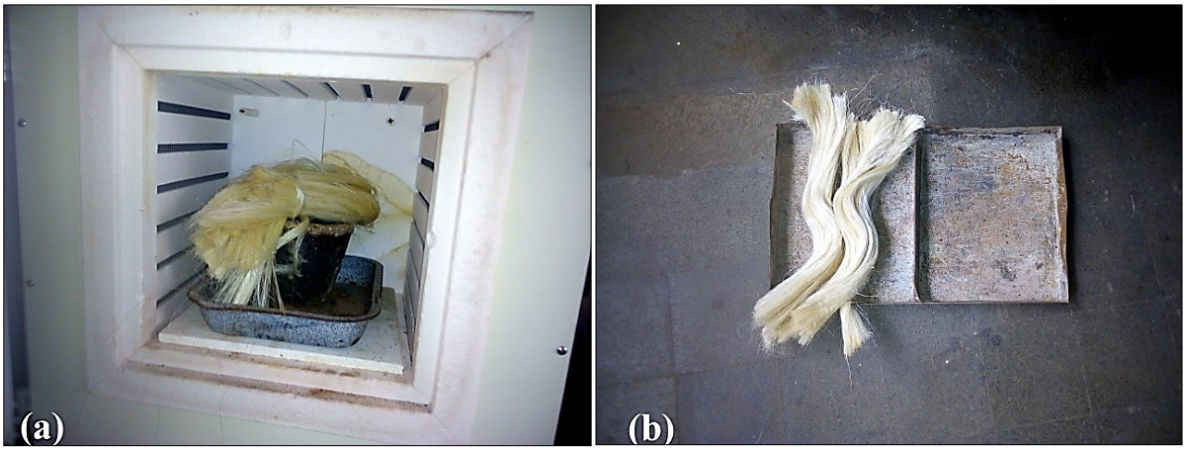

Figure 3. 2: Image showing (a) sisal fibres cornifying in an electric oven (b) combed cornified sisal fibres ready for use as fibre reinforcement.

3.1.1.4 Fibre Morphology

Vickers hardness testing machines are generally fitted with a high-magnification optical microscope. This microscope is powerful enough to observe the various phases and grain boundaries in metal alloys. Optical microscopy to determine untreated and surface-modified sisal fibres was carried out by observing the fibres under a Vickers machine optical microscope. The accuracy of the equipment was set to 0.01 μm. Figure 3.3 shows the optical microscope used in the current study at the materials laboratory, the Mechanical Engineering Building, UoN.

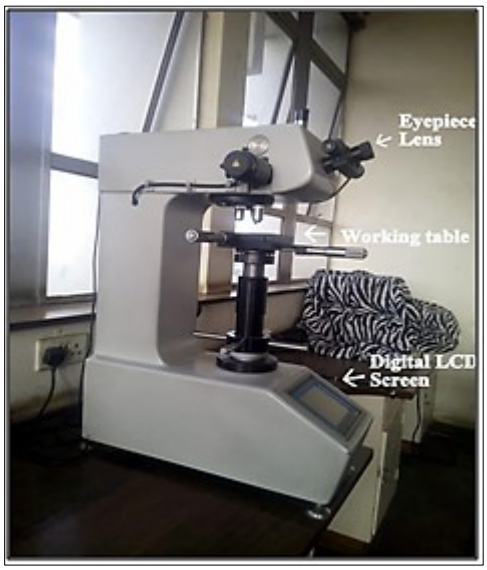

Figure 3.3: Image showing Vickers hardness testing machine at the Materials Laboratory, UoN, used in this research

3.1.1.5 Fibre Absorbency

Moisture absorption test was done in accordance with C 948-81 standard method for dry and wet bulk density, absorption and apparent porosity of thin glass fibre composites [211]. Three (3) samples each weighing 50 grams of untreated, mercerised and cornified sisal fibres were dried in an oven at 60°C for 6hrs. The dry samples weight was then recorded, and the samples then were soaked in clean tap water for 48hrs. Finally, the samples were pat dried using a cotton towel, reweighed and then oven-dried at 60°C with weighing every 1hr until they attained constant weight. In between weighing, the fibres were kept in desiccators to prevent re-absorption of atmospheric moisture. Figure 3.4 is an image showing sisal fibre absorbency test specimens in (a) convection oven and (b) desiccator jar before weighing.

The equation used to determine the moisture absorption of the fibres was as follows:

$$\%\ Moisture = \frac{Wet\ fibre\ Mass - Final\ Oven\ Dry\ Mass}{Final\ Oven\ Dry\ Mass} x100\% \quad \text{.....(3. 4)}$$

Figure 3.4: Image showing absorbency specimens in (a) convection oven and (b) desiccator jar before weighing.

3.1.1.6 Fibre Diameter

The sisal fibre diameter (in μm) was determined by observing and measuring individual fibre strand diameters using the Vickers Hardness Testing Machine at the Materials Laboratory, the Mechanical Engineering Building, UoN. A randomly selected single fibre strand was put under the Vickers microscope and brought to focus. The diagonals were then aligned with the left side of the fibre strand by turning the adjustment knob in the appropriate direction. Once the diagonals were both aligned (and joined), the machine was reset to zero, and the mobile diagonal moved to the right side of the fibre by turning the adjustment knob. The fibre diameter, in micrometres, was then read off the screen. Only the butt-end and mid-span sisal fibre diameters were measured since these were the only portions used in this research.

The mean sisal fibre diameter was then determined by modelling the diameters as a Weibull Cumulative Density function (CDF). Detailed calculations, including Ms Excel® (2003) commands, are presented in Appendix A, Table A3. Inacio *et al.* [212] have demonstrated that

the Weibull CDF is an accurate tool for analysing sisal fibre tensile strength dependence on fibre diameter. The Weibull distribution model adopted in the current research follows one done by Poudel and Cao [213] in their 2013 evaluation of methods to predict Weibull parameters for characterising diameter distributions. The following Weibull CDF expressions were used:

$$Mean\ diameter = D_o\Gamma\left(1 + {}^{1}/_{m}\right) \quad \text{(3. 5)}$$

$$Standard\ error = \frac{\sqrt[2]{\left(D_0{}^{2}\left[\Gamma\left(1+{}^{2}/_{m}\right)-\Gamma^{2}\left(1+{}^{1}/_{m}\right)\right]\right)}}{\sqrt[2]{n}} \quad \text{(3. 6)}$$

where:

D_o - Reference diameter (scale parameter)

Γ - Gamma function, defined as $\Gamma_{(n)} = \int_0^\infty (x^{n-1}e^{-x})dx$

m - Weibull Modulus (shape parameter)

n - Number of samples

3.1.1.7 Fibre Density

In light of sisal fibres hygroscopic nature, conventional methods of determining fibre density could not work. A modified version of the linear density and diameter calculation method employed by Soykeabkaew *et al.* [214] to determine the densities of jute and flax fibres was used. This method was employed on the basis of its simplicity and its reputation of giving accurate results in the determination of high density natural fibres such as sisal fibres. Individual fibre strands of length 100 mm were randomly picked from the butt and middle portions of the untreated sisal fibres. The fibres were then grouped into bunches consisting of 100, 120, 150 and 200 fibre strands and the fibre bunches dried in a convection oven at 60°C

for 1 hour. The fibre bunches were then removed from the oven and then weighed on an electronic scale. The densities were determined from the fibre bunch mass and total fibre volume determined using the 100 mm length and average fibre diameter determined in section **3.1.1.6.**

3.1.1.8 Fibre Tensile Test

The fibre tensile test was done on a Hounsfield Tensometer (type W) at the Timber Laboratory, Department of Civil and Construction engineering, UoN. The machine is equipped with self -aligning wedge type jaws that automatically increased grip pressure with increasing tensile force. The magnification was set at x8. Fibre samples were picked randomly and separately from each batch of fibres (untreated, mercerised and cornified batches.) This was done in a manner that made the samples representative of their respective fibre batches. From these samples, test pieces between 150 - 200 mm long were cut from the butt-end and mid-portion of the fibres. Further random samples were then picked from these cut pieces and grouped into bunches of 15, 20, 30, 40, 60, 90, 120 and 180 fibre strands. This fibre bunching method has been successfully utilized by several researchers in determining the strength properties of ligno-cellulosic fibres [34, 215]. The fibres were tested in bunches comprising of randomly selected individual fibre strands to counter the inverse proportionality relationship between fibre diameter and strength reported by Denise *et al.* [216] in their Weibull analysis of the tensile strength of Piassava fibres. The Young's Modulus of natural fibres has also been shown by Jouannot-Chesney *et al.* [217] to have an inverse relationship with the fibre diameter. Monteiro *et al.* [218] research into high strength natural fibres corroborates Denise *et al.*'s [216] findings and shows that indeed, sisal fibres of diameters less than 50 μm are the strongest sisal fibres in a bunch.

The respective fibre bunches were then glued at the extremities onto emery paper using wood glue and the glue allowed to cure for 24 hrs.

The fibre bunches were then each tested in tension on the Hounsfield Tensile Testing Machine at a constant crosshead speed of 3.75 mm min^{-1} as shown in Figure 3.8 under normal atmospheric conditions (20°C and 60% relative humidity, RH) and Load-extension curves plotted. All tensile tests were carried out in the morning hours between 7.00 am and 10.00 am when temperatures were 20°C - 23°C following Chand and Hashmi's [219] findings that sisal fibre strain increased with increasing temperature. Figure 3.5 is an image showing (a) A 30 fibre strand tensile test in progress on a Hounsfield tensile testing machine at the Timber Laboratory, UoN. (b) Specimen after failure.

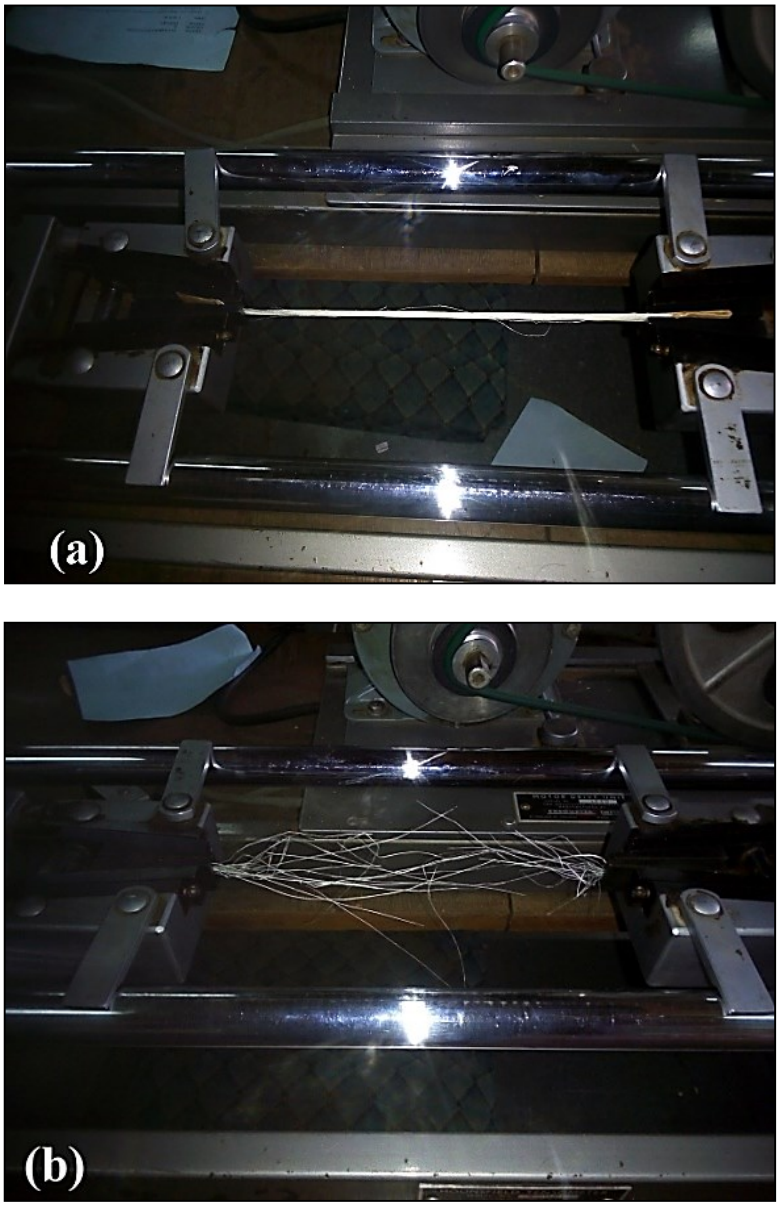

Figure 3.5: Image showing (a) A 30 fibre strand tensile test in progress on a Hounsfield tensile testing machine at the Timber Laboratory, UoN. (b) Specimen after failure

The actual change in length (Δl) of the specimen was calculated following the machine manufacturer's manual [220] and FCE 245 – Materials Science for Civil Engineers Laboratory Procedure [221]. From the manufacturer's data, it is ascertained that the machine extension is proportional to the load. A machine deformation characteristic straight line (at the same load and crosshead speed as the specimen) was generated and superimposed onto the

specimen's load-displacement curve which then formed the datum line for extension measurements. This effectively subtracted the machine deformation from the total deformation recorded on the graphical extensometer.

Engineering 'stress-strain' curves were then generated from the load-displacement graphs by simply multiplying the ordinate scale by $1/A_o$ and the abscissa by $1/l_o$ where $'A_o'$ and $'l_o'$ are the specimen's original cross-sectional area and gauge length respectively. This operation effectively transformed the load-displacement '*domain'* into a stress-strain *'range'* where *every* point within the load displacement graph was mapped into a corresponding stress-strain point through the following mathematical operation:

$$(\Delta l \quad P)\begin{bmatrix} 1/l_o & 0 \\ 0 & 1/A_o \end{bmatrix} = (\varepsilon \quad \sigma) \qquad \textit{(3. 7)}$$

where:

Δl – specimen deformation

P – load

l_o – specimen gauge length

A_o – original cross sectional area (given by $\left(n\pi \, d_f^2/4\right)$ where *'n'* is the number of fibre strands)

ε – engineering strain

σ – engineering stress

The engineering fracture stress and engineering fracture strain were then read-out and recorded from the stress-strain curves (remembering to measure the strain using the characteristic machine deformation line as datum and taking into consideration the machine magnification when recording the strain). The Young's Modulus of the fibres was then

calculated from the engineering stress and engineering strain by determining the gradient of the stress-strain curve (within the elastic range) using the formula:

$$E_s = \frac{\Delta\sigma}{\Delta\varepsilon} = \frac{\sigma_2 - \sigma_1}{\varepsilon_2 - \varepsilon_1} \quad \text{(3. 8)}$$

Finally, the fibre fracture stress was modelled as a Weibull CDF as done by Masudur *et al.* [222] in their 2015 work on the tensile and statistical analysis of sisal fibres. Tabulated results of the analysis done in the present work, including Ms Excel® (2003) commands, are presented in Appendix A, Table A8.

The Weibull Modulus of the fibres fracture stress was determined using the two-parameter Weibull CDF:

$$F = 1 - exp\left[-\left(\frac{\sigma_{fr}}{\sigma_0}\right)^m\right] \quad \text{(3. 9)}$$

where:

F - Cumulative probability of failure as a function of fibre fracture stress

σ_{fr} - Fibre fracture stress

σ_0 - Reference stress (scale parameter)

m - Weibull Modulus

The value of the probability index *F*, in equation 3.9 was calculated as recommended by Lingyan *et al.* [223] in their 2003 statistical work on optimal probability estimators for determining Weibull parameters when the number of samples, *n>20*. The formula used was:

$$F_i = \frac{i - 0.5}{n} \quad \text{(3. 10)}$$

where n is the number of samples tested, and F_i is the cumulative probability of failure for the i[th] ranked stress data. In some literature, F_i is referred to as 'the average value of the empirical density function before and after the jump at σ_i' [224].

The mean fibre fracture and standard error was then computed from the two-parameter Weibull distribution model using the equations:

$$\mu = \sigma_0 \Gamma\left(1 + {}^{1}/_{m}\right) \quad \text{(3. 11)}$$

$$Standard\ error = \frac{\sqrt[2]{\left(\sigma_0{}^2\left[\Gamma\left(1+{}^{2}/_{m}\right) - \Gamma^2\left(1+{}^{1}/_{m}\right)\right]\right)}}{\sqrt[2]{n}} \quad \text{(3. 12)}$$

where:

μ - Mean fibre fracture stress

σ_0 - Reference stress (scale parameter)

Γ - Gamma function, defined as $\Gamma_{(n)} = \int_0^\infty (x^{n-1}e^{-x})dx$

m - Weibull Modulus (shape parameter)

n - Number of samples

3.1.2 Experimental Procedure II - Mortar Composites

3.1.2.1 Preparation of Sisal Fibre Specimens for Mortar Reinforcement

Fibre samples were picked randomly and separately from each batch of fibres (untreated, mercerised and cornified batches.) This was done in a manner that made the samples representative of their respective fibre batches. Known weights of fibres from these different batches were then chopped into predetermined lengths (30 mm, 400 mm and 500 mm) and stored in airtight polyethene paper bags marked with the batch they were picked from (untreated, mercerised or cornified) and their respective weights clearly labelled on the packaging.

3.1.2.2 Preparation of Wooden Moulds for Mortar Composite Specimen

Figure 3.9 shows the OPC mortar composite mould design made at the Timber Laboratory, Department of Civil and Construction Engineering, UoN. They were made using 1-inch-thick Plywood and fastened together using self-tapping wood screws. Figures 3.6 – 3.7 shows the design drawings for the mortar composite flexural and tensile test specimens respectively.

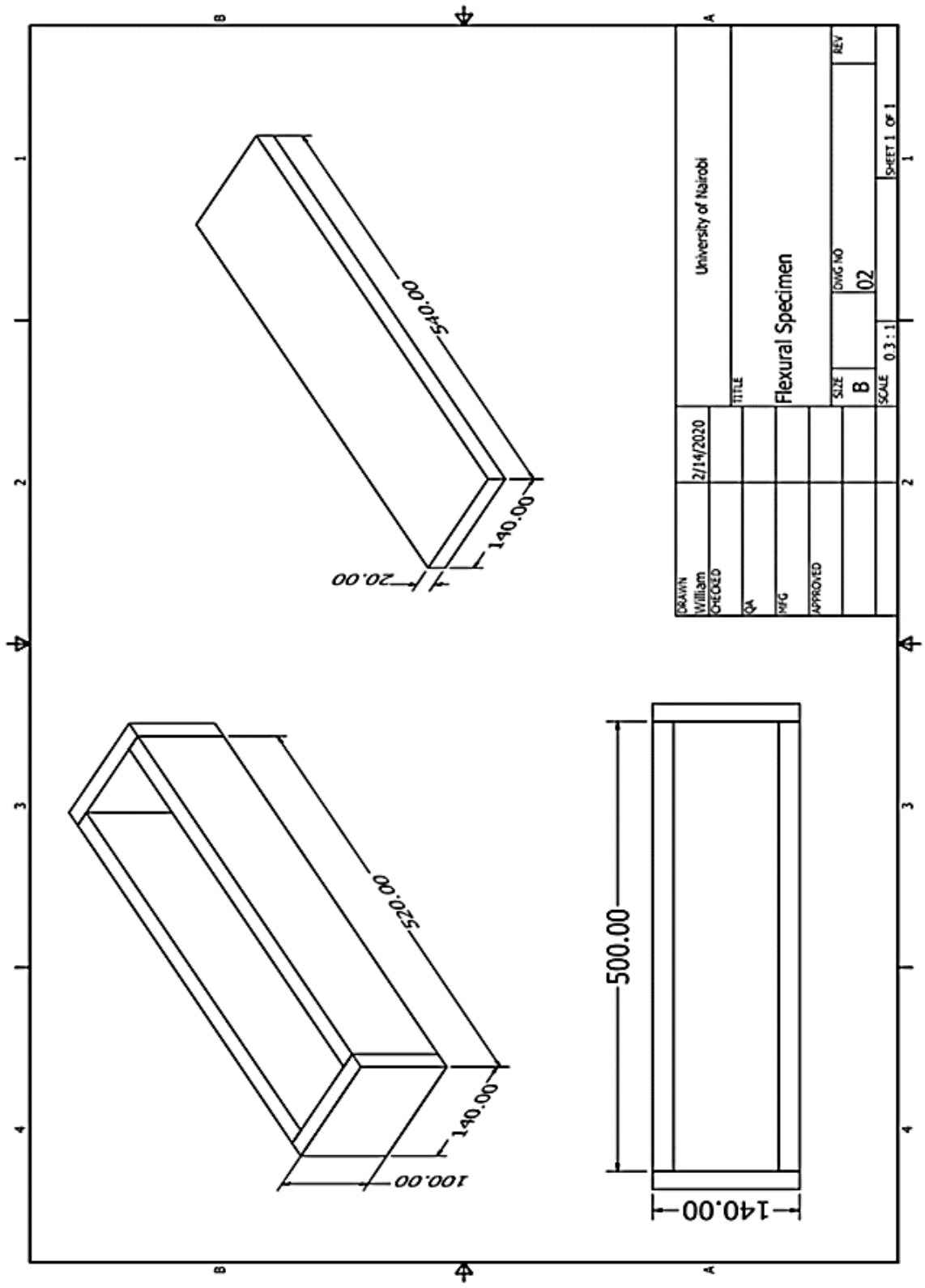

Figure 3.6: Wooden mould design for mortar flexural specimen (dimensions in mm)

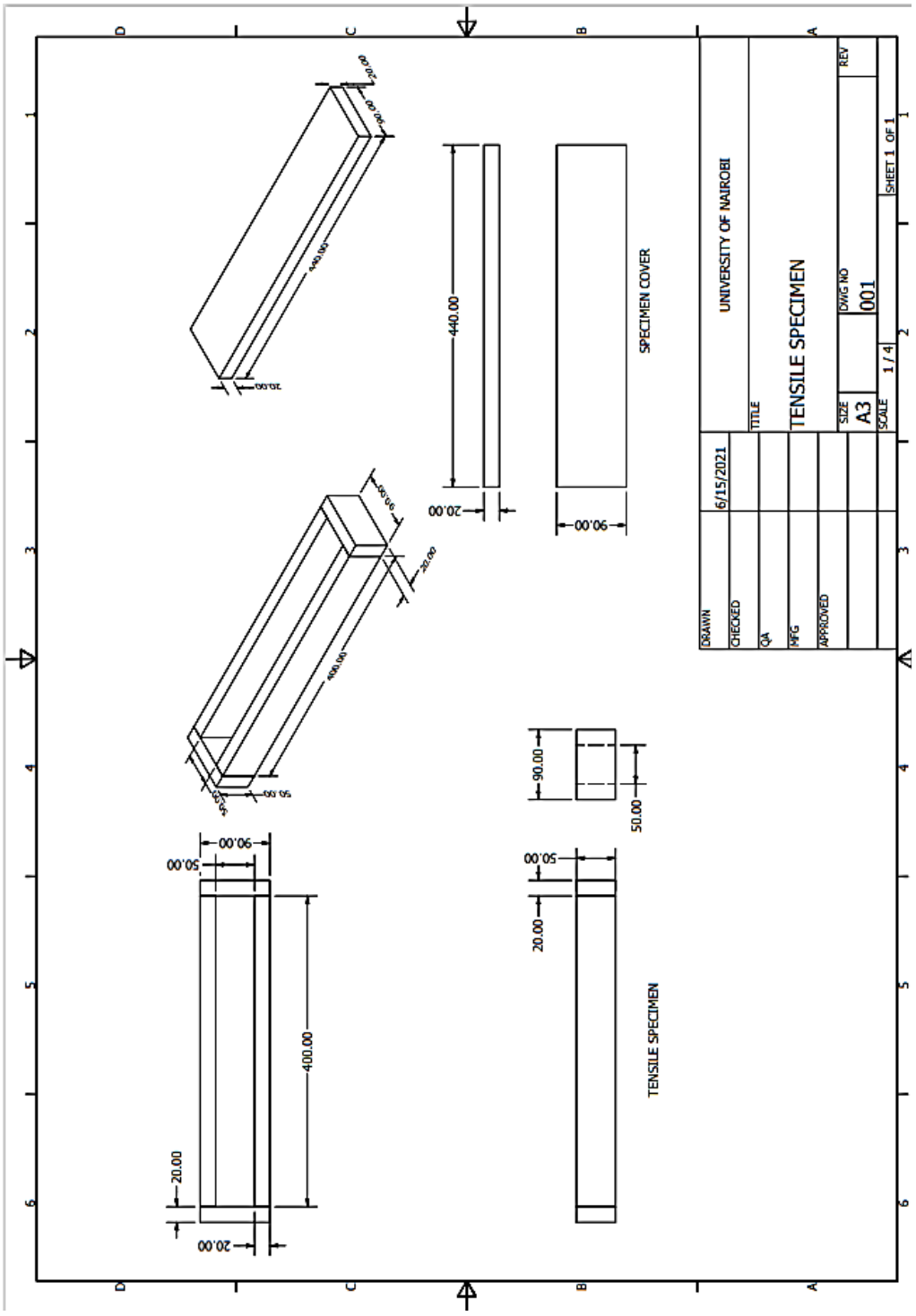

Figure 3.7: Wooden mould design for mortar tensile specimen (dimensions in mm)

3.1.2.3 Sand Particle Size Distribution

The sand was graded in accordance with BS882:1992 specification for aggregates from natural sources for concrete [225]. First, a sample of sand in a tray was dried in an oven at 105°C for 24 hrs. The dried sand's weight was recorded. The sand was then washed over a 75µm sieve (BS No. 200) and oven-dried yet again in an oven at 105°C for a further 24 hrs. The dried sand weight after washing and drying was recorded. The sand was then dry sieved through 10 mm, 5 mm, 2.36 mm, 1.18 mm, 600 µm, 300 µm and150 µm sieves with the recording of the weight retained on each sieve. A graph of the cumulative percentage retained by each sieve against sieve size was plotted. The graph was then used to grade the standard by comparing it against the acceptance criteria as stipulated by the standard. In this research, before being used in the preparation of OPC mortar, the sand was always dry sieved through a 5 mm sieve to remove any coarse aggregate.

3.1.2.4 Mortar Specimens

3.1.2.4.1 Unreinforced OPC Mortar Specimens

Bending beams (100 mm x 100 mm x 500 mm) and tensile specimens (50mm x 50mm x 400mm) were prepared at the Concrete Laboratory, Department of Civil and Construction Engineering, UoN. Used engine oil was smeared on the mould surface to prevent the sample from adhering to the mould. OPC mortar with water, sand cement ratio of 1:2:5 (*w/c* 0.5) as used by HABRI in the making of fibre-reinforced OPC roofing tiles was prepared in a mechanical mortar mixer, with speed set at 60 rpm and poured into the well-oiled mould. (Tensile test specimens mortar was made using 32.5 Bamburi pozzolanic cement using the same ratios). The mould was then vibrated for 3 minutes for proper compaction and then covered with a moist hessian cloth for 24 hrs. It was then demoulded, labelled and the specimen submerged in a curing tank for 28 days.

The tensile strength, flexural strength, void volume fraction and density of the composite were then calculated. Figure 3.8 is an image of the moulds used to cast the sisal fibre-reinforced mortar specimens.

Figure 3.8: Image showing well-oiled flexural specimen wooden moulds at the Concrete Laboratory, Mechanical Engineering building, UoN

3.1.2.4.2 Uniaxially Oriented Sisal Fibre-reinforced OPC Mortar Specimens

Bending beams of dimensions 100 mm x 100 mm x 500 mm were used for the flexural test while beams of dimensions 50mm x 50mm x 400mm were used in the tensile test to determine the tensile and interfacial bond strength. Used engine oil was smeared on the mould surface to prevent the sample from adhering to the mould. The hand lay-up technique was employed, and a constant fibre aspect ratio (*l/d*) of 2149 and 1719 was maintained for all the flexural and tensile specimens respectively. OPC mortar with water, sand cement ratio of 1:2:5 (*w/c* 0.5) (used by HABRI in the making of fibre-reinforced OPC roofing tiles) was then prepared in a mechanical mortar mixer with speed set at 60 rpm. The mortar was then spread on the mould base followed by a layer of uniaxially oriented fibres from a pre-weighed fibre

bundle of untreated, mercerised and cornified sisal fibres. A layer of OPC mortar was then added, followed by more fibre from the same pre-weighed fibre bundle and covered with more OPC mortar. The process was repeated until all the fibres from the pre-weighed bundle had been used. The mould was vibrated for 3 minutes for proper compaction and then covered with a moist hessian cloth for 24 hrs. It was then demoulded, labelled and the specimen submerged in a curing tank for 28 days.

The effect of untreated, mercerised and cornified sisal fibre reinforcement on OPC mortar in uniaxial orientation was then determined in the laboratory. Strength tests were carried out on the cured samples. The results were recorded and modelled as a 4^{th}-degree polynomial regression equation. A polynomial regression curve was then plotted and analysed using Graph [226], open-source computer software under the GNU, General Public License.

The flexural strength, void volume fraction and density of the composite were then calculated.

3.1.2.4.3 Randomly Oriented Sisal Fibre-Reinforced OPC Mortar Specimens

Bending beams of dimensions 100 mm x 100 mm x 500 mm were used for the flexural test. A constant fibre aspect ratio *(l/d)* of 129 was maintained for all specimens. Used engine oil was smeared on the mould surface to prevent the sample from adhering to the mould. A known weight of chopped fibres from a pre-weighed fibre bundle of either untreated or mercerised sisal fibres was added by hand and thoroughly mixed with OPC mortar (water, sand cement ratio of 1:2:5 as used by HABRI) as shown in Figure 3.9 and the mixture placed in the oiled mould. The mould was vibrated for 3 minutes for proper compaction and then covered with a moist hessian cloth for 24 hrs. It was then demoulded, labelled and the specimen submerged in a curing tank for 28 days.

Figure 3.9: Image showing 30 mm chopped sisal fibre mixing with OPC mortar in the cement mixer at the Concrete Laboratory, UoN.

The effect of untreated and mercerised sisal fibre reinforcement on OPC mortar in random orientation was then determined in the laboratory. Strength tests were done on the cured samples. The results were recorded and modelled as a 4^{th}-degree polynomial regression equation. A polynomial regression curve was then plotted and analysed using Graph [226], open-source computer software under the GNU, General Public License.

The composite flexural strength was then calculated.

3.1.2.5 Composite Void Volume Fraction

Water absorption tests were done in accordance with BS 1881 Part 122: 2011 method of determination of water absorption in concrete [227]. Oven-dried sisal fibre-reinforced OPC mortar composites were submerged in tap water (a minimum of 50 mm under the water meniscus) at room temperature (22°C) for 48 hrs. The specimens were then removed from the water, wiped using a cotton towel to remove excess surface water and then weighed. This weight was recorded as the saturated specimen mass W_s. The saturated specimens were then

dried in an electric oven with the temperature set at 100°C for a period of 24hrs. The specimens were then removed from the oven, allowed to cool for a period of 12hrs and then reweighed. This weight was recorded as the specimen dry mass W_d.

The average mass of water absorbed by the specimens at each fibre fraction was then calculated as a percentage using the formula:

$$W_a = \frac{W_s - W_d}{W_d} \, x \, 100\% \quad \text{.....(3. 13)}$$

The percentage void volume was then calculated in accordance with ASTM C642-13 [228] Standard test method for density, absorption and voids in hardened concrete as follows:

$$\%V_v = \rho_c W_a \quad \text{.....(3. 14)}$$

where:

V_v - Percentage void volume

P_c - OPC mortar composite density

The percentage void volume and composite density were calculated as an average of 2 specimens at each fibre volume fraction. Graphs of composite density and percentage void volume against fibre volume fraction were then plotted.

3.1.2.6 Gravimetric Method of Determination of Sand/Cement Ratio in Mortar

This test was carried out in a fume chamber at the Chemistry Laboratory in the Department of Chemistry, the University of Nairobi (Chiromo Campus). Randomly selected, cured and unreinforced mortar specimens were selected for this test. Each specimen was hammered into

rough gravel using a small ball peen hammer and later ground in a mortar and pestle into a fine powder. The following procedure was then carried out:

1. Take 100 grams of the ground mortar.
2. In a beaker, mix concentrated (11 M) Hydrochloric acid (HCL) with H_2O in the ratio of 1:1 and then add the 100 grams of ground mortar.
3. In a fume cupboard, boil the HCl/H_2O/ground mortar mixture while stirring vigorously until there is no further reaction.
4. Let the mixture cool.
5. Add water at room temperature to the now cool HCl/H_2O/ground mortar mixture as you decant the mixture with care being taken not to lose any solid particles. This is done to neutralise the acid and to prevent the mixture from corroding the filter paper in step number 6.
6. Filter with filter paper No. 42
7. Dry in the oven at 105 °C until a constant final weight is obtained.

Since the original sample weight was 100 grams, the final weight is the percentage of sand (fine aggregate) in the mortar.

3.1.2.7 Determination of Moisture Content in Mortar

Randomly selected, cured and unreinforced mortar specimens were selected for this test. Each specimen was hammered into rough gravel using a small ball peen hammer and later ground in a mortar and pestle into a fine powder. The following procedure was then carried out:

1. Take 100 grams of the ground mortar powder.

2. Put it in a crucible and cure it in furnace at 1000 °C for 6 hours (or until a constant weight is achieved)
3. Remove the crucible from the oven, remove the powder, and, store it in a desiccator to prevent moisture reabsorption.
4. Once cooled, weigh the powder and record the final weight.

Since the original sample weight was 100 grams, the difference between the initial sample weight and the final weight was the percentage of absorbed and chemically bound water (and any other volatiles) in the mortar. Figure 3.10 shows crushed mortar specimen drying at 1000°C in a Daihan scientific furnace.

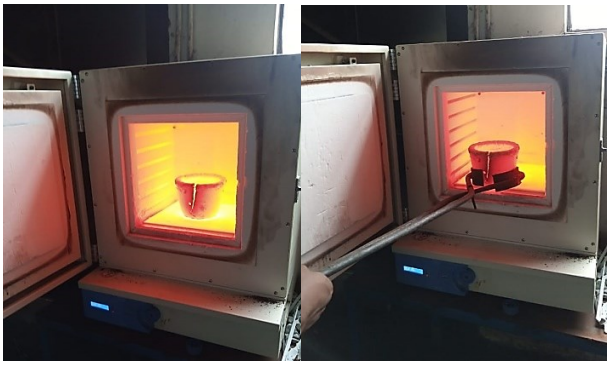

Figure 3.10: Images showing a pulverised mortar specimen in a crucible drying at 1000°C in a scientific furnace at the Mechanical Engineering Laboratory and Workshop, UoN.

3.1.3 Experimental Procedure III - Unsaturated Polyester and Epoxy Resin Composites

3.1.3.1 Preparation of Sisal Fibre Specimens for Polyester Resin Reinforcement

Fibre samples were picked randomly and separately from each batch of fibres (untreated, mercerised and cornified batches.) This was done in a manner that made the samples representative of their respective fibre batches. Known weights of fibres from these different batches were then chopped into a predetermined length (300 mm) and stored in airtight polyethene paper bags marked with the batch they were picked from (untreated, mercerised or cornified) and their respective weights clearly labelled on the packaging.

3.1.3.2 Preparation of Moulds for Polyester Resin Composite Specimen

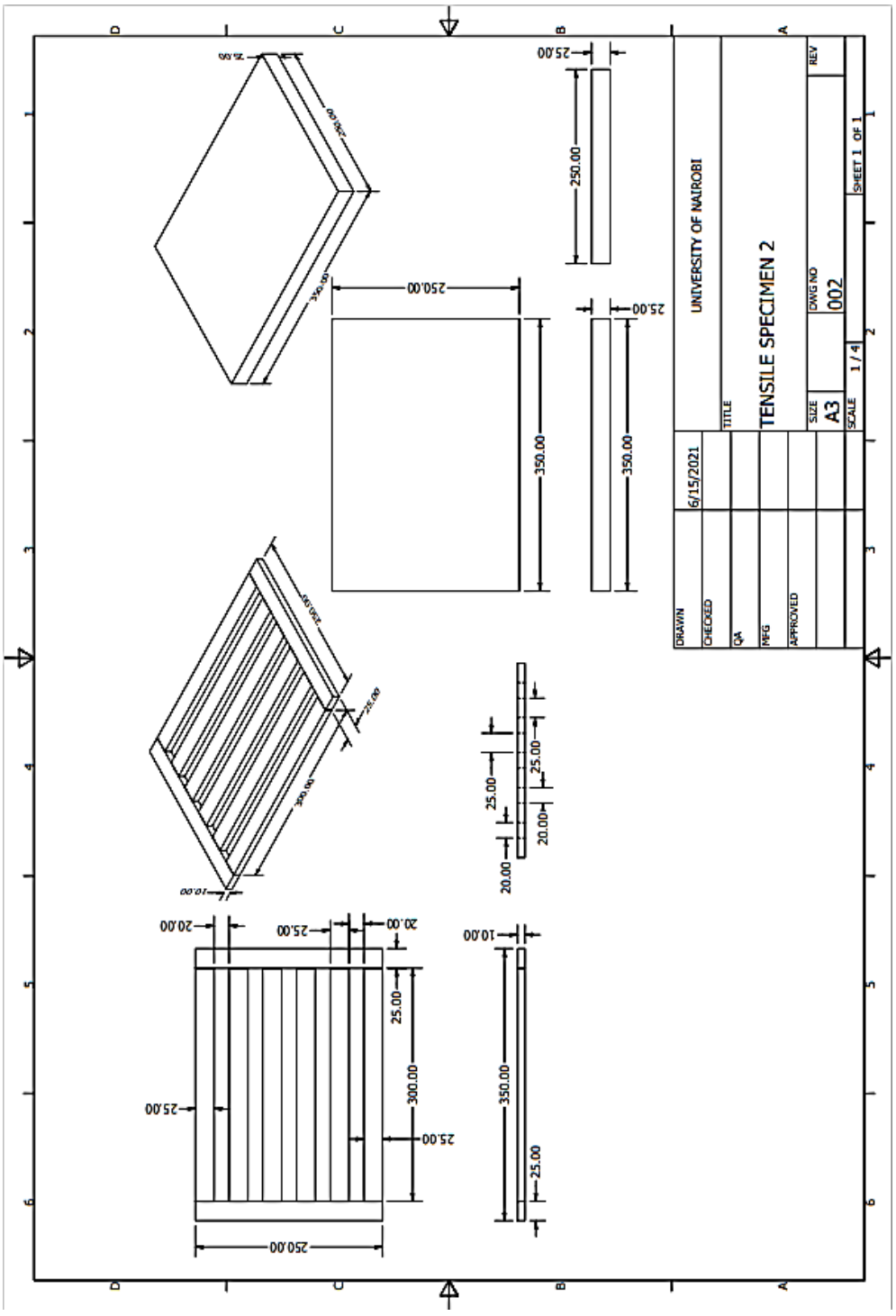

Figure 3.11: Wooden mould for polyester and epoxy resin specimens (dimensions are in mm)

Figure 3.12: Image showing cured polyester resin specimens in mould ready for demoulding

Figure 3.11 shows the resin composite wooden mould design made at the Timber workshop, Department of Civil and Construction engineering, UoN. Figure 3.12 shows cured sisal fibre-reinforced polyester resin specimens ready for demoulding.

3.1.3.3 Polyester and Epoxy Resin Specimens

Henkel E.A supplied the unsaturated polyester resin used in this research (together with 1% *vol* methyl ethyl ketone peroxide initiator.) while the 2:1 clear epoxy resin was supplied by Epoxy Druntech Dev EA construction chemicals. The effect of untreated, mercerised and cornified sisal fibre reinforcement on the polyester and epoxy resin composites in uniaxial orientation was determined in the laboratory. Strength tests were done on the cured samples, and the fracture stress, fracture strain, flexural strength (in the case of polyester resin) and the Secant Modulus (at 100% strain) calculated.

3.1.3.4 Unreinforced Polyester and Epoxy – Resin Specimens

Unreinforced test specimens were prepared by covering the inside of wooden mould with a thin layer of petroleum jelly to prevent sticking. The unsaturated polyester resin was mixed with 1% *vol* methyl ethyl ketone peroxide initiator in a jar, and the mixture then poured into the mould with care being taken not to introduce air bubbles into the matrix. In a similar manner, to prepare the epoxy specimens, the 2:1 clear epoxy resin was mixed following manufacturer's directions and the mixture poured into the mould with care being taken not to introduce air bubbles into the matrix. A blow torch was then used to remove any bubbles that might have formed during the casting process of the specimens. The mould was then covered and left to cure under atmospheric conditions (22 ° C) for 24 hrs before demoulding. Strength tests were done on the cured samples, and the fracture stress, fracture strain, flexural strength (in the case of the polyester resin specimens) and the Secant Modulus (at 100% strain) calculated.

3.1.3.5 Sisal Fibre-Reinforced Polyester and Epoxy – Resin Composites

Chopped sisal fibres of known weight were pre-soaked in polyester and epoxy – resin respectively. The resin mixtures were prepared by: (a) mixing unsaturated polyester resin with 1% *vol* methyl ethyl ketone peroxide initiator, and (b) mixing epoxy resin in the ratio of 2:1 following manufacturer's directions. A thin layer of petroleum jelly was then applied on the inside of a wooden mould to prevent sticking. A small quantity of the resin mixture was poured into the mould followed by laying of chopped sisal fibre from a pre-weighed fibre bundle in uniaxial (one direction) fashion. This was followed by pouring of more resin mixture and further laying of chopped sisal fibre from the same pre-weighed fibre bunch. Care was taken to prevent air bubbles from becoming entrapped in the sisal fibre-resin mixture. The process was repeated until all the pre-weighed fibres were embedded in the matrix. A blow

torch was then used to remove any bubbles that might have formed during the casting process. The mould was covered and left to cure under atmospheric conditions (22°C) for 24 hrs before demoulding. Strength tests were done on the cured samples, and the fracture stress, fracture strain, flexural strength (in the case of polyester resin composite) and the Secant Modulus (at 100% strain) calculated.

3.2 Mechanical Testing

3.2.1 Sisal Fibre-Reinforced Mortar Specimens

3.2.1.1 Tensile Test

Direct application of a tensile load onto a cementitious specimen is difficult for the following reasons:

1) Sliding of the gripping system.
2) Secondary stresses being generated in adjacent zones.

Various direct and indirect methods have been developed to attempt addressing the aforementioned problems such as determining the splitting tensile strength of cylindrical concrete specimens by the application of diametric compressive force on the specimen.

In the current study, the difficulty of conducting a direct tensile test on cementitious specimens was overcome by employing a tensile test rig proposed by Bessel and Mutuli [46] This is shown in Figure 3.13.

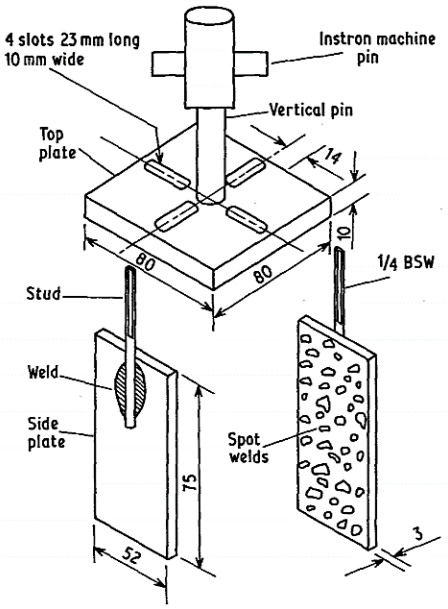

Figure 3.13: Assembly drawing of tensile test rig showing two square side plates [46] (dimensions are in mm)

The rig is designed to grip the four sides of the specimen. The rig comprises of a top-plate with four slots, at 90° to each other with four bolted square plates that form an open box when in place. The faces of the specimen were first brushed using a wire brush to remove loose dust and then KAPCI polyester putty (car-body filler, see Figure 3.14) mixed with dibenzoyl peroxide hardener, following manufactures instructions, applied on to the cleaned specimen surface.

Figure 3.14: Image showing KAPCI polyester putty and dibenzyl peroxide hardener used in the study

This was done on both sides of the specimen. The four square plates were then fastened on the specimen using G-clamps and the polyester putty allowed to cure for 24 hrs before testing. The fastening of the G-clamps was meant to just hold the plates onto the specimens as the polyester putty was curing and binding the plates to the specimen's sides.

The specimen gauge length was first measured using a digital Vernier calliper. The specimen was then loaded onto the universal tensile testing machine and the specimen subjected to a tensile load at a crosshead speed of 1.489 mm min^{-1} (see Figure 3.15 (a)). The ultimate tensile load was then read-out and recorded from the machine's digital read-out. The inter-crack spacing, breadth and depth of the specimen at the point of fracture (first crack) was measured (and recorded) using a digital Vernier calliper (see Figure 3.15 (b)), and, the composite's ultimate tensile stress was then determined and the interfacial bond strength calculated using the Aveston [209] equation (eq. 2.28)

Figure 3.15: Image showing (a)50x50x300mm tensile test specimen with affixed rig during a tensile test (b) Specimen after tensile test displaying MMF and (c) Kerosene blow torch being used to de-bond rig from polyester putty on specimen.

After the test, the rig was removed from the specimen by unscrewing the G-clamps and de-bonding the plates from the polyester putty by heating. For this purpose, a kerosene blow torch as shown in Figure 3.15 (c) was used. The rig's bolted square plates were heated to a temperature of 650°C using the kerosene blow torch and the hot metal plates were then de-bonded from the polyester putty with gentle taps using a 2 Pound ball peen hammer.

3.2.1.2 Flexural Test

In this research, the Modulus of Rupture of sisal fibre-reinforced OPC mortar composites was determined using a three-point bending test. The test was carried out using a bending and transverse testing machine at the concrete laboratory, the Mechanical Engineering Building, at the UoN in accordance with ASTM C 293-02 standard method for flexural strength of concrete [229]. The arrangement consisted of two support rollers of semi-circular cross-section and a single load application roller, as shown in Figure 3.16

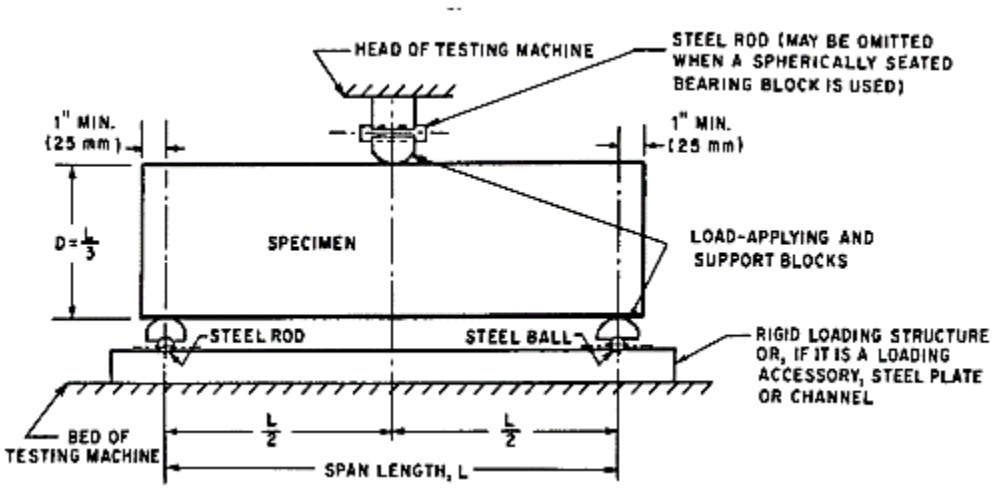

Figure 3.16: ASTM C 293-02 Diagrammatic view of 3-point bending arrangement used in this research [229]

The cured unreinforced and sisal fibre-reinforced OPC mortar composite specimens made as described in section **3.1.2.4** with dimensions 100 mm x 100 mm x 500 mm were tested. The

span length, as per the standard was set to 300 mm with an overhang of 100 mm on either side. The specimens were removed from the curing tank, wiped with a cotton towel and air-dried for 30 minutes prior to testing.

Flexural tests were performed with the specimen at right angles to the support and loading rollers, as shown in Figure 3.17. The machine was manually operated, and the loading rate was approximately 2 mm per minute.

The machine is calibrated in imperial units and equipped with a dial gauge from which the ultimate flexural load (in Lbs) for each specimen was read, converted into metric units and recorded.

Three beams were tested for each volume fraction and the average ultimate flexural load per fibre volume fraction calculated from the three specimens.

Figure 3.17: Image showing 3-point bending test on a fibre-reinforced OPC mortar specimen in progress on a bending and transverse testing machine at the Timber Laboratory, UoN.

The Modulus of Rupture was then calculated from the expression

$$\sigma_b = \frac{3PL}{2bd^2} \quad \text{.....(3. 15)}$$

where:

P - Ultimate flexural load (Newtons)

L - Distance between supporting rollers (span)

b - Specimen breadth

d - Specimen depth

3.2.2 Polyester and Epoxy Resin Specimens

3.2.2.1 Tensile Test

Specimen preparation and tensile tests were carried out in accordance with BS 2782-3 standard methods of testing plastics mechanical properties, tensile strength, elongation and elastic Modulus [230]. Rectangular test pieces measuring 5 mm x 20 mm x 160 mm were cut from the cured unsaturated resin specimens using a band saw. The specimen rectangular geometry was deliberately chosen since the typical dog bone specimen used on flat coupons of isotropic materials is not suitable for laminates [17]. This is due to the fact that, a dog bone-shaped specimen under uniaxial tension with 0° fibre orientation results in formation of matrix cracks, parallel to the fibres, and ultimately, premature failure in the regions highlighted in Figure 3.18

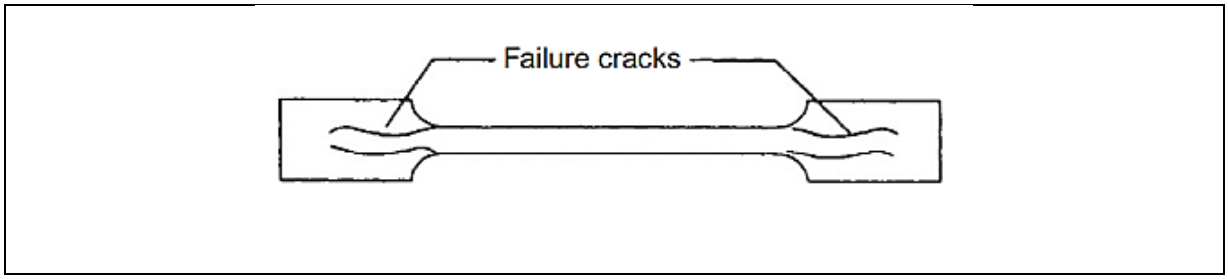

Figure 3.18: Image showing failure mechanism for a dog bone-shaped composite specimen

[17]

The specimens were then tested in tension on a Hounsfield tensometer *(Type W)* at a constant crosshead speed of 3.75 mm min^{-1} under normal atmospheric conditions (20°C and 60% relative humidity, RH) with the major axis in the direction of pull. A gauge length of 110 mm was used for all the specimens tested. Figure 3.19 shows a sisal fibre specimen after failure under a tensile load on a Hounsfield tensometer.

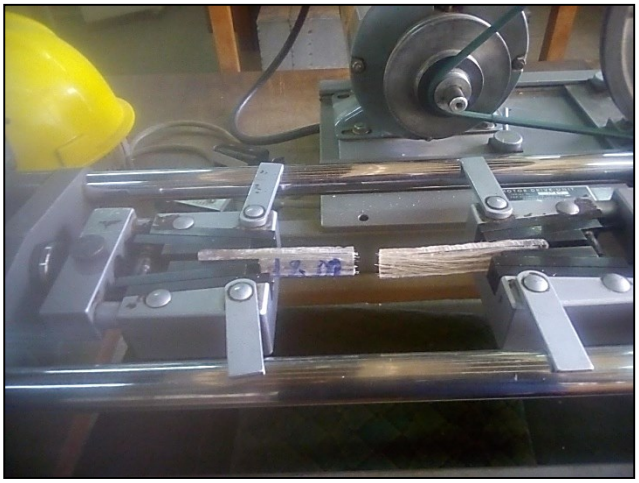

Figure 3.19: Image showing sisal fibre-reinforced polyester resin specimen after failure during a tensile test on a Hounsfield tensometer at the Concrete Laboratory, UoN.

3.2.2.2 Three-Point Bending Test

Specimen preparation and bending tests were carried out in accordance with BS 2782-3 standard methods of testing plastics mechanical properties, tensile strength, elongation and

elastic Modulus [230]. Rectangular test pieces, 20 mm x 8 mm x 300 mm, were demoulded and the specimens were then tested in 3-point bending on a Hounsfield tensometer *(Type W)* at a constant crosshead speed of 3.75 mm min^{-1} under normal atmospheric conditions (20°C and 60% relative humidity, RH). A span of 280 mm was used for all the specimens tested. The Modulus of Rupture was then calculated using equation 3.15. Figure 3.20 is an image showing sisal fibre-reinforced polyester resin composite undergoing a 3-point bending test on a Hounsfield tensometer.

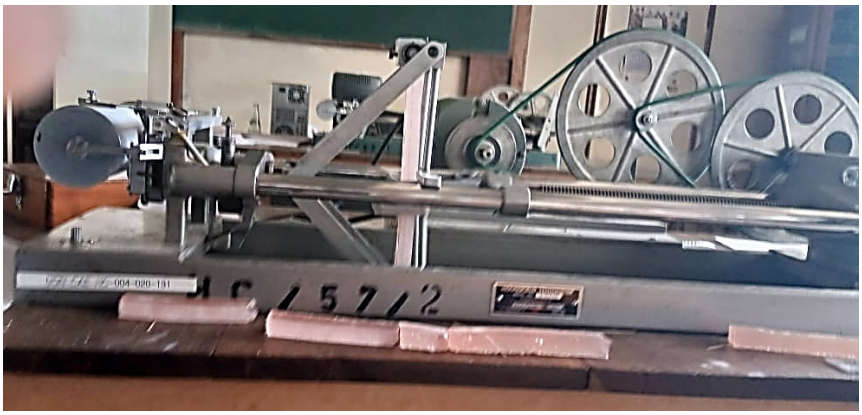

Figure 3.20: Image showing sisal fibre-reinforced polyester resin specimen undergoing a 3-point bending test on a Hounsfield tensometer.

3.3 Data Analysis and Interpretation

After completion of experimental work in the laboratories and workshops, data was collected and entered into Ms Excel® (2003.) Using ANOVA (an analysis tool pack 'add-in' in Ms Excel® (2003),) considerable scatter was observed in some of the captured data. To deal with the scatter, Weibull, a statistical distribution model with broad applicability developed by Swedish engineer, scientist and mathematician Waloddi Weibull [231] and explained in detail by Hertzberg *et al.* [232] in 'Deformation and Fracture Mechanics of Engineering Materials' was used to characterise and analyse the data. The graphical method was employed to determine the value of the shape and scale parameters of the Weibull CDF. Equation 3.9*,* being a power function, was 'linearised' by gathering like terms together and taking the natural logarithm of both sides to yield:

$$\log_e\left(\log_e\left({}^{1}/_{(1-F)}\right)\right) = m\log_e\sigma_f - m\log_e\sigma_0 \ldots\ldots\ldots\ldots\ldots\ldots\ldots\ldots (3.16)$$

The 'linearised' equation was then plotted as a linear regression line, and the gradient *(m)* was equal to the shape parameter while the scale parameter (σ_0) was calculated from the y-intercept.

Data that could be modelled as polynomial regression equations were further analysed using Graph [226], an open-source computer software that is under the GNU, General Public License. The equations were of the form:

$$f_{(x)} = Ax^n + Bx^{n-1} + Cx^{n-2} + Dx^{n-3} + Ex^{n-4} + \cdots \alpha x^{n-n} \ldots\ldots\ldots (3.17)$$

where 'x' is the fibre volume fraction (%V_f), '$f_{(x)}$' is the Modulus of rupture (MOR) in the flexural strength tests and, A, B, C, D…...α are correlation constants.

CHAPTER FOUR

4.0 RESULTS AND DISCUSSION

4.1 Sisal Fibres

The following are the results obtained from **experimental procedure I.**

4.1.1 Sisal Fibre Surface Morphology

Figure 4.1 (a, b & c) shows the results of optical microscopy of surface-modified and untreated sisal fibres under a magnification of x 20.

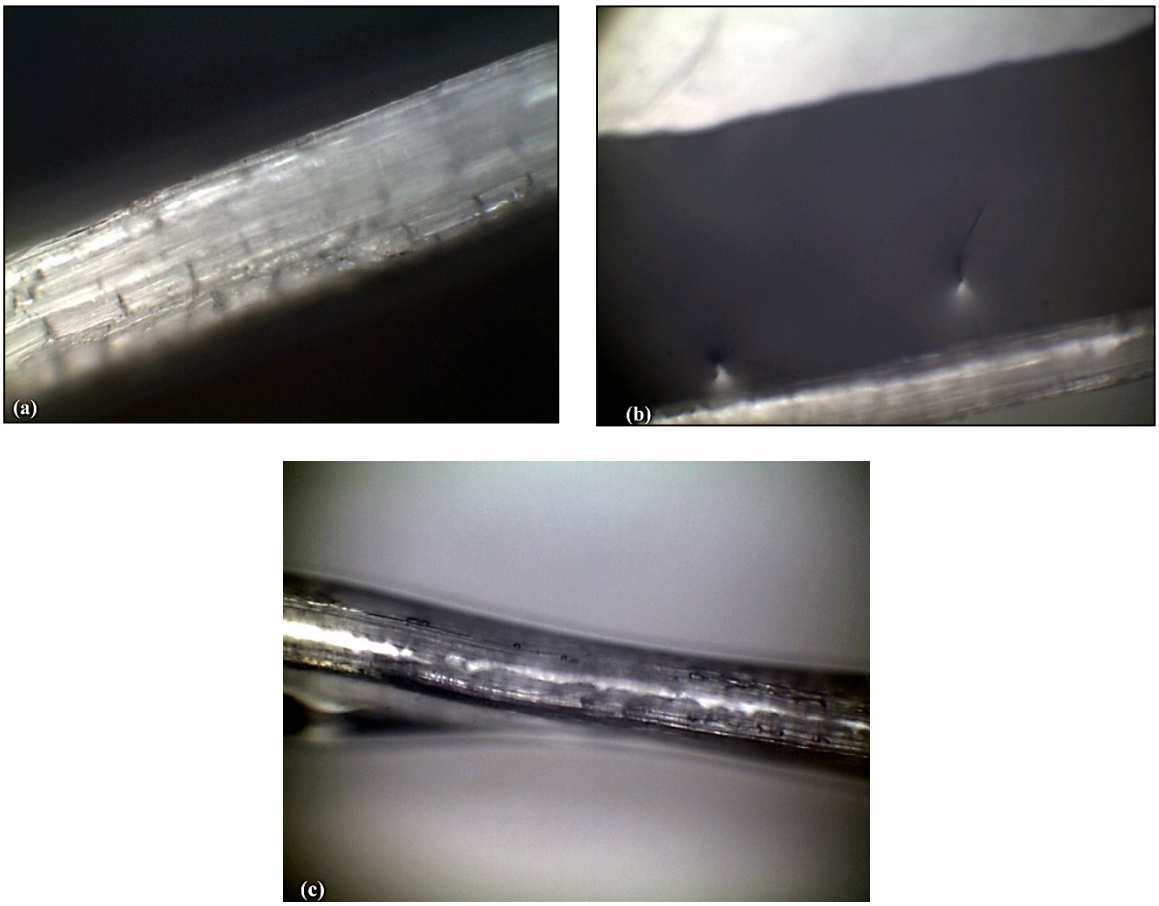

Figure 4.1(a, b & c): Optical microscopy image showing surface-modified and untreated sisal fibres

Figure 4.1 (a) shows a mercerised sisal fibre. As can be seen from the image, the fibre has a roughened surface and protruding fibrillar. The non-reflective nature of the fibre surface is indicative of the absence of the waxy layer on the fibre. The mercerised sisal fibres had protruding fibrillar and a surface devoid of the waxy covering. The removal of wax and other impurities from the fibre surface, according to Ferreira [64] and Wu *et al.* [138], leads to an increased area of contact between the fibre and polymeric matrices.

According to Bassyouni [93] and Merlini *et al.* [164], a dewaxed fibre surface results in better interfacial bonding between the fibre and the matrix. Calado *et al.* [181] investigation into the effect of mercerisation on the structure and morphology of coir fibre also concluded that a mercerised ligno-cellulosic fibre surface provides more interlocking between fibre and matrix. The optical microscopy results shown in Figure 4.1 (a) corroborate the findings of these researchers (Bassyouni [93], Wu *et al.* [138] and Calado *et al.* [181]).

Figure 4.1 (b) shows a cornified sisal fibre. The cornification procedure used in this work was based on one performed by Claramunt *et al.* [177] and by Ballesteros *et al.* [39]. While in his work, Ballesteros advocated the use of 60°C ($\pm$ 5°C), in the current research, a temperature of 100°C was employed. This was because the electric oven that was used in the current work had a minimum temperature setting of 100°C. The fibre surface is darkened as a result of the heating effect during cornification. The fibre surface also has visible cracks. From the image, it can be seen that the high cornification temperature (100°C) resulted in charring of the sisal fibres surface. According to Stevulova *et al.* [186], and Mukhopadyay and Srikanta [110], charring of lignin, hemicellulose and other amorphous ligno-cellulosic fibre constituents occurs at a drying temperature of 150°C, resulting in improved fibre crystallinity. From the findings of this current work, charring seems to have occurred at a drying temperature of

100°C. The fibres were also embrittled, and cracks could be seen on the fibre surface indicating reduced flexibility of the fibres, which according to Ferreira *et al.* [61], is a property that characterises cornified ligno-cellulosic fibres.

Figure 4.1 (c) shows the fibre surface of an untreated sisal fibre strand. The image shows the smooth, waxy sisal fibre surface with the fibre lignin intact and no observable defibrillation. The untreated sisal fibres were observed to have a smooth, waxy surface. It is this waxy surface that Li *et al.* [92] reports as the reason behind the incompatibility observed between ligno-cellulosic fibres and hydrophilic matrices. Peng *et al.* [165] recommend fibre pre-treatment as a possible way of improving the fibre matrix adhesion characteristics, which, in the current study, was accomplished via mercerisation and cornification.

4.1.2 Absorbency

Appendix A (Table A1) shows the absorbency test results for untreated, mercerised and cornified sisal fibres. The Table shows the dry sample mass, the wet sample mass, change in dry mass (with time) and the calculated moisture absorption. Figure 4.2 is a graphical representation of the results.

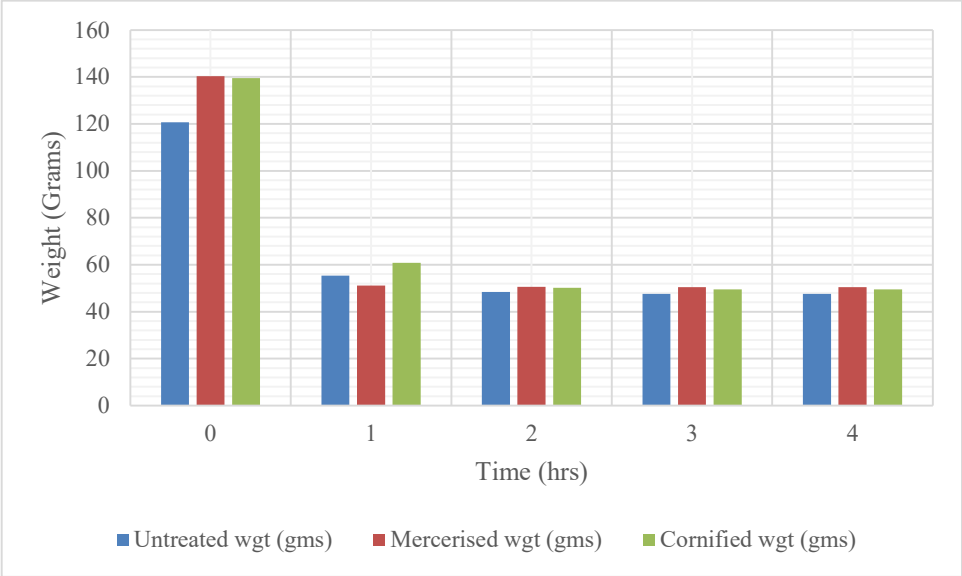

Figure 4.2: Bar graph showing change in mass of untreated, mercerised and cornified sisal fibres with time during drying

Three samples each of untreated, mercerised and cornified sisal were tested for moisture absorption behaviour. In all the samples tested, the final oven-dry mass was found to be lower than the original dry mass of the specimen.

Untreated sisal fibres displayed the lowest moisture absorption value of 172.48% (standard error $\pm$ 0.25 %.) This is much higher than the reported value of 60-70% by Mutuli *et al.* [45]. Ballesteros [39], on the other hand, gave an untreated cellulosic pulp fibre-moisture absorption value of 164% under a 7 hour soaking duration.

In comparison, cornified sisal fibres exhibited the highest moisture absorption value of 182.24% (standard error $\pm$ 0.79 %.) Mercerised sisal fibres had a moisture absorption value of 178.3% (standard error $\pm$ 0.64 %).

Overall, in this research, following surface-modification, an increase in moisture absorption was observed. These results contradict those reported by Ferreira [61] and Ballesteros [39],

where an overall decrease in moisture absorption was observed following fibre surface-modification.

This disparity in moisture absorbency results could be attributed to:

a) Some researchers have not specified the fibre soaking period.
b) Regular tap water was used in this research. Other researchers reported using distilled water
c) In the case of cornified fibres, other researchers cornified the fibres at a temperature of 60°C. In this research, a temperature of 100°C was employed.

According to Favaro *et al.* [65], a high percentage moisture absorption value is an indicator of increased hydrophilicity in natural fibres. This is a desirable trait when using the fibres as reinforcement in cementitious matrices such as cement mortar. In the case of polymeric matrices such as unsaturated polyester resin, this is, however, not a desirable characteristic.

4.1.3 Sisal Fibre Diameter

Appendix A (Table A2) shows the fibre diameter results, measured under room temperature and atmospheric conditions.

The maximum butt-end diameter measured was 396.80 µm and the minimum measured was 196.52 µm. The maximum mid-span diameter measured was 261.20µm, and the minimum was 148.7 µm.

The mean fibre diameter and standard error were computed from the combined butt-end and mid-span data using equations 3.5 and 3.6 and found to be 232.70 µm with a standard error of $\pm$ 8.98 µm. (see Appendix A (Table A3) for Weibull analysis). The mean sisal fibre diameter

calculated in the current study is well within documented sisal fibre diameter values of between 100 - 300 μm [3, 18, 65, 85, 109, 182].

4.1.4 Fibre Density

Appendix A (Table A4) shows the density test results for sisal fibres. The Table shows the number of sisal fibre strands in a bunch, mass of the bunch, measured volume of the bunch, and, the calculated fibre density.

The mean density of UG grade Kenyan sisal fibres was calculated using the linear density and diameter calculation method and found to be1.30 gcm^{-3} (standard error $\pm$ 0.38 gcm^{-3}). This figure is much higher than that reported by Mutuli [91] of 0.70 gcm^{-3}. Other researchers such as Saxena [124], Chand and Jain [200] and Mukherjee and Radhakrishnan [233], give a higher sisal fibre density of 1.45 gcm^{-3}. Idicula *et al.* [81], on the other hand, report a sisal fibre density of 1.41 gcm^{-3}. Rao and Rao [159] have posited that natural fibre density is dependent on plant age, genetics and growth environment. This could explain the different sisal fibre densities reported by various researchers. It is also important to note that only the butt-end and mid-span fibre diameters and densities were measured since these were the only portions of the fibre used in this research.

4.1.5 Fibre Tensile Test

Appendix A (Tables A5, A6 & A7) show the data collected during the tensile testing untreated and surface-modified sisal fibres. The Tables show the results for the ultimate tensile stress, fracture strain and the Young's Modulus at 100% strain for untreated, mercerised and cornified sisal fibres. The test was conducted at room temperature and normal atmospheric conditions.

Significant scatter was observed between test samples, and this is explained by the fact that natural flaws within the fibre structure, and flaws that get introduced during the decortication process, are randomly distributed along the length of the fibre. These flaws act as crack initiation points and fracture prematurely during a tensile test. The failure mechanism of a sisal fibre bundle subjected to a tensile load has been shown to be due to the uncoiling of the microfibrils and tearing of the cell walls [108]. It is because of this failure mechanism that the behaviour of ligno-cellulosic fibres under a tensile load is linear followed by catastrophic failure with no evident plasticity [234].

Apart from variations occasioned by defects along the fibre length, the growth and maturity of ultimate cells as described in section **2.1.2** within the sisal fibre could also account for the scatter in tensile results. Less developed ultimates at the extreme butt-end are bound to give lower fracture stress readings compared to the middle and apex fibre sections where more mature and fully developed ultimate cells are to be found.

It is in light of this scatter that the Weibull graphical analysis method was used to obtain the mean fracture stress of the fibres. Appendix A (Table A8) shows the Weibull analysis data, including Microsoft Excel® (2003) commands that were used to analyse the data.

Table 4.1 presents a summary of results.

Table 4.1: Tensile test results summary for untreated, mercerised and cornified sisal fibres

Fibre	**Mean Fracture Stress (x10^6 Nm^{-2})**	**Mean Fracture Strain (%)**	**Mean Young's Modulus (x10^9 Nm^{-2})**
Untreated Fibres	161.02 $\pm$ 5.46	4.51 $\pm$ 0.18	3.60 $\pm$ 0.10
Mercerised Fibres	271.00 $\pm$ 11.16	5.50 $\pm$ 0.19	5.02 $\pm$ 0.17
Cornified Fibres	196.57 $\pm$ 10.46	5.07 $\pm$ 0.27	4.00 $\pm$ 0.19
Legend: $\pm$ - Standard error			

With untreated sisal fibre as the standard control, cornified sisal fibres showed an increase in mean fracture stress, fracture strain and Young's Modulus of 23.32%, 12.33% and 11.11% respectively.

Similarly, using untreated sisal fibres as standard control, mercerised sisal fibres showed an increase in mean fracture stress, fracture strain and Young's Modulus of 68.30%, 21.99% and 39.44% respectively. These results are markedly higher than those reported by Mokaloba and Batane [60] of a 12.04%, and by Gan˜an *et al.* [182] of an 18.67% increase in sisal fibre fracture stress following mercerisation. Rong *et al.* [152] gives a Young's Modulus value of 4.5 ± 0.30 GN/m^2 for mercerised, acetylated sisal fibres. In the current study, the Young's Modulus for mercerised sisal fibres was calculated to be 5.502 ± 0.17 GN/m^2. The difference in results could either be attributed to the high lignin and hemicellulose content of Kenyan sisal fibres reported by Phologolo *et al.* [118], or to the lower concentration of NaOH (0.06M) used in the current research. Mokaloba and Batane [60] used a 6M NaOH solution, while Gan˜an *et al.* [182] used a 0.5M NaOH solution to mercerise the fibres. Rong *et al.* [152] mercerised the sisal fibres using a 4.5 M NaOH solution. A high NaOH concentration when used in mercerisation of sisal fibres has been shown by Ansell and Mwaikambo [210], to have a negative effect on the mercerised fibre's strength properties. It is from the results of Ansell and Mwaikambo [210] that the optimal NaOH concentration of 0.06 M was used to mercerise sisal fibres in the current study.

Cornified ligno-cellulosic fibres have been observed by Chand and Hashmi [219], to have more ductile phases in their composition compared to untreated fibres. This could explain the increased fracture strain observed in the cornified sisal fibres in the current study.

The Weibull Modulus (shape parameter, *m*) of the untreated sisal fibres was determined from equation 3.16 and found to equal 7.616 ($R^2_{0.98}$). This figure is higher than the 5.521Weibull Modulus reported by Inacio *et al.* [212] (without specifying the source of fibres) and of 2.5 reported by Masudur *et al.* [222] for untreated Brazilian sisal fibres. The results in the current research agree with Phologolo *et al.*'s [118] characterization of Kenyan sisal as having markedly higher lignin and hemicellulose content than sisal from other parts of the world. The wax, lignin and hemicellulose serves as a matrix, sheathing and thus protecting the load-bearing cellulose ultimates from kinks and flaws that get introduced during decortication and general handling of the fibres. It is these kinks and flaws that act as stress concentration points, ultimately leading to fracture of the fibre strand during tensile loading.

Mercerised and cornified fibre Weibull moduli found to equal 6.175 ($R^2_{0.54}$) and 4.723 ($R^2_{0.66}$) respectively. These results are represented graphically in Figure 4.3.

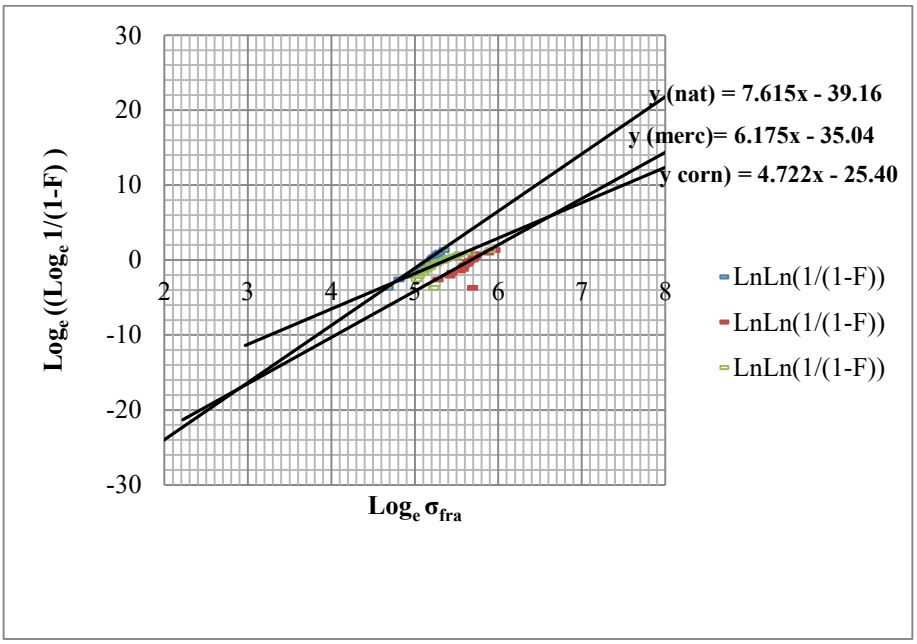

Figure 4.3: Weibull Plot of untreated, mercerised and cornified sisal fibres fracture stress (with plotlines extended for clarity)

The reference stress σ_0 (the stress by which 63.20% of the specimen tested had failed) for untreated, mercerised and cornified sisal fibres was calculated from the linear equations displayed in Figure 4.3 and found to equal 171.14 MN/m^2 ($R^2_{0.98}$), 291.34 MN/m^2 ($R^2_{0.54}$) and 216.82 MN/m^2 ($R^2_{0.66}$) respectively.

These results can be interpreted to mean that despite mercerised fibres having higher reference stress, physical flaws and defects in the fibres are more evenly distributed in the untreated sisal fibres than they are in the mercerised and cornified sisal fibres. By having a higher value of *'m,'* untreated sisal had a lower variability in fracture stress. If we consider stresses higher than the respective reference stresses, untreated sisal fibres failed over a narrower stress range compared to mercerised and cornified fibres. The delignification associated with mercerisation, and the collapse of the fibre lamella structure that accompanies cornification (see Figure 2.10), both seemed to either have exacerbated existing flaws or, introduced new defects into the fibre. According to Chand and Hashmi [219], the introduction of new flaws following thermal treatment of natural fibres is as a result of the change in ratio and proportions of the fibre chemical constituents. During the drying phase of cornification, the fibres lose not only water but also volatiles that form part of the wax and lignin, leaving behind voids. It is these voids that act as stress concentration points during a tensile test and lead to premature failure and a lower Weibull Modulus for cornified sisal fibres. The same can thus be said of mercerisation, which involves chemical removal of the wax and lignin from the fibres. Following the high lignin, wax and hemicellulose characterisation of Kenyan sisal by Phologolo *et al.* [118], the results in the current research are thus in agreement with the findings of Chand and Hashmi [219].

Overall, with untreated sisal fibres as standard control, mercerised sisal fibres displayed the most significant improvement in tensile properties. However, untreated sisal fibres recorded the highest Weibull Modulus.

4.2 Cement Mortar Composites

The following are the results obtained from **experimental procedure II**

4.2.1 Sand Particle Size Distribution

Appendix B (Table B1(d)) shows the tabulated results of the sieve analysis carried out on the river sand used in this research. The sand met the acceptance criteria necessary for civil work in accordance with BS882:1992 specification for aggregates from natural sources for concrete [225]. The cumulative percentage passing through the 150μm sieve exceeded the acceptance criteria by 2.9%, and through the 75μm sieve exceeded the criteria by 6.7%.

Figure 4.4 shows a plot of the cumulative passed particle size (%) against the sieve size in millimetres and the acceptance criteria adopted. The blue and the green lines show the minimum and maximum acceptance criterion, respectively, while the red dotted line shows the results for the river sand used in this research. This results were acceptable as in the current study, the sand was used in comparative experimental work.

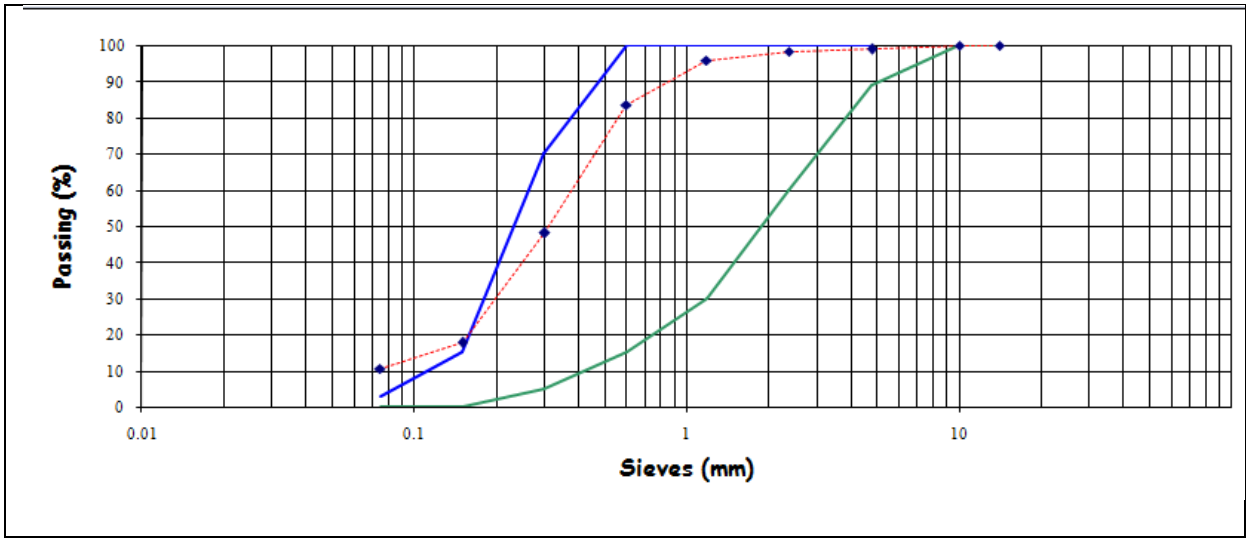

Figure 4.4: River sand sieve analysis grading curve

4.2.2 OPC Mortar Specimens

4.2.2.1 Flexural Rigidity

4.2.2.1.1 Uniaxially Aligned Continuous Fibre-Reinforced Mortar (Untreated Sisal Fibres)

The 3-point bending test results for uniaxially aligned, untreated, mercerised and cornified sisal fibre-reinforced OPC mortar composites are shown in Appendix B (Tables B2, B6 and B10) The Tables show the specimen dimensions, average mass of embedded fibre, fibre volume fraction, maximum applied load for each sample, average applied load and the calculated Flexural strength (Modulus of Rupture). The test was conducted at a constant fibre aspect ratio (l/d) of 2149.

Figure 4.5 is a graph showing the Modulus of Rupture of uniaxially aligned, CFRC of mortar with the fibres in their untreated, mercerised and cornified states.

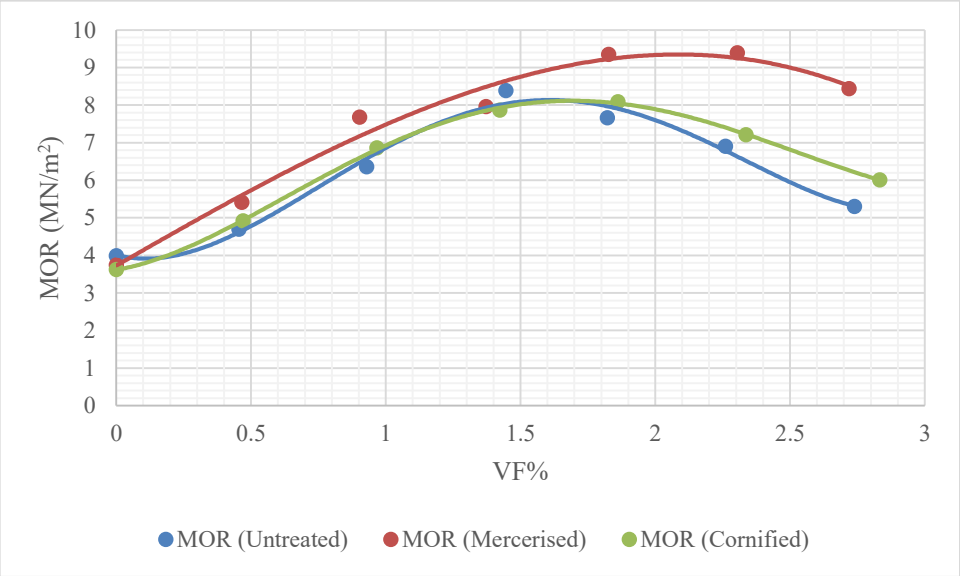

Figure 4.5: Graph showing MOR of uniaxially aligned continuous fibre-reinforced mortar (untreated, mercerised and cornified sisal fibres) against fibre V_f %

The graphs have been superimposed for ease of comparison. A trend of increasing ultimate flexural load with increasing fibre volume fraction was observed in all the specimen groups (untreated, mercerised and cornified sisal fibre–reinforced composites). The increase in flexural strength with increasing fibre V_f % indicates that the fibre length of 500 mm used in this research is greater than the critical fibre length (l_c). According to Seshan *et al.* [235], at this fibre length, there is complete load transfer from the matrix to the reinforcing fibres.

The Modulus of Rupture was calculated using equation (3.15) from the ultimate flexural load recorded and the specimen dimensions. The highest average value of the Modulus of Rupture equal to 9.39 MN/m^2 was recorded from the samples comprising 2.30% V_f mercerised sisal beyond which, the composite flexural strength steadily decreased. This shows a 151.07% increase in flexural strength of the mercerised sisal fibre-reinforced composite compared to the unreinforced (standard control) specimen.

Cornified sisal fibre-reinforced composites on the other hand, had a maximum Modulus of Rupture of 8.09 MN/m^2 at an average fibre volume fraction of 1.86% beyond which, the composite flexural strength steadily decreased. This in turn, represented a 123.48% increase in flexural strength of the untreated fibre-reinforced composite compared to the unreinforced (standard control) specimen.

Untreated sisal fibre-reinforced composites displayed a maximum Modulus of Rupture value of 8.39 MN/m^2 at an average fibre volume fraction of 1.45% beyond which, the composite flexural strength steadily decreased. This represented a 110.28% increase in flexural strength of the untreated fibre-reinforced composite compared to the unreinforced (standard control) specimen.

The analysis of variation (ANOVA), and, polynomial regression equations (to 3 decimal places) for the Modulus of Rupture of untreated, mercerised and cornified sisal fibre-reinforced OPC mortar composites are shown in Appendix B (Tables B3, B7 and B11). The regression equations all had an R^2 value ≥ 0.98 which shows a very good match between the data points and the regression curve.

In the case of the unreinforced (standard control) specimens, a single crack, perpendicular to the neutral axis and parallel to the load application roller characterised the failure mode of all the unreinforced specimens. In contrast, in the case of the fibre-reinforced specimens, at low fibre volume fractions (<3% V_f), a single crack, perpendicular to the neutral axis and parallel to the load application roller, with simultaneous fibre pull-out was observed as shown in Figure 4.6.

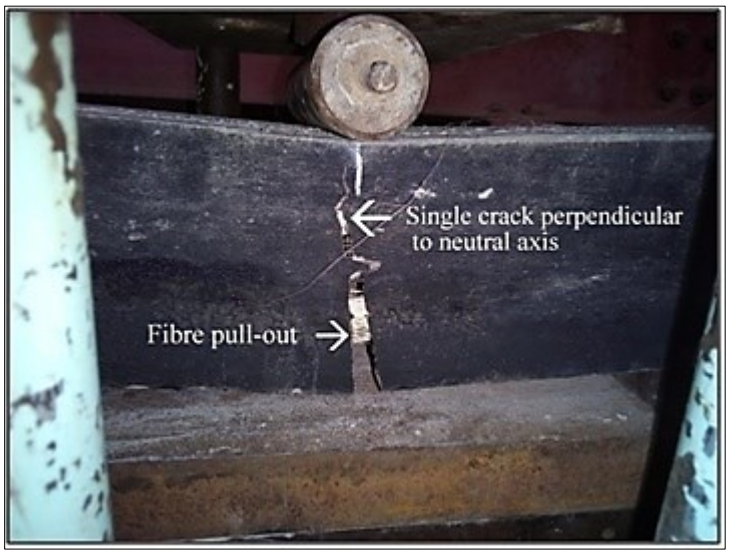

Figure 4.6: A uniaxially aligned, 2% V_f continuous fibre-reinforced mortar specimen showing single crack failure mode and fibre pull-out during a flexural test.

At higher volume fractions (>3% V_f), multiple cracking with one crack perpendicular to the neutral axis and parallel to the load application roller characterised the composite failure mode. Several other cracks formed parallel to the neutral axis, indicative of failure as a result of shear stresses. This is consistent with Swift and Smith's [236] finding that at high fibre volume fractions, the predominant composite failure mode is by shear as shown in Figure 4.7

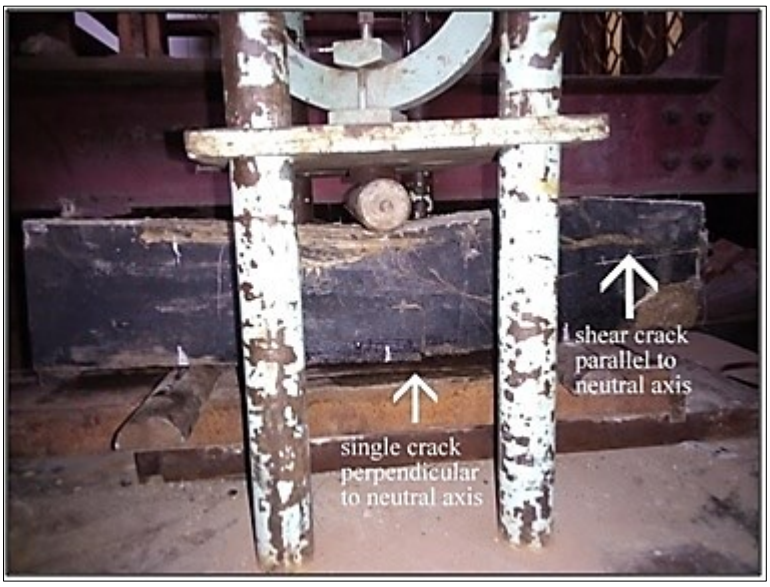

Figure 4.7: A uniaxially aligned, 5% V_f continuous fibre-reinforced mortar specimen showing multiple cracking during a flexural test.

When a specimen is loaded in bending, flexural and shear stresses develop across the beam cross-section. A maximum value of the flexural stress is developed on the outermost surface of the beam while the maximum shear occurs in the middle of the beam cross-section. In the case of high volume fraction reinforcement, the beam seems to behave as a laminate with the shear stresses slicing through the fibre matrix interface leading to the formation of 'shear cracks' parallel to the beam's neutral axis.

The optimal fibre volume fractions reported in the current study are significantly lower than the 4.8% optimal fibre volume fraction of reported by Mutua [48] for continuous uniaxially aligned fibre-reinforced composites. This can be attributed to the fact that in his work, Mutua made use of a concrete matrix. The coarse aggregate within a concrete matrix deflects the fibres effectively 'misaligning' them. In such a scenario, according to Stang *et al.* [198], the efficiency factor is lowered and therefore, a higher fibre volume fraction will be required in a concrete matrix to achieve reinforcement as compared to a mortar matrix.

Beyond a fibre volume of 2% there was a steady reduction in the flexural strength in the untreated and cornified sisal fibre-reinforced composite. Mercerised sisal fibre-reinforced composites exhibited this steady reduction at ≈ 2.4% fibre volume fraction. This reduction can be attributed to:

a) Increased number of voids at high volume fractions due to poor compaction.
b) High water absorption by the sisal fibres at high volume fractions lowering the water/cement ratio in the mortar.

From the results presented in Appendix B (Table B1(c)) of this report, composite void volume fraction was observed to have a directly proportional relation with fibre volume fraction. Composite density was, on the other hand, observed to have a more or less inversely proportional relationship with fibre volume fraction. These results are graphically presented in Figures 4.8 and 4.9.

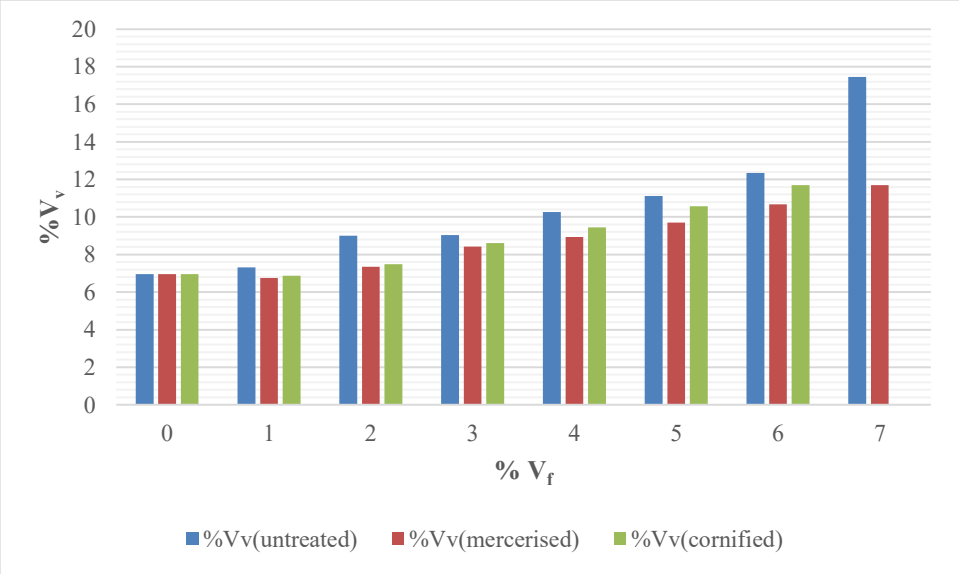

Figure 4.8: Column graph comparing the variation of void volume fraction with the fibre volume fraction of sisal fibre-reinforced mortar.

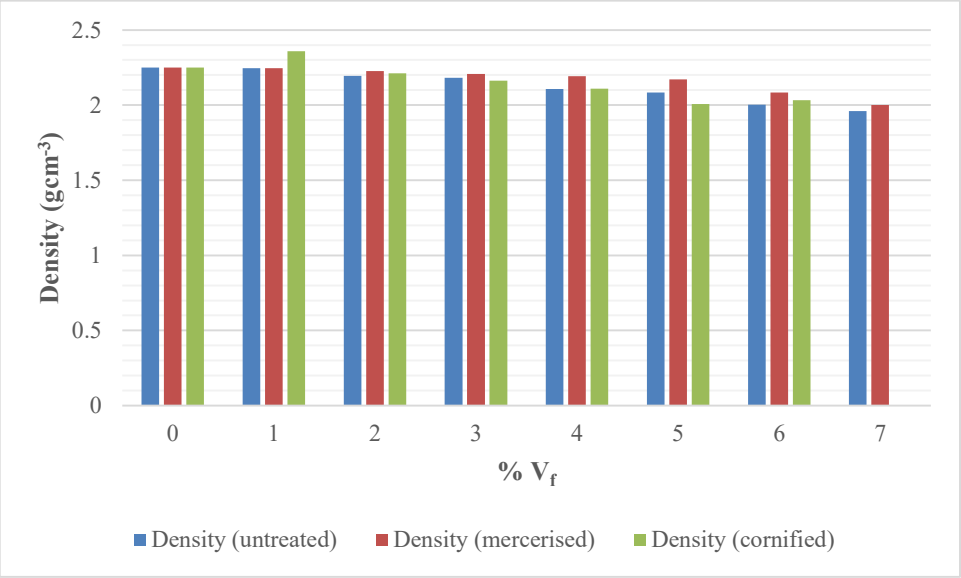

Figure 4.9: Column comparing mortar composite density with the fibre volume fraction of sisal fibre-reinforced mortar

It can be seen from Figures 4.8 and 4.9 that mercerised sisal fibre mortar composites generally had a higher density (and a lower void volume fraction) than untreated and cornified sisal fibre-reinforced composites at the same fibre volume fraction.

It can thus be deduced that alongside possible water absorption by the fibres, the increased number of voids at high fibre volume fractions is partially responsible for the observed decrease in flexural strength of the composite. This explains (in part) why the mercerised sisal fibre-reinforced mortar had a 151.07% increase in flexural strength compared to cornified (123.48%) and untreated (110.28%) sisal fibre-reinforced mortar composites.

4.2.2.1.2 Randomly Oriented Discontinuous Fibre-Reinforced Mortar (Untreated Sisal Fibres)

The 3-point bending test results for discontinuous, randomly aligned, untreated, mercerised and cornified sisal fibre-reinforced OPC mortar composites are shown in Appendix B (Tables B14, B16 and B18) The Tables show the specimen dimensions, average mass of embedded

fibre, fibre volume fraction, maximum applied load for each sample, average applied load and the calculated Flexural strength (Modulus of Rupture). The test was conducted at a constant fibre aspect ratio (*l/d*) of 129. Figure 4.10 is a graph showing the Modulus of Rupture of randomly aligned, DFRC of mortar with the fibres in their untreated, mercerised and cornified states.

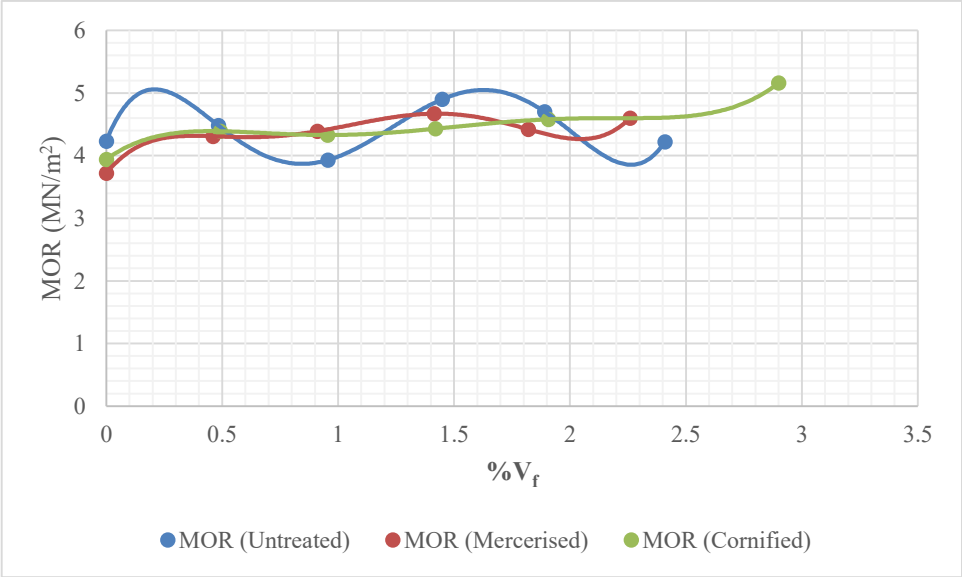

Figure 4.10: Graph showing MOR of randomly aligned, discontinuous fibre-reinforced mortar (untreated, mercerised and cornified sisal fibres) against fibre V_f %

The graphs have been superimposed for ease of comparison. The analysis of variation (ANOVA), and, polynomial regression equations (to 3 decimal places) for the Modulus of Rupture of untreated, mercerised and cornified sisal discontinuous fibre-reinforced OPC mortar composites are shown in Appendix B (Tables B15, B17 and B19). The regression equations all had an R^2 value ≥ 0.98 which shows a very good match between the data points and the regression curve.

A variation in ultimate flexural load with increasing fibre volume fraction was observed in all three specimen groups (untreated, mercerised and cornified sisal fibre-reinforced mortar composites). The Modulus of Rupture was calculated using equation (3.15) from the ultimate flexural load recorded and the specimen dimensions. This MOR also varied randomly from specimen to specimen in all the specimen groups hence the wavy regression line in Figure 4.10.

In the case of the unreinforced (standard control) specimens, a single crack, perpendicular to the specimen neutral axis characterised the standard control specimens' failure mode. Similarly, in the case of the fibre-reinforced specimens, a single crack, perpendicular to the neutral axis was the observed mode of failure. However, the fibre-reinforced specimens failed with fibres pulling out once crack propagation had commenced, and the specimen eventually split into two halves. This observed behaviour is consistent with the results reported by Fujiyama [42], Mutua [48], Mutuli [91] and Kirima [237]. Figure 4.11 is an image showing (a) A single crack with fibre pull-out and (b) fracture surface in a discontinuous fibre-reinforced mortar specimen.

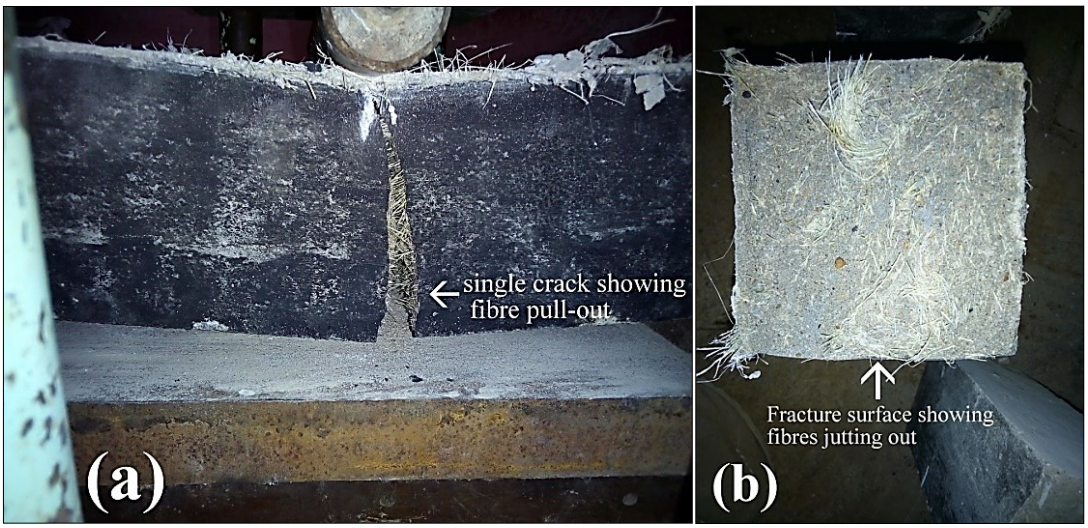

Figure 4.11: Image showing (a) single crack with fibre pull-out and (b) fracture surface with fibres jutting out of a 3% V_f discontinuous, randomly aligned fibre-reinforced mortar

Compared to the continuous uniaxially aligned fibre-reinforced mortar, the improvement in flexural strength for these specimens was markedly reduced. This result agrees well with Stang *et al.* [198] since it is difficult to achieve a high-efficiency factor with chopped, randomly oriented fibres courtesy of their lower aspect ratio. The rule of mixtures predicts this result.

Much can be said about the workability of the randomly oriented fibre-OPC mortar mixture. At fibre volume fractions above 5%, workability was a near-impossible task and during mixing, the fibres balled up in the mixer forming clumps. This phenomenon has also been reported by Mutuli [91], and Ngala [142] in chopped sisal fibre-reinforced cement composites at volume fractions above 6%. From Figure 4.12, the resulting composite specimens can be seen to be having fibre clumps on the surface and increased porosity on the inside. Evidence of this was the bubbling of escaping air when the specimens were initially submerged in the curing tank for the 28-day curing period prior to testing.

Figure 4.12: Image showing fibre clumps on a 7% randomly oriented discontinuous fibre-reinforced mortar surface.

The slight albeit fluctuating improvement in mechanical properties of the randomly oriented fibre-reinforced mortar compared to the uniaxially oriented continuous fibre-reinforced mortar can be partly attributed to this phenomenon. Mutua [48] found no improvement in flexural strength with discontinuous, randomly aligned fibre-reinforced concrete. This could be in part due to the presence of coarse aggregate in the concrete. Other researchers, including Swift and Smith [236], Mutuli [91] and Kirima [237] reported a slight increase in flexural strength of chopped, randomly aligned fibre-reinforced composites. The results presented in the current study for discontinuous, randomly aligned fibre-reinforced mortar are consistent with their findings.

4.2.2.2 Tensile and Interfacial Bond Strength

The results for the tensile and interfacial bond strength for uniaxially aligned continuous sisal-fibre-reinforced mortar are presented in Appendix B (Tables B4, B8 & B12). The Tables show the specimen dimensions, average mass of embedded fibre, fibre volume fraction, mean

crack spacing, maximum applied load for each sample, average applied, the calculated Flexural strength (Modulus of Rupture) and the calculated Interfacial bond strength. The test was conducted at a constant fibre aspect ratio (*l/d*) of 1719.

Figure 4.13 is a graph showing the ultimate tensile stress (UTS) of uniaxially aligned, CFRC of mortar with the fibres in their untreated, mercerised and cornified states.

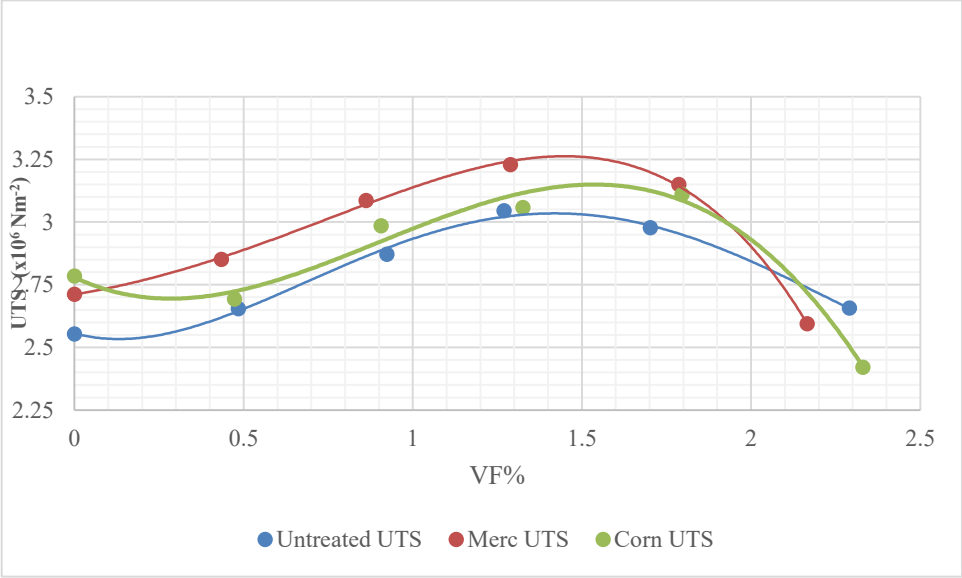

Figure 4.13: Graph showing tensile test results for untreated, mercerised and cornified sisal fibre-reinforced mortar.

In Figure 4.13, the graphs have been superimposed for ease of comparison. A trend of increasing maximum tensile stress with increasing fibre volume fraction was observed in all the specimen groups (untreated, mercerised and cornified sisal fibre –reinforced composites).

The highest value of the maximum tensile stress of 3.23 MN/m^2 at a fibre volume fraction of 1.29% was calculated from the mercerised sisal fibre-reinforced composites. This represented a 19.10% increase in ultimate tensile stress compared to the unreinforced specimens.

Cornified sisal fibre-reinforced mortar on the other hand, had a maximum fracture stress of 3.11 MN/m^2 at a fibre volume fraction of 1.80 % which shows an 11.70% increase in fracture stress compared to the unreinforced specimens. Untreated sisal fibre-reinforced mortar had a maximum UTS value of 3.05 MN/m^2 at 1.27% fibre volume fraction which represented a 19.20% increase in UTS of the fibre-reinforced specimens compared to the unreinforced specimens.

The ultimate tensile stress of the three specimen groups (untreated, mercerised and cornified sisal fibre-reinforced mortar) was observed to increase with increasing fibre volume fraction and could accurately be modelled as polynomial regression equations as shown in Figure 4.13.

The analysis of variation (ANOVA), and, polynomial regression equations (to 3 decimal places) for the ultimate tensile strength of untreated, mercerised and cornified sisal fibre-reinforced mortar composites are shown in Appendix B (Tables B5, B9 and B13). The regression equations all had an R^2 value ≥ 0.97 which shows a very good match between the data points and the regression curve.

From the data collected during the tensile test, an attempt to calculate the interfacial bond strength at $\approx 0.5\%$ fibre volume fraction was made using Aveston's [209] equation (eq. 2.28).

Figure 4.14 is a graphical representation of the interfacial bond strength for the untreated, mercerised and cornified sisal fibre-reinforced mortar composites.

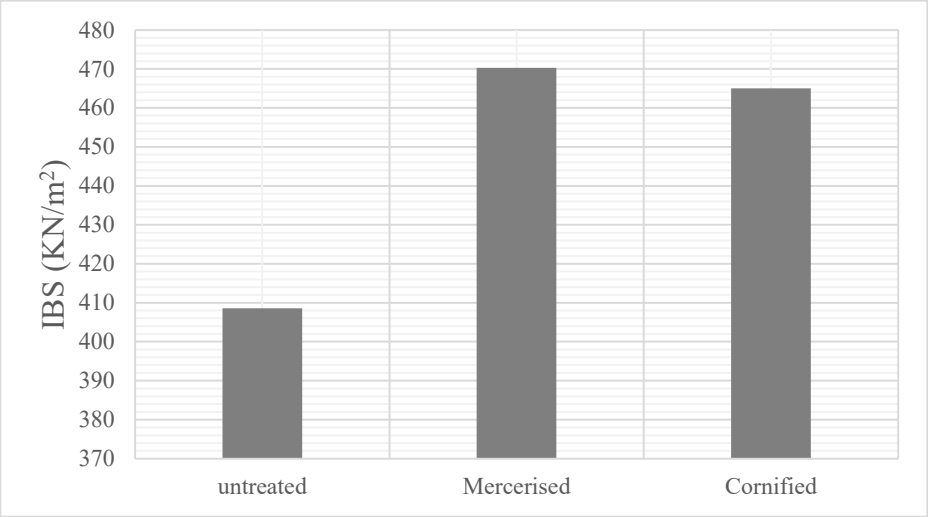

Figure 4.14: Graph showing interfacial bond strength (IBS) results for untreated, mercerised and cornified sisal fibre-reinforced mortar (@≈ 0.5% V_f).

From the graph, it can be observed that at ≈ 0.5% V_f, the surface-modified sisal fibre-reinforced mortar composites had a higher value of interfacial bond strength than the untreated sisal fibre-reinforced mortar specimens.

Mercerised sisal fibre-reinforced mortar composites recorded the highest interfacial bond strength value of 470.30 KN/m^2 at an average fibre volume fraction of 0.43%. Cornified sisal fibre-reinforced mortar composites had an interfacial bond strength value of 465 KN/m^2 at a fibre volume fraction of 0.47%. Untreated sisal fibre-reinforced mortar composites recorded the lowest interfacial bond strength value of 408.60 KN/m^2 at a fibre volume fraction of 0.48%.

Silva *et al*. [203] report a much higher interfacial bond strength value of 920 KN/m^2 for sisal fibre-embedded in an OPC mortar matrix. In their study, Silva *et al*. employed the single fibre strand pull-out method while in the current study, multiple fibres embedded in a cementitious matrix at a low fibre volume fraction were tested in direct tension. The results reported in the

current study are, however, comparable to results posted by Ngala [142] of a maximum interfacial bond strength value of 453 KN/m^2 at a fibre volume fraction of 0.98% for untreated sisal fibre-reinforced rice husk ash cement mortar. Bessel and Mutuli [46] report an interfacial bond strength value of 600 KN/m^2 for untreated sisal fibre-reinforced cement paste. From the results of this study, and by comparing the results with those of Bessel and Mutuli [46], one can conclude that the presence of fine aggregate (sand) in the matrix (as is the case in the current study) has a negative effect on the interfacial bond strength between the reinforcing fibre, and, the matrix. This has been shown to be the case in the MOR of cementitious matrices comprising aggregate by other researchers such as Mutua [48] and Stang *et al.* [198]

The matrix constituent composition (cement/sand ratio) and moisture content were also determined experimentally and the tabulated results are shown in Appendix B (Tables B1(a) and B1(b)). The mortar specimen's total moisture content was determined to be 13.77% (standard deviation 0.29%). This moisture could easily ingress into the fibres, causing dimensional instability and thus negatively affecting the interfacial bond strength between the sisal fibre reinforcement, and the matrix. The fine aggregate proportion of 74.45 % in the mortar specimens shows that the mortar was properly mixed and there were minimal areas of fine aggregate coalescing within the specimens. This would similarly have impacted the interfacial bond strength negatively

Overall, it was observed that the average crack spacing in all the fibre-reinforced specimens reduced with increasing fibre volume fraction. This phenomenon has also been reported by Ngala [142]. It is also worth noting that at high fibre volume fractions, the predominant mode of failure of the composites was multiple matrix failure (MMF), a result consistent with Ngala

[142] which made the accurate measurement of inter-crack spacing of high fibre-volume composites in the current study ($V_f \geq 2\%$) impractical.

4.3 Sisal Fibre-reinforced Polyester Resin Composites

The following are the results obtained from **experimental procedure III**

4.3.1 Tensile Strength

Appendix B (Tables B20 (a, b c & d)) shows the results for fracture stress, fracture strain and Secant Modulus for untreated, mercerised and cornified sisal fibre-reinforced unsaturated polyester resin alongside the analysis of variation (ANOVA). Table B20 (a) shows the volume fraction of embedded fibre, composite cross-sectional area, maximum applied load for each sample, fracture stress, fracture strain and Secant Modulus calculated for each specimen. The test was conducted at a constant fibre aspect ratio (*l/d*) of 687.60. Figure 4.15 is a graphical representation of the results.

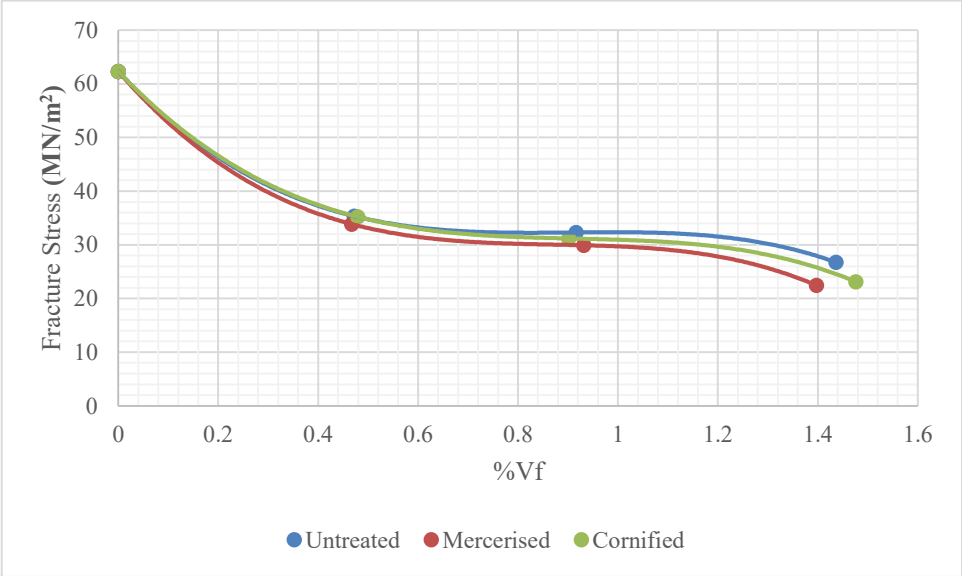

Figure 4.15: Graph showing tensile test results for untreated, mercerised and cornified sisal fibre-reinforced unsaturated polyester resin.

The graphs have been superimposed for ease of comparison. All three types of sisal fibre reinforcement (untreated, mercerised and cornified) exhibited *negative reinforcement*[18] in polyester resin. Other researchers have reported this negative reinforcement phenomenon of natural fibres in polyester resin. Satyanarayana *et al.* [238] reported negative reinforcement of coir fibre-reinforced polyester resin and attributed his findings to weak bonding between the fibres and the matrix. Zhu *et al.* [127] and Marwa *et al.* [234] on the other hand, attributes poor mechanical properties of natural fibre-reinforced polymeric matrices on the thermal degradation of the fibres by the relatively high polymer processing temperatures. This phenomenon has also been reported by Melkamu *et al.* [239] concerning the tensile strength of sisal fibre-reinforced unsaturated polyester resin. Negative reinforcement, a behaviour where the composite behaviour is in contradiction with the rule of mixtures, has also been reported in synthetic fibres by Marom *et al.* [240] while investigating mechanical behaviour of AS-carbon fibre-reinforced epoxy resin, with the reason being attributed to the type of fibre used and the composite's loading configuration. Further investigation into the curing temperatures of the fibre-reinforced polyester resin gave the results shown in Figure 4.16.

[18] A phenomenon where addition of reinforcement to a matrix reduces the strength properties of the composite.

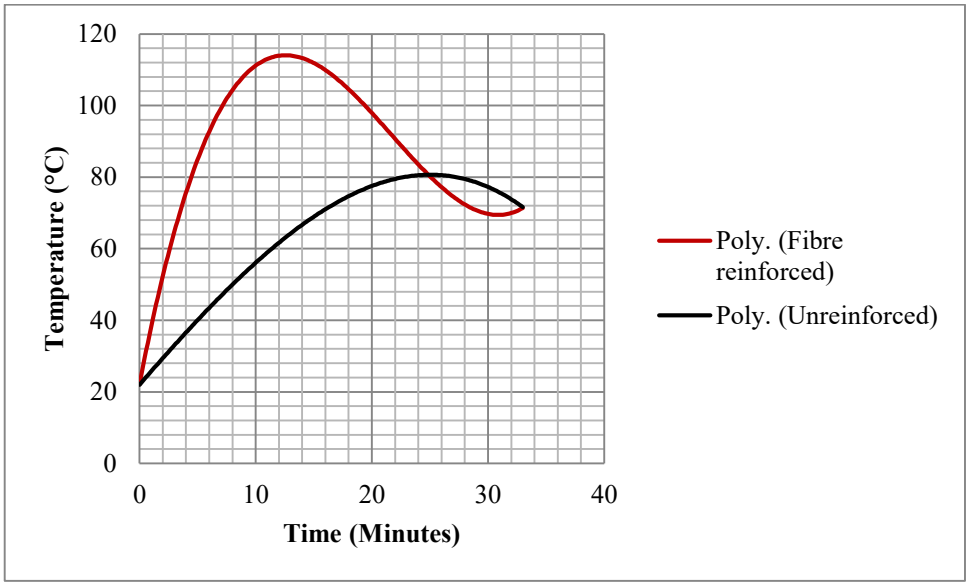

Figure 4.16: Temperature variation within the mould during curing of unreinforced and fibre-reinforced polyester resin (See Appendix B, Tables B8(a, b &c))

Figure 4.16 shows the variation of temperature with time for unreinforced and fibre-reinforced polyester resin during curing (See Appendix B Tables B23 (a, b & c) for temperature measurement results and ANOVA).

The unreinforced polyester resin was observed to cure with a gradual rise from room temperature to a peak temperature of 82.40° C, over a 26-minute period.

The fibre-reinforced polyester resin, on the other hand, was observed to cure with a gradual rise from room temperature to a peak of 113.8° C, over a 12-minute 30-second period. According to Mukhopadyay and Srikanta [110], koronis *et al.* [94] and Zhu *et al.* [127], ligno-cellulosic fibres tend to degrade at or near the processing temperature of thermoplastics such as polyesters and polyamides. Studies into the mechanical properties of sisal fibres at elevated temperatures by Chand and Hashmi [219] have shown that sisal fibres display a reduction in tensile strength at temperatures exceeding 100°C.

This sharp rise in temperature over a short duration has been shown to cause 'thermal shock' to natural fibres by Claramunt *et al.* [177]. In the current research, we posit that the most likely explanation for the negative reinforcement of fibre-reinforced polyester resin is a combination of the high curing temperature and the thermal shock factor.

4.3.2 Flexural Strength

The 3-point bending test results for uniaxially oriented untreated, mercerised and cornified sisal fibre-reinforced polyester composites alongside the analysis of variation (ANOVA) are shown Appendix B (Table B21(a, b c & d)). Table B21 (a) shows the fibre volume fraction, composite cross-section, the breaking load, the Modulus of Rupture and beam deflection. The test was conducted at a constant fibre aspect ratio (*l/d*) of 1289. Figure 4.17 is a graphical representation of the results.

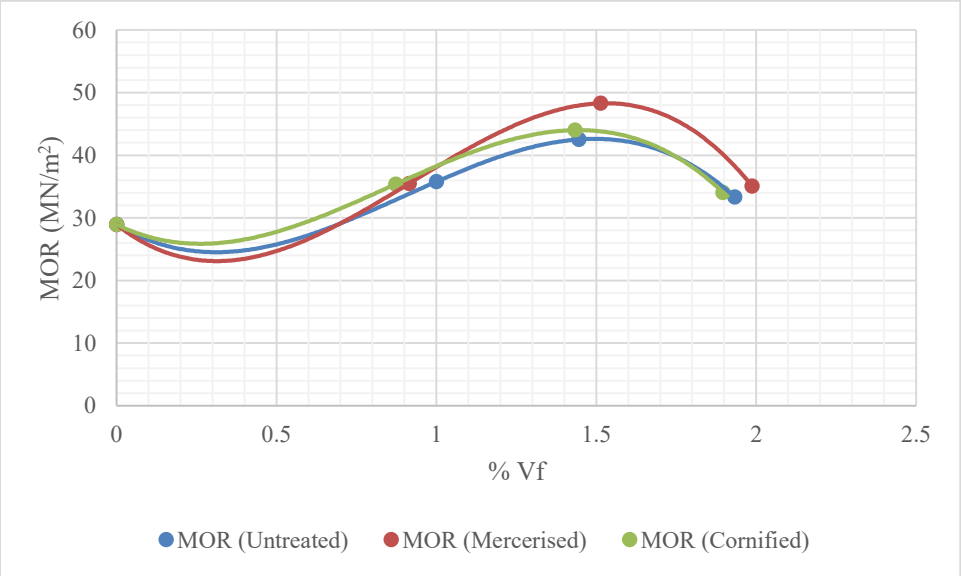

Figure 4.17: Graph showing flexural test results for untreated, mercerised and cornified sisal fibre-reinforced unsaturated polyester resin.

In this test, by curing the flexural specimens in an uncovered mould by an open window overnight, positive reinforcement was achieved as shown in Figure 4.17. A trend of increasing flexural load with increasing volume fraction was observed. The Modulus of Rupture was calculated using equation (3.15) from the ultimate flexural load and the specimen dimensions. The highest average value of the Modulus of Rupture equal to 48.29 MN/m^2 was recorded from the samples containing 1.51% mercerised sisal fibre reinforcement. This showed a 66.93% increase in flexural strength compared to the unreinforced specimens. Cornified sisal fibre-reinforced polyester resin specimens registered a peak MOR of 44.01 MN/m^2 at 1.43 %Vf which translates to a 52.13% increase in the Modulus of rupture compared to the unreinforced specimens. Untreated sisal fibre-reinforced polyester resin had a maximum MOR of 42.53 MN/m^2 at a fibre volume fraction of 1.45%. This represented a 47.01% increase in the Modulus of Rupture compared to the unreinforced (standard control specimens). At 1.45 % V_f, this result is lower than the optimal V_f reported by Idicula *et al.* [81] of 4% for untreated sisal fibre-reinforced polyester resin. However, it is essential to note that Idicula employed short, randomly distributed sisal and banana fibres dispersed in an unsaturated polyester resin matrix. The mechanical properties of polyester resin have also been shown to be affected by the volume of MEKP initiator used in the mixing of the resin and also by the presence of catalysts [241]. In the current study, 1% vol. MEKP with no catalyst was employed while in an earlier study by Abd El-Baky [234] where a Modulus of rupture of 14.01 MN/m^2 was reported for unsaturated polyester resin, 1.5% MEKP and Cobalt Naphthenate catalyst was employed. An even earlier study by Pasdar and Mohseni [194] reports a Modulus of rupture of 78 MN/m^2 for neat unsaturated polyester resin. However, in that study, just like in the study by Abd El-Baky [234], a metal salt catalyst (Cobalt Octoate) was used.

4.4 Sisal Fibre-reinforced Epoxy Resin Composites

4.4.1 Tensile Strength

Appendix B (Tables B22 a, b c & d) shows the results for fracture stress, fracture strain and Secant Modulus alongside the analysis of variation (ANOVA) for untreated, mercerised and cornified sisal fibre-reinforced epoxy resin. Table B22 (a) shows the volume fraction of embedded fibre, composite cross-sectional area, maximum applied load for each sample, fracture stress, fracture strain and Secant Modulus calculated for each specimen. The test was conducted at a constant fibre aspect ratio (*l/d*) of 687.60. Figure 4.18 is a graphical summary of the results.

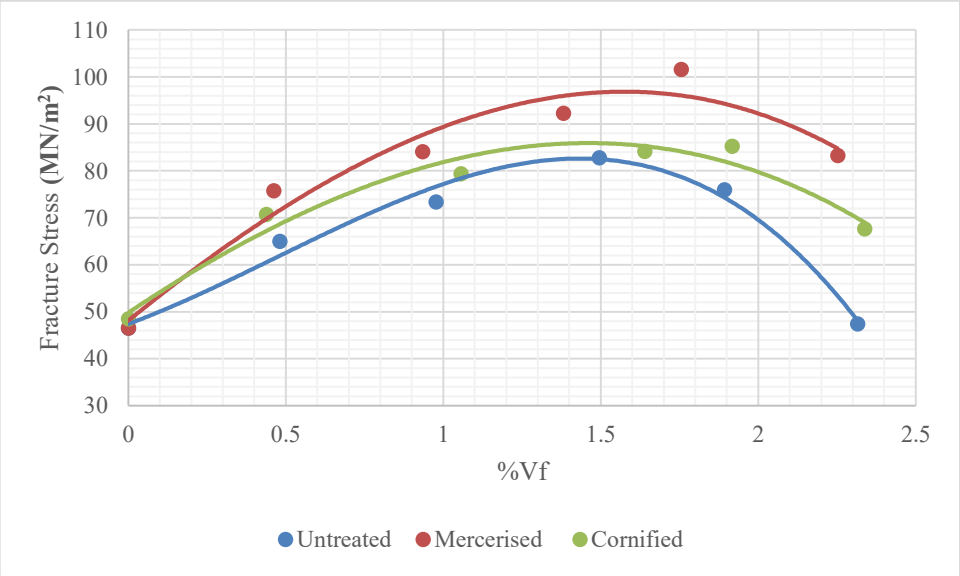

Figure 4.18: Graph showing tensile test results for untreated, mercerised and cornified sisal fibre-reinforced epoxy resin.

In Figure 4.18, the graphs have been superimposed for ease of comparison. In all the specimen groups (untreated, mercerised and cornified sisal fibre-reinforced epoxy resin), the composite tensile strength and also the secant modulus (at 100% strain) were observed to

increase with increasing fibre volume fraction. Mercerised sisal fibre-reinforced epoxy resin displayed the greatest gain in tensile strength with a maximum fracture value of 101.57 MN/m^2 at a fibre volume fraction of 1.76%. This translated to an 118.52% increase in tensile strength compared to the standard control (unreinforced specimen). Cornified sisal fibre-reinforced epoxy resin attained a maximum fracture stress value of 85.24 MN/m^2 at a fibre volume fraction of 1.92%. This represented an 83.39% increase in fracture stress compared to the unreinforced epoxy resin. Untreated sisal fibre-reinforced epoxy resin displayed the least gain in tensile strength with a maximum fracture stress value of 82.77 MN/m^2 at a fibre volume fraction of 1.50%. This in turn translated to a 78.08% increase in tensile strength compared to the standard control (unreinforced specimen). Significant standard deviation was observed in the fracture stress data. This could be due to uneven fibre distribution in the composite due to the hand lay-up method employed in the current study. It could also be as a result of the type of epoxy resin used in the current study. There are many different types of epoxy resin in the market with varying physical, chemical and mechanical properties. The epoxy resin used in the current study had mechanical properties comparable to the epoxy resins used by Yusof *et al.* [76] and Ngala [142] ($\sigma_{uts} \approx 44\ MN/m^2$; $E \approx 1\ GN/m^2$).

The motivation behind using an epoxy resin matrix in the current study was to see the effect of the exothermic curing temperature of polyester resin on untreated and surface-modified sisal fibres. By using the fibres in both polyester and epoxy resin matrices, and comparing the results, the fibres were able to positively reinforce the epoxy resin unlike was the case with polyester resin. More so, the average Secant Modulus of the epoxy resin was about twice that of the unsaturated polyester (0.91 GN/m^2 vs 0.58 GN/m^2). The reinforcing effect of fibre reinforcement is most pronounced when the stiffness of the fibres is much greater than that of

the matrix i.e. ($E_f >> E_m$). Yet in the current study the matrix with a higher Modulus value, was better reinforced than the one with a lower Modulus value. This can be attributed to the exothermic curing temperature of the lower Modulus unsaturated polyester resin matrix.

Overall, sisal fibre surface-modification led to greater improvement in the strength properties of the epoxy composite system than in the untreated sisal fibre-reinforced epoxy composite. These results confirm the predictions of Ngala [142] and Bisanda [166] that sisal fibre surface-modification prior to incorporation into a polymeric matrix will result in a composite system with better/improved strength properties compared to the untreated sisal fibre-reinforced composite.

CHAPTER FIVE

5.0 CONCLUSIONS AND RECOMMENDATIONS FOR FURTHER WORK

5.1 Conclusions

The following conclusions can be drawn from this study

1) The mean sisal fibre diameter of the butt-end and mid-span portions of UG grade Kenyan sisal was measured to be 232.70 μm with a standard error of $\pm$ 8.98 μm.
2) The density of untreated sisal fibres under normal atmospheric conditions was determined using the linear density and diameter calculation method [214] and found to be equal to 1.3 gcm^{-3} with a standard error of $\pm$ 0.38 gcm^{-3}
3) The tensile strength of Kenyan sisal fibre in its untreated, mercerised and cornified states was determined and found to equal 161.02 MN/m^2, 271.00 MN/m^2 and 198.57 MN/m^2 respectively.
4) Cornified sisal fibres have the highest water absorption, about 182.24% of their weight, compared to mercerised sisal fibres 178.30%.
5) Both mercerisation and cornification either introduced new flaws or exacerbated existing defects in untreated sisal fibres.
6) The flexural strength of untreated, mercerised, and cornified sisal fibre-reinforced OPC mortar matrix was higher than that of the unreinforced matrix.
7) Uniaxially oriented continuous fibre-reinforced OPC mortar composites displayed an increase in flexural strength with increasing fibre volume fraction. At the optimum fibre volume fraction, a two to three-fold gain in flexural strength was observed, a result that has also reported by Savastano [36] and by Tonoli *et al.* [38].

8) Mercerised sisal continuous fibre-reinforced mortar composites displayed a higher increase in flexural strength of 151.07% compared to untreated sisal fibre-reinforced specimens of 110.28%.
9) Randomly oriented discontinuous sisal fibre mortar composites displayed a marginal increase in flexural strength that was significantly lower than that of the uniaxially oriented, continuous fibre-reinforced mortar composites. These findings are consistent with those reported by Mutua [48], Mutuli [91], Kirima [237] and Swift & Smith [236].
10) There were two modes of failure identified in the flexural test of uniaxially aligned continuous fibre-reinforced composites. At low fibre volume fractions, specimens failed with a single crack parallel to the load application roller indicative of flexural failure while at higher fibre volume fractions, the specimens failed in shear, with multiple cracks forming parallel to the neutral axis.
11) The tensile strength results of the uniaxially aligned continuous fibre-reinforced polyester resin specimens displayed negative reinforcement while the flexural strength results showed positive reinforcement. This was attributed to the effect of elevated temperature on sisal tensile strength that is also reported by Chand and Hashmi [219].
12) Mercerised sisal fibre-reinforced unsaturated polyester resin specimens displayed the highest gain in flexural strength of 66.93% compared to cornified and untreated sisal fibre-reinforced specimens of 52.13% and 47.01% respectively.
13) Mercerised sisal fibre-epoxy resin specimens displayed the highest gain in in tensile strength of 118.52% compared to cornified and untreated sisal fibre-reinforced specimens of 88.16% and 78.08% respectively. Compared to the results of sisal fibre-reinforced polyester resin, these results further corroborate the findings of Claramunt

et al. [177] and Chand & Hashmi [219] that high processing temperatures (above 100°C) are potentially detrimental to sisal fibres.

5.2 Recommendations

The following are recommendations for future work.

1) The density of untreated UG grade Kenyan sisal fibres was determined using the linear density and diameter method employed by Soykeabkaew *et al.* [214] in the determination of the densities of jute and flax fibres. This method was adopted on the basis of its low cost, simplicity and its reputation of giving accurate results in the determination of high density natural fibres such as sisal fibres. Although the density arrived at in this research is well within documented results, more advanced density determination methods such as the ASTM-1505-03 gradient column method [242] or the liquid pycnometry method [243] can be considered to get a more accurate measurement of the density of UG grade Kenyan sisal fibres. There is also a need to employ either one of these more precise density calculation methods to determine whether the surface-modification treatments had any effect on the diameter and density of the sisal fibres.
2) In this research, both mercerisation and cornification have resulted in improvement of the mechanical properties of Kenyan sisal fibres. However, many researchers such as Sathishkumar *et al.* [13], Chandramohan and Bharanichandar [26], Idicula *et al.* [81], Marom *et al.* [240] and Jacob *et al.* [199] have shown that hybrid fibre compositions lead to synergistic improvement of composite mechanical properties than that of the individual fibre types used alone. There is, therefore, a need to establish the reinforcing effect of mercerised/cornified sisal fibre hybrid in both cementitious and polymeric matrices.
3) At high fibre volume fractions, the flexural strength results have pointed towards a predominantly shear failure mode of the composite. The true flexural strength of

uniaxially aligned continuous fibre-reinforced OPC mortar composites needs further investigation.

4) The durability of mercerised and cornified sisal fibres in the predominantly alkaline OPC mortar needs investigation before a conclusive decision can be arrived at as to which surface-modification method best suits Kenyan sisal fibres.
5) Semsarzadeh [59] has shown that polyvinyl acetate has an insulating effect on natural fibres. There is a need to investigate if spraying the fibres with polyvinyl acetate before embedding them in the polyester resin can reverse the negative reinforcement effect reported by Zhu *et al.* [127], Satyanarayana *et al.* [238] and Abd El-Baky *et al.* [244], and also observed in the current research.
6) Chand and Hashmi [219] have shown that untreated (untreated) sisal fibres display a gradual reduction in strength properties at temperatures above 100°C. Given the negative and positive reinforcement observed in the tensile and flexural strengths of sisal fibre-reinforced polyester resin, a comparative study on the thermal stability of untreated and surface-modified sisal fibres needs further investigation.
7) In this research work, cornification was carried out at a drying temperature of 100°C with the temperature set to increase from room temperature at a rate of 1°C/min. Claramunt *et al.* [177] and Ballesteros *et al.* [39] advocated the use of a drying temperature of 60°C and this was not realised in the current research due to challenges with the electric oven discussed in section **4.1.1** of this study. There is a need, therefore, to investigate the effect of cornifying Kenyan sisal fibres at 60°C and to compare the cornified fibres strength properties with those reported in this research.

REFERENCES

[1] Townsend, T. and Sette, J.: *Natural Fibres and the World Economy*. In: Natural Fibres: Advances in Science and Technology Towards Industrial Applications. Dordrecht, Netherlands: SpringerNature, 2016, p. 381–390.

[2] Mohammad, J., Mohamed, T. and Naheed, S.: *Mechanical and Physical Testing of Biocomposites, Fibre-Reinforced Composites and Hybrid Composites*. Cambridge, United Kingdom: Woodhead Publishing ltd, 2019.

[3] Rowell, R.M.: *Natural Fibres: Types and Properties*. In: Properties and Performance of Natural-Fibre Composites. Cambridge, England: Woodhead Publishing ltd, 2008, p. 3–66.

[4] Gentry, H.S.: *Agaves of Continental North America*. Arizona, USA: University of Arizona Press, 2004.

[5] Narváez-Zapata, J.A. and Sánchez-Teyer, L.F.: Agaves as a Raw Material: Recent Technologies and Applications. *Recent Patents on Biotechnology*, **3** (3), 2009, p. 185–191.

[6] Sabea, H.: Reviving the Dead: Entangled Histories in the Privatisation of the Tanzanian Sisal Industry. *Africa: Journal of the International African Institute*, **71** (2), 2001, p. 286–313.

[7] Sabea, H.: Mastering the Landscape? Sisal Plantations, Land, and Labor in Tanga Region, 1893-1980s. *The International Journal of African Historical Studies*, **41** (3), 2008, p. 411–432.

[8] Sheikh Ali, A.: Effects of Foreign Exchange Rate on Foreign Trade in Financial Performance of the Agricultural Sector in Kenya. *International journal of social sciences and entrepreneurship (IJSSE)*, **4** (6), 2015, p. 1–19.

[9] *Rea Vipingo - World Leaders in Sisal*. 2020.

[10] Rading, G.O.: *Concise Notes on Materials Science and Engineering*. Victoria, BC, Canada: Trafford Publishing, 2007.

[11] Mallick, P.K.: *Fibre Reinforced Composites-Materials, Manufacturing and Design*. 6000 Broken Sound Parkway NW, Suite 300, Boca Raton, Florida, USA: CRC press, 2008.

[12] Campbell, F.C.: *Structural Composite Materials*. Materials Park, Ohio, USA: ASM Press, 2010.

[13] Sathishkumar, T., Naveen, J. and Satheeshkumar, S.: Hybrid Fiber Reinforced Polymer Composites – A Review. *Journal of Reinforced Plastics and Composites*, **33** (5), 2014, p. 454–471.

[14] Cai, J., Qiu, L., Yuan, S., Shi, L., Liu, P. and Liang, D.: *Structural Health Monitoring of Composite Materials*. In: Composites and their Applications. Rijeka, Croatia: InTech, 2012, p. 37–60.

[15] Yimer, T.: *Development of Natural Fiber Composites for Automotive Applications*. Addis Ababa, Ethiopia: Addis Ababa Institute of Technology, 2013.

[16] Namvar, F., Mohammad, J., Paridah, M.T., Rosfarizan, M. and Azizi, S.: Potential Use of Plant Fibres and their Composites for Biomedical Applications. *BioResources*, **9** (3), 2014, p. 5688–5706.

[17] Staab, G.H.: *Laminar Composites*. The Boulevard, Langford Lane, Kidlington, Oxford OX5, 1GB, United Kingdom: Butterworth-Heinemann © Elsevier Inc, 2015.

[18] Kumar, K.P. and Sekaran, A.S.J.: Some Natural Fibers used in Polymer Composites and their Extraction Processes: A Review. *Journal of Reinforced Plastics and Composites*, **33** (20), 2014, p. 1879–1892.

[19] Biagiotti, J., Puglia, D. and Kenny, J.M.: A Review on Natural Fibre-Based Composites-Part I. *Journal of Natural Fibers*, **1** (2), 2004, p. 37–68.

[20] Senseney, J.R.: Review: Ancient Building Technology. Volume 3: Construction by G. R. H. Wright; Constructing the Ancient World: Architectural Techniques of the Greeks and Romans by Carmelo G. Malacrino, Jay Hyams. *Journal of the Society of Architectural Historians*, **70** (4), 2011, p. 547–549.

[21] Pachta, V., Stefanidou, M., Konopisi, S. and Papayianni, I.: Technological Evolution of Historic Structural Mortars. *Journal of Civil Engineering and Architecture*, **8** (7), 2014, p. 846–854.

[22] Selvaraj, T., Ramadoss, R., Sekar, S. and Nambirajan, M.: Knowing from the Past - Ingredients and Technology of Ancient Mortar used in Vadakumnathan Temple, Tirussur, Kerala, India. *Journal of Building Engineering*, **4**, 2015, p. 101–112.

[23] Mbeche, S.M. and Omara, T.: Effects of Alkali Treatment on the Mechanical and Thermal Properties of Sisal/Cattail Polyester Commingled Composites. *PeerJ Materials Science*, **2**, 2020, p. e5.

[24] Milosevic, M., Valášek, P. and Ruggiero, A.: Tribology of Natural Fibers Composite Materials: An Overview. *Lubricants*, **8** (4), 2020, p. 42.

[25] Kesikidou, F. and Stefanidou, M.: Natural Fiber-Reinforced Mortars. *Journal of Building Engineering*, **25**, 2019, p. 100786.

[26] Chandramohan, D. and Bharanichandar, J.: Impact Test on Natural Fiber Reinforced Polymer Composite Materials. *Carbon-Science and Technology*, **5** (3), 2013, p. 314–320.

[27] Kaushik, V.K., Kumar, A. and Susheel, K.: Effect of Mercerization and Benzoyl Peroxide Treatment on Morphology, Thermal Stability and Crystallinity of Sisal Fibers. *International Journal of Textile Science*, **1** (6), 2012, p. 101–105.

[28] Naidu, L. and Kumar, D.A.: A Study on Different Chemical Treatments for Natural Fiber Reinforced Composites. *International Journal of Mechanical and Production Engineering Research and Development*, **8** (5), 2018, p. 143–152.

[29] Ramamoorthy, S.K., Skrifvars, M. and Persson, A.: A Review of Natural Fibers Used in Biocomposites: Plant, Animal and Regenerated Cellulose Fibers. *Polymer Reviews*, **55** (1), 2015, p. 107–162.

[30] Srinivasa, C.V., Arifulla, A., Goutham, N., Santhosh, T., Jaeethendra, H.J., Ravikumar, R.B., Anil, S.G., Santhosh Kumar, D.G. and Ashish, J.: Static Bending and Impact Behaviour of Areca Fibers Composites. *Materials & Design*, **32** (4), 2011, p. 2469–2475.

[31] Khalil, A.H.P.S., Jawaid, M., Hassan, A., Paridah, M.T. and Zaidon, A.: *Oil Palm Biomass Fibres and Recent Advancement in Oil Palm Biomass Fibres Based Hybrid Biocomposites*. In: Composites and their Applications. Rijeka, Croatia: InTech Open Access Books, 2012, p. 209–242.

[32] Chandramohan, D. and Marimuthu, K.: A Review on Natural Fibers. *International Journal of Recent Research and Applied Studies*, **8** (2), 2011, p. 194–206.

[33] Sarikanat, M., Seki, Y., Sever, K. and Durmuşkahya, C.: Determination of Properties of Althaea Officinalis L. (Marshmallow) Fibres as a Potential Plant Fibre in Polymeric Composite Materials. *Composites Part B: Engineering*, **57**, 2014, p. 180–186.

[34] Mokhtar, M., Rahmat, A.R. and Hassan, A.: *Characterization and Treatments of Pineapple Leaf Fibre ThermoplasticComposite for Construction Application*. VOT 75147. Johor, Malaysia: Universiti Teknologi Malaysia, 2007.

[35] Brahmakumar, M., Pavithran, C. and Pillai, R.M.: Coconut Fibre Reinforced Polyethylene Composites: Effect of Natural Waxy Surface Layer of the Fibre on Fibre/Matrix Interfacial Bonding and Strength of Composites. *Composites Science and Technology*, **65** (3–4), 2005, p. 563–569.

[36] Savastano, H, Warden, P G and Coutts, R P S: Brazilian Waste Fibers as Reinforcement for Cement-Based Composites. *Cement and Concrete Composites*, **22** (5), 2000, p. 379–384.

[37] Bernard, S.S., Suresh, G., Srinivasan, T., Srinivasan, S., Kaarmugilan, N., Naveed, L.M., Kiranmouli, N. and Mahalakshmi, C.S.: Analyzing the Mechanical Behaviour of Sisal Fiber Reinforced IPN Matrix. *Materials Today: Proceedings*, 2020.

[38] Tonoli, G.H.D., Joaquim, A.P., Arsène, M.-A., Bilba, K. and Savastano, H.: Performance and Durability of Cement Based Composites Reinforced with Refined Sisal Pulp. *Materials and Manufacturing Processes*, **22** (2), 2007, p. 149–156.

[39] Ballesteros, J.E.M., Mármol, G., Filomeno, R., Rodier, L., Savastano, H. and Fiorelli, J.: Synergic effect of Fiber and Matrix Treatments for Vegetable Fiber Reinforced Cement of Improved Performance. *Construction and Building Materials*, **205**, 2019, p. 52–60.

[40] Yu, T., Ren, J., Li, S., Yuan, H. and Li, Y.: Effect of Fiber Surface-Treatments on the Properties of Poly(Lactic Acid)/Ramie Composites. *Composites Part A*, **41** (4), 2010, p. 499–505.

[41] Hestiawan, H., Jamasri and Kusmono: Effect of Chemical Treatments on Tensile Properties and Interfacial Shear Strength of Unsaturated Polyester/Fan palm fibers. *Journal of Natural Fibers*, **15** (5), 2018, p. 762–775.

[42] Fujiyama, R., Darwish, F. and Pereira, M.V.: Mechanical Characterization of Sisal Reinforced Cement Mortar. *Theoretical and Applied Mechanics Letters*, **4** (6), 2014, p. 061002.

[43] Angiolilli, M., Gregori, A., Pathirage, M. and Cusatis, G.: Fiber Reinforced Cementitious Matrix (FRCM) for Strengthening Historical Stone Masonry Structures: Experiments and computations. *Engineering Structures*, **224**, 2020, p. 111102.

[44] Wu, Y., Li, Y. and Niu, B.: Assessment of the Mechanical Properties of Sisal Fiber-Reinforced Silty Clay Using Triaxial Shear Tests. *The Scientific World Journal*, **2014**, 2014, p. 1–9.

[45] Mutuli, S.M., Bessel, T.J. and Talitwala, E.S.J.: The Potential of Sisal as a Reinforcing Fibre in Cement Base Materials. *African Journal of Science and Technology*, **1** (1), 1982, p. 5–16.

[46] Bessel, T.J. and Mutuli, S.M.: The Interfacial Bond Strength of Sisal-Cement Composites Using a Tensile Test. *Journal of Materials Science Letters*, **1** (6), 1982, p. 244–246.

[47] Aruna, M.: Mechanical Behaviour of Sisal Fibre Reinforced Cement Composites. *International Journal of Materials and Metallurgical Engineering*, **8** (4), 2014, p. 650–653.

[48] Mutua, J.: *Mechanical Properties of Sisal Fibre Reinforced Concrete*. Nairobi: University of Nairobi, 1993.

[49] Ghali, L., Aloui, M., Zidi, M., Bendaly, H., M'sahli, S. and Sakli, F.: Effect of Chemical Modification of Luffa Cylindrica Fibers on the Mechanical and Hygrothermal Behaviours of Polyester/Luffa Composite. *BioResources*, **6** (4), 2011, p. 3836–3849.

[50] Islam, M.S., Church, J.S. and Miao, M.: Effect of Removing Polypropylene Fibre Surface Finishes on Mechanical Performance of Kenaf/Polypropylene Composites. *Composites Part A: Applied Science and Manufacturing*, **42** (11), 2011, p. 1687–1693.

[51] Alwani, S.M., Khalil, A.H.P.S., Asniza, M., Suhaily, S.S., Amiranajwa, A.S.N. and Jawaid, M.: *Agricultural Biomass Raw Materials: The Current State and Future Potentialities*. In: Agricultural Biomass Based Potential Materials. Germany: Springer, Cham Heidelberg, 2015, p. 505.

[52] Dicker, M.P.M., Duckworth, P.F., Baker, A.B., Francois, G., Hazzard, M.K. and Weaver, P.M.: Green Composites: A Review of Material Attributes and Complementary Applications. *Composites Part A: Applied Science and Manufacturing*, **56**, 2014, p. 280–289.

[53] Chaitanya, S. and Singh, I.: Novel Aloe Vera Fiber Reinforced Biodegradable Composites—Development and Characterization. *Journal of Reinforced Plastics and Composites*, **35** (19), 2016, p. 1411–1423.

[54] Kim, H.C., Kim, D., Lee, J.Y., Zhai, L. and Kim, J.: Effect of Wet Spinning and Stretching to Enhance Mechanical Properties of Cellulose Nanofiber Filament. *International Journal of Precision Engineering and Manufacturing-Green Technology*, **6** (3), 2019, p. 567–575.

[55] Thakur, V.K., Thakur, M.K. and Gupta, R.K.: Graft Copolymers of Natural Fibers for Green Composites. *Carbohydrate Polymers*, **104**, 2014, p. 87–93.

[56] Eichhorn, S.J., Baillie, C.A., Mwaikambo, Y.L., Ansell, P.M. and Zafeiropoulos, N.: Current International Research into Cellulosic Fibres and Composites. *Journal of Materials Science*, **36** (9), 2001, p. 2107–2131.

[57] Aracri, E., Fillat, A., Colom, J.F., Gutiérrez, A., del Río, J.C., Martínez, Á.T. and Vidal, T.: Enzymatic Grafting of Simple Phenols on Flax and Sisal Pulp Fibres using Laccases. *Bioresource Technology*, **101** (21), 2010, p. 8211–8216.

[58] Çinçik, E. and Günaydin, E.: The Influence of Calendering Parameters on Performance Properties of Needle-Punched Non-Woven Cleaning Materials including r-PET Fiber. *The Journal of the Textile Institute*, **108** (2), 2017, p. 216–225.

[59] Semsarzadeh, Mohammed.A., Lotfali, A.R. and Mirzadeh, H.: Jute Reinforced Polyester Structures. *Polymer Composites*, **5** (2), 1984, p. 141–142.

[60] Mokaloba, N. and Batane, R.: The Effects of Mercerization and Acetylation Treatments on the Properties of Sisal Fiber and its Interfacial Adhesion Characteristics on Polypropylene. *International Journal of Engineering, Science and Technology*, **6** (4), 2014, p. 83–97.

[61] Ferreira, S.R., Silva, F. de A., Lima, P.R.L. and Toledo Filho, R.D.: Effect of Hornification on the Structure, Tensile Behavior and Fiber Matrix Bond of Sisal, Jute

and Curauá Fiber Cement Based Composite Systems. *Construction and Building Materials*, **139**, 2016, p. 551–561.

[62] Colom, X. and Carrillo, F.: Crystallinity Changes in Lyocell and Viscose-type Fibres by Caustic Treatment. *European Polymer Journal*, **38** (11), 2002, p. 2225–2230.

[63] Diniz, J.M.B.F., Gil, M.H. and Castro, J.A.A.M.: Hornification—Its Origin and Interpretation in Wood Pulps. *Wood Science and Technology*, **37** (6), 2004, p. 489–494.

[64] Ferreira, S.R., Lima, P.R.L., Silva, F. de A. and Filho, T.D.R.: Effect of Sisal Fibre Hornification on the Fibre Matrix Bonding Characteristics and Bending Behaviour of Cement-Based Composites. *Key Engineering Materials*, **600**, 2014, p. 421–432.

[65] Favaro, S.L., Ganzerli, T.A., Neto, A.G.V. de C., da Silva, O.R.R.F. and Radovanovic, E.: Chemical, Morphological and Mechanical Analysis of Sisal Fiber-Reinforced Recycled High-Density Polyethylene Composites. *eXPRESS Polymer Letters*, **4** (8), 2010, p. 465–473.

[66] Ramanathan, A. and Subramanian, V.: Present Status of Asbestos Mining and Related Health Problems in India —A Survey. *Industrial Health*, **39** (4), 2001, p. 309–315.

[67] Patel, K., Wakhisi, J., Mining, S., Mwangi, A. and Patel, R.: Esophageal Cancer, the Topmost Cancer at Moi Teaching and Referral Hospital (MTRH) in the Rift Valley, and its Potential Risk Factors. *International Scholarly Research Notices*, 2013, p. 1–9.

[68] Goswami, E., Craven, V., Dahlstrom, D.L., Alexander, D. and Mowat, F.: Domestic Asbestos Exposure: A Review of Epidemiologic and Exposure Data. *International Journal of Environmental Research and Public Health*, **10** (11), 2013, p. 5629–5670.

[69] Vainio, H.: Epidemics of Asbestos-Related Diseases – something old, something new. *Scandinavian Journal of Work, Environment & Health*, **41** (1), 2015, p. 1–4.

[70] Murphy, T.L.G.: *Asbestos Exposure and Incidence of Disease among a group of former Chrysotile Miners and Millers from Baie Verte, NL, Canada*. Newfoundland, Canada: Memorial University of Newfoundland, 2015.

[71] Piche, A., Revel, I. and Peres, G.: *Experimental and Numerical Methods to Characterize Electrical Behaviour of Carbon Fiber Composites Used in Aeronautic Industry*. In: Advances in Composite Materials - Analysis of Natural and Man-Made Materials. Rijeka, Croatia: InTech, 2011, p. 481–496.

[72] Toldy, A., Szolnoki, B. and Marosi, G.: Flame Retardancy of Fibre-Reinforced Epoxy Resin Composites for Aerospace Applications. *Polymer Degradation and Stability*, **96** (3), 2011, p. 371–376.

[73] Young-Jun, Y., Jang-Ho, J.-K., Ki-Tae, P., Dong-Woo, S. and Tae-Hee, L.: Modification of Rule of Mixtures for Tensile Strength Estimation of Circular GFRP Rebars. *Polymers*, **9** (12), 2017, p. 682–695.

[74] Segerström, S., Astbäck, J. and Ekstrand, K.D.: A Retrospective Long Term Study of Teeth Restored with Prefabricated Carbon Fiber Reinforced Epoxy Resin Posts. *Swedish Dental Journal*, **30** (1), 2006, p. 1–8.

[75] Dikbas, I. and Tanalp, J.: *An Overview of Clinical Studies on Fiber Post Systems*. Hindawi, 2013, 2013, p. e171380.

[76] Yusof, N., Dewi, D., Salih, N.M., Supriyanto, E., Syahrom, A. and Faudzi, A.: Epoxy resin characterization for imaging phantom: X-ray, textural, and mechanical properties. *2016 IEEE EMBS Conference on Biomedical Engineering and Sciences (IECBES)*, 2016, p. 617–622.

[77] Giri, J. and Adhikari, R.: A Brief Review on Extraction of Nanocellulose and its Application. *BIBECHANA*, **9**, 2012, p. 81–87.

[78] Sreekumar, P.A., Joseph, K., Unnikrishnan, G. and Thomas, S.: A Comparative Study on Mechanical Properties of Sisal-Leaf Fibre-Reinforced Polyester Composites prepared by Resin Transfer and Compression Moulding Techniques. *Composites Science and Technology*, **67** (3), 2007, p. 453–461.

[79] Wulfsberg, J., Herrmann, A., Ziegmann, G., Lonsdorfer, G., Stöß, N. and Fette, M.: Combination of Carbon Fibre Sheet Moulding Compound and Prepreg Compression Moulding in Aerospace Industry. *Procedia Engineering*, **81**, 2014, p. 1601–1607.

[80] Bledzki, A.K., Jaszkiewicz, A. and Scherzer, D.: Mechanical Properties of PLA Composites with Man-Made Cellulose and Abaca Fibres. *Composites Part A: Applied Science and Manufacturing*, **40** (4), 2009, p. 404–412.

[81] Idicula, M., Malhotra, S.K., Joseph, K. and Thomas, S.: Dynamic Mechanical Analysis of Randomly Oriented Intimately Mixed Short Banana/Sisal Hybrid Fiber Reinforced Polyester Composites. *Composites Science and Technology*, **65** (7–8), 2005, p. 1077–1087.

[82] Blackburn, R.: *Biodegradable and Sustainable Fibres*. Cambridge, England: Woodhead Publishing ltd, 2005.

[83] Dunne, R., Desai, D., Sadiku, R. and Jayaramudu, J.: A Review of Natural Fibres, their Sustainability and Automotive Applications. *Journal of Reinforced Plastics and Composites*, **35** (13), 2016, p. 1041–1050.

[84] Karthik, T. and Rathinamoorthy, R.: *Sustainable Synthetic Fibre Production*. In: Sustainable Fibres and Textiles (Editor: S. S. Muthu). Coimbatore, India: Woodhead Publishing, 2017, p. 191–240.

[85] Senthilkumar, K., Saba, N., Rajini, N., Chandrasekar, M., Jawaid, M., Siengchin, S. and Alotman, O.Y.: Mechanical properties evaluation of sisal fibre reinforced polymer composites: A review. *Construction and Building Materials*, **174**, 2018, p. 713–729.

[86] Holmberg, K., i Kivikytö-Reponen, P., Härkisaari, P., Valtonen, K. and Erdemir, A.: Global Energy Consumption due to Friction and Wear in the Mining Industry. *Tribology International*, **115**, 2017, p. 116–139.

[87] Kiarie, E.: Biogas as a Potential Alternative Source of Energy for Industrial Sector: Case Study of Kilifi Sisal Plantation Biogas Plant. *International Journal of Advanced Research and Publications*, **3** (7), 2019, p. 30–38.

[88] Kumar, M.A., Reddy, G.R., Siva, Y., Bharathi, Naidu, S.V., Naga, V. and Naidu, P.: Frictional Coefficient, Hardness, Impact Strength, and Chemical Resistance of Reinforced Sisal/Glass Fiber Epoxy Hybrid Composites. *Journal of Composite Materials*, **44** (26), 2010, p. 3195–3202.

[89] Dwivedi, U.K. and Chand, N.: Influence of Fibre Orientation on Friction and Sliding Wear Behaviour of Jute Fibre Reinforced Polyester Composite. *Applied Composite Materials*, **16** (2), 2009, p. 93–100.

[90] Xin, X., Xu, C.G. and Qing, L.F.: Friction Properties of Sisal Fibre Reinforced Resin Brake Composites. *Wear*, **262** (5–6), 2007, p. 736–741.

[91] Mutuli, S.M.: *The Properties of Sisal Fibres and Sisal Fibre Reinforced Composite Materials*. Nairobi, Kenya: University of Nairobi, 1979.

[92] Li, Y., Mai, Y.-W. and Ye, L.: Sisal Fiber and its Composites: A Review of Recent Developments. *Composites Science and Technology*, **60** (11), 2000, p. 2037–2055.

[93] Bassyouni, M.: Dynamic Mechanical Properties and Characterization of Chemically treated Sisal Fiber-Reinforced Polypropylene Biocomposites. *Journal of Reinforced Plastics and Composites*, **37** (23), 2018, p. 1402–1417.

[94] Koronis, G., Silva, A. and Fontul, M.: Green Composites: A Review of Adequate Materials for Automotive Applications. *Composites Part B: Engineering*, **44** (1), 2013, p. 120–127.

[95] Ogaha, A.O. and Chukwujike, I.C.: Physiomechanical Properties of Agro Waste filled High-Density Polyethylene Bio-Composites. *Journal of Institute of Polymer Engineers*, **1** (2), 2017, p. 1–10.

[96] Cooke, J.A. and Johnson, M.S.: Ecological Restoration of Land with Particular Reference to the Mining of Metals and Industrial Minerals: A Review of Theory and Practice. *Environmental Reviews*, **10** (1), 2002, p. 41–71.

[97] Mborah, C., Bansah, K. and Boateng, M.: Evaluating Alternate Post-Mining Land-Uses: A Review. *Environment and Pollution*, **5** (1), 2016, p. 14–22.

[98] Fields, S.: The Earth's Open Wounds: Abandoned and Orphaned Mines. *Environmental Health Perspectives*, **111** (3), 2003, p. 154–161.

[99] Dris, R., Gasperi, J., Saad, M., Mirande, C. and Tassin, B.: Synthetic Fibers in Atmospheric Fallout: A Source of Microplastics in the Environment? *Marine Pollution Bulletin*, **104** (1–2), 2016, p. 290–293.

[100] Carney Almroth, B.M., Åström, L., Roslund, S., Petersson, H., Johansson, M. and Persson, N.-K.: Quantifying Shedding of Synthetic Fibers from Textiles; a Source of Microplastics Released into the Environment. *Environmental Science and Pollution Research*, **25** (2), 2018, p. 1191–1199.

[101] Zhang, C., Garrison, T.F., Madbouly, S.A. and Kessler, M.R.: Recent Advances in Vegetable Oil-Based Polymers and their Composites. *Progress in Polymer Science*, **71**, 2017, p. 91–143.

[102] Mwasha, A.: Using Environmentally Friendly Geotextiles for Soil Reinforcement: A Parametric Study. *Materials and Design*, **30** (5), 2009, p. 1798–1803.

[103] Methacanon, P., Weerawatsophon, U., Sumransin, N., Prahsarn, C. and Bergado, D.T.: Properties and Potential Application of Selected Natural Fibres as Limited Life Geotextiles. *Carbohydrate Polymers*, **82** (4), 2010, p. 1090–1096.

[104] The National Economic and Social Council of Kenya, (NESC): *Kenya's Vision 2030 (The Popular Version)*. Nairobi, Kenya: Government of Kenya, 2007.

[105] Thatoi, H.N., Panda, S.K., Rath, S.K. and Dutta, S.K.: Antimicrobial Activity and Ethnomedicinal Uses of Some Medicinal Plants from Similipal Biosphere Reserve, Orissa. *Asian Journal of Plant Sciences*, **7** (3), 2008, p. 260–267.

[106] Brown, K.: Agave Sisalana Perrine. *University of Florida Center for Aquatic and Invasive Plants*, **7922**, 2002, p. 18–21.

[107] Naik, R.K., Dash, R.C. and Goel, A.K.: Mechanical Properties of Sisal (A. Sisalana) Relevant to Harvesting and Fibre Extraction. *International Journal of Agricultural Engineering*, **6** (2), 2013, p. 423–426.

[108] Rajesh, D., Anandjiwala and Maya, J.: *Sisal – Cultivation, Processing and Products*. In: Industrial Applications of Natural Fibres: Structure, Properties and Technical Applications. West Sussex, England: John Wiley & Sons, 2010, p. 181–196.

[109] Garcia de Rodriguez, N.L., Thielemans, W. and Dufresne, A.: Sisal Cellulose Whiskers Reinforced Polyvinyl Acetate Nanocomposites. *Cellulose*, **13** (3), 2006, p. 261–270.

[110] Mukhopadhyay, S. and Srikanta, R.: Effect of Ageing of Sisal Fibres on Properties of Sisal – Polypropylene Composites. *Polymer Degradation and Stability*, **93** (11), 2008, p. 2048–2051.

[111] PKF Consulting Ltd, International Research Network: *Kenya's Sisal Industry*. Nairobi, Kenya: Export Processing Zone Authority, 2005.

[112] Munson, R.B.: *The Landscape of German Colonialism: Mt. Kilimanjaro and Mt. Meru, CA. 1890-1916*. Boston, USA: Boston University, 2005.

[113] Overton, J.: War and Economic Development: Settlers in Kenya, 1914– 1918. *The Journal of African History*, **27** (1), 1986, p. 79–103.

[114] Hartemink, A.E. and Wienk, J.F.: Sisal Production and Soil Fertility Decline in Tanzania. *International Soil Reference and Information Center*, **95** (8), 1995, p. 1–15.

[115] Yoshida, M.: Agricultural Marketing Reorganization in Post-war East Africa. *The Developing Economies*, **11** (3), 1973, p. 244–271.

[116] *Kenya Sisal Industry Act*. 1946, p. 32.

[117] Westcott, N.: The East African Sisal Industry, 1929–1949: The Marketing of a Colonial Commodity During Depression and War. *The Journal of African History*, **25**, 1984, p. 445–461.

[118] Phologolo, T., Yu, C., Mwasiagi, J.I., Nobert, M. and Li, Z.F.: Production and Characterization of Kenyan Sisal. *Asian Journal of Textile*, **2** (2), 2012, p. 17–25.

[119] Snyder, B.J., Bussard, J., Dolak, J. and Weiser, T.: A Portable Sisal Decorticator for Kenyan Farmers. *International Journal for Service Learning in Engineering, Humanitarian Engineering and Social Entrepreneurship*, **1** (2), 2006, p. 92–116.

[120] Müssig, J.: *Industrial Applications of Natural Fibres: Structure, Properties and Technical Applications*. West Sussex, England: John Wiley & Sons, 2010.

[121] Burgwin, W.A.: Notes from the High Level Sisal Research Station. *Kenya Sisal Board Bulletin*, **75**, 1971, p. 17–19.

[122] Pothan, L.A., Oommen, Z. and Thomas, S.: Dynamic Mechanical Analysis of Banana Fiber Reinforced Polyester Composites. *Composites Science and Technology*, **63** (2), 2003, p. 283–293.

[123] Hariharan, A.B. and Khalil, A.: Lignocellulose-based Hybrid Bilayer Laminate Composite: Part I – Studies on Tensile and Impact Behavior of Oil Palm Fiber–Glass Fiber-Reinforced Epoxy Resin. *Journal of Composite Materials*, **39** (8), 2005, p. 663–684.

[124] Saxena, M., Pappu, A., Sharma, A., Haque, R. and Wankhede, S.: *Composite Materials from Natural Resources: Recent Trends and Future Potentials*. In: Advances in Composite Materials - Analysis of Natural and Man-Made Materials. Rijeka, Croatia: InTech Open Access Books, 2011, p. 121–162.

[125] Mansor, M.R., Sapuan, S.M., Zainudin, E.S., Nuraini, A.A. and Hambali, A.: Stiffness Prediction of Hybrid Kenaf/Glass Fiber Reinforced Polypropylene Composites using

Rule of Mixtures (ROM) and Rule of Hybrid Mixtures (RoHM). *Journal of Polymer Materials*, **30** (3), 2013, p. 321–334.

[126] Chandramohan, D. and Bharanichandar, J.: Natural Fiber-Reinforced Polymer Composites for Automobile Accessories. *American Journal of Environmental Sciences*, **9** (6), 2013, p. 494–504.

[127] Zhu, J., Njuguna, J. and Abhyanka, H.: Recent Development of Flax Fibres and their Reinforced Composites based on Different Polymeric Matrices. *Materials*, **6** (11), 2013, p. 5171–5198.

[128] George, J., Sreekala, M.S. and Thomas, S.: A Review on Interface Modification and Characterization of Natural Fiber Reinforced Plastic Composites. *Polymer Engineering & Science*, **41** (9), 2001, p. 1471–1485.

[129] Karus, M., Kaup, M. and Ortmann, S.: Use of Natural Fibres in Composites in the German and Austrian Automotive Industry—Market Survey 2002. *Journal of Industrial Hemp*, **8** (2), 2003, p. 73–78.

[130] Rubin, E.: The Trabant: Consumption, Eigen-Sinn, and Movement. *History Workshop Journal*, **68** (1), 2009, p. 27–44.

[131] Wambua, P., Ivens, J. and Verpoest, I.: Natural Fibres: Can they Replace Glass in Fibre Reinforced Plastics? *Composites Science and Technology*, **63** (9), 2003, p. 1259–1264.

[132] Baker, A.F.: *Effects of the Use of Agave Juice in the Treatment of Seeds, Control of Spider Mite [Tetranychus urticae (Koch, 1836)] and Phytotoxicity in Cotton (Gossypium Hirsutum L. r. latifolium Hutch)*. Brazil: Federal University of Paraíba, 2003.

[133] Silveira, R.X., Chagas, A.C.S., Botura, M.B., Batatinha, M.J.M., Katiki, L.M., Carvalho, C.O., Bevilaqua, C.M.L., Branco, A., Machado, E.A.A., Borges, S.L. and Almeida, M.A.O.: Action of Sisal (Agave Sisalana, Perrine) Extract in the In-Vitro Development of Sheep and Goat Gastrointestinal Nematodes. *Experimental Parasitology*, **131** (2), 2012, p. 162–168.

[134] Muruke, M.H.S., Hosea, K.M., Pallangyo, A. and Heijthuijsen, J.H.F.G.: Production of Lactic Acid from Waste Sisal Stems Using a Lactobacillus Isolate. *Discovery and Innovation*, **18** (1), 2006, p. 5–10.

[135] Elisante, E. and Msemwa, V.: Dry Method for Preparation of Inulin Biomass as Feedstock for Ethanol Fermentation. *African Crop Science Journal*, **18** (4), 2010, p. 215–222.

[136] Damião Xavier, F., Santos Bezerra, G., Florentino Melo Santos, S., Sousa Conrado Oliveira, L., Luiz Honorato Silva, F., Joice Oliveira Silva, A. and Maria Conceição, M.: Evaluation of the Simultaneous Production of Xylitol and Ethanol from Sisal Fiber. *Biomolecules*, **8** (1), 2018, p. 2–15.

[137] Berger, J.: The World's major Fiber Crops, Their Cultivation and Manuring. *Centre Detude De L'azote*, **6**, 1969, p. 294.

[138] Wu, M., Sun, Z. and Zhao, X.: Effects of Different Modification Methods on the Properties of Sisal Fibers. *Journal of Natural Fibers*, **17** (7), 2020, p. 1048–1057.

[139] Khedari, J., Nankongnab, N., Hirunlabh, J. and Teekasap, S.: New Low-Cost Insulation Particleboards from Mixture of Durian Peel and Coconut Coir. *Building and Environment*, **39** (1), 2004, p. 59–65.

[140] Filho, T.D.R., Silva, A. de F., Fairbairn, E.M.R. and Filho, J.A.: Durability of Compression Molded Sisal Fiber Reinforced Mortar Laminates. *Construction and Building Materials*, **23** (6), 2009, p. 2409–2420.

[141] Barros, J.A.O., Silva, F. de A. and Toledo Filho, R.D.: Experimental and Numerical Research on the Potentialities of Layered Reinforcement Configuration of Continuous Sisal Fibers for Thin Mortar Panels. *Construction and Building Materials*, **102** (Part 1), 2016, p. 792–801.

[142] Ngala, W.O.: *The Mechanical Properties of Sisal Fibre Reinforced Composites of Epoxy Resin and Rice Husk Ash Pozzolanic Cement*. Nairobi, Kenya: University of Nairobi, 2001.

[143] Fonseca Coelho, A.W., da Silva Moreira Thiré, R.M. and Araujo, A.C.: Manufacturing of Gypsum–Sisal Fiber Composites using Binder Jetting. *Additive Manufacturing*, **29**, 2019, p. 100789.

[144] Jia, R., Wang, Q. and Feng, P.: A Comprehensive Overview of Fibre-Reinforced Gypsum-Based Composites (FRGCs) in the Construction Field. *Composites Part B: Engineering*, **205**, 2021, p. 108540.

[145] Abiola, O.S., Kupolati, W.K., Sadiku, E.R. and Ndambuki, J.M.: Utilisation of Natural Fibre as Modifier in Bituminous Mixes: A Review. *Construction and Building Materials*, **54**, 2014, p. 305–312.

[146] Danso, H., Martinson, D.B., Ali, M. and Williams, J.B.: Physical, Mechanical and Durability Properties of Soil Building Blocks Reinforced with Natural Fibres. *Construction and Building Materials*, **101**, 2015, p. 797–809.

[147] Namango, S.S.: *Development of Cost-Effective Earthen Building Material for Housing Wall Construction: Investigations into the Properties of Compressed Earth Blocks Stabilized with Sisal Vegetable Fibres, Cassava Powder and Cement Compositions*. Cottbus, Germany: Brandenburg Technical University, 2006.

[148] Mwaniki, A.: *Factors Affecting Sisal Cultivation and Adoption in Kiomo Division, Kitui County, Kenya*. Kitui County, Kenya: South Eastern Kenya University, 2018.

[149] Silva, A. de F., Chawla, N. and Filho, T.D.R.: Tensile Behavior of High Performance Natural (Sisal) Fibers. *Composites Science and Technology*, **68** (15–16), 2008, p. 3438–3443.

[150] Reddy, N. and Yang, Y.: Bio-fibers from Agricultural By-Products for Industrial Applications. *TRENDS in Biotechnology*, **23** (1), 2005, p. 22–27.

[151] Khalil, A.H.P.S., Alwani, S.M. and Omar, M.A.K.: Chemical Composition, Anatomy, Lignin Distribution, and Cell Wall Structure of Malaysian Plant Waste Fibers. *BioResources*, **1** (2), 2006, p. 220–232.

[152] Rong, Z.M., Zhang, Q.M., Liu, Y., Yang, C.G. and Zeng, M.H.: The Effect of Fiber Treatment on the Mechanical Properties of Unidirectional Sisal-Reinforced Epoxy Composites. *Composites Science and Technology*, **61** (10), 2001, p. 1437–1447.

[153] Oksman, K., Wallstrom, L., Berglund, A.L. and Filho, T.D.R.: Morphology and Mechanical Properties of Unidirectional Sisal–Epoxy Composites. *Journal of Applied Polymer Science*, **84** (13), 2002, p. 2358–2365.

[154] Foulk, J.A., Akin, D.E., Dodd, R.B. and McAlister III, D.D.: *Flax Fiber: Potential for a New Crop in the Southeast*. In: Trends in New Crops and New Uses (Editors: J. Janick and A. Whipkey). Alexandria, VA, USA: ASHS Press, 2002, p. 361–370.

[155] Jacquet, N., Quiévy, N., Vanderghem, C., Janas, S., Blecker, C., Wathelet, B., Devaux, J. and Paquot, M.: Influence of Steam Explosion on the Thermal Stability of Cellulose Fibres. *Polymer Degradation and Stability*, **96** (9), 2011, p. 1582–1588.

[156] Kukle, S., Grāvītis, J., Putniņa, A. and Stikute, A.: The Effect of Steam Explosion Treatment on Technical Hemp Fibres. *ETR*, **1**, 2015, p. 230.

[157] Wilson, P.I.: Sisal, Vol II. *Hard Fibres Research Series*, **8**, 1971, p. 618–653.

[158] Kuruvilla, J., Sabu, T. and Pavithran, C.: Effect of Chemical Treatment on the Tensile Properties of Short Sisal Fibre-Reinforced Polyethylene Composites. *Polymer*, **37** (23), 1996, p. 5139–5149.

[159] Rao, K.M.M. and Rao, K.M.: Extraction and Tensile Properties of Natural Fibers: Vakka, Date and Bamboo. *Composite Structures*, **77** (3), 2007, p. 288–295.

[160] Young, T.: An Essay on the Cohesion of Fluids. *Philosophical Society of the Royal Society of London*, **95**, 1805, p. 65–87.

[161] Schrader, M.E.: Young-Dupre Revisited. *Langmuir*, **11**, 1995, p. 3585–3589.

[162] Kaelble, D.H.: *Physical Chemistry of Adhesion*. Canada: John Wiley & Sons Canada, Ltd, 1971.

[163] Rubio-López, A., Olmedo, A., Díaz-Álvarez, A. and Santiuste, C.: *Parametric Study on the Manufacturing of Biocomposite Materials*. In: Natural Fibres: Advances in Science and Technology Towards Industrial Applications. Dordrecht, Netherlands: SpringerNature, 2016, p. 243–254.

[164] Merlini, C., Soldi, V. and Barra, G.M.O.: Influence of Fiber Surface Treatment and Length on Physico-Chemical Properties of Short Random Banana Fiber-Reinforced Castor Oil Polyurethane Composites. *Polymer Testing*, **30** (8), 2011, p. 833–840.

[165] Peng, X., Zhong, L., Ren, J. and Sun, R.: Laccase and Alkali Treatments of Cellulose Fibre: Surface Lignin and its influences on Fibre Surface Properties and Interfacial Behaviour of Sisal Fibre/Phenolic Resin Composites. *Composites Part A: Applied Science and Manufacturing*, **41** (12), 2010, p. 1848–1856.

[166] Bisanda, E.T.N. and Ansell, M.P.: The Effect of Silane Treatment on the Mechanical and Physical Properties of Sisal-Epoxy Composites. *Composites Science and Technology*, **41** (2), 1991, p. 165–178.

[167] Zhou, F., Cheng, G. and Jiang, B.: Effect of Silane Treatment on Microstructure of Sisal Fibers. *Applied Surface Science*, **292**, 2014, p. 806–812.

[168] Calvo-Flores, F.G. and Dobado, J.A.: Lignin as Renewable Raw Material. *ChemSusChem*, **3** (11), 2010, p. 1227–1235.

[169] Radu, C.D., Danila, A., Sandu, I., Muresan, I.E., Sandu, I.G. and Branisteanu, E.D.: Fibrous Polymers in Textile Prospect for Tissue Engineering Development. *Revista de Chimie*, **68** (6), 2017, p. 1345–1351.

[170] Brancato, A.A.: *Effect of Progressive Recycling on Cellulose Fibre Surface Properties*. Atlanta, Georgia, USA: Georgia Institute of Technology, 2008.

[171] Huber, T., Müssig, J., Curnow, O., Pang, S., Bickerton, S. and Staiger, M.P.: A Critical Review of all-Cellulose Composites. *J Mater Sci*, **47** (3), 2012, p. 1171–1186.

[172] Vanholme, R., Morreel, K., Ralph, J. and Boerjan, W.: Lignin engineering. *Current Opinion in Plant Biology*, **11** (3), 2008, p. 278–285.

[173] Sergio, N.M., Felipe, P.D.L., Anderson, P.B., Bevitori, A.B., da Silva, I.L.A. and Da Costa, L.L.: Natural Lignocellulosic Fibers as Engineering Materials - An Overview. *Metallurgical and Materials Transactions A*, **42A**, 2011, p. 2963–2974.

[174] Wallenberger, F.T. and Weston, N. eds.: *Natural Fibers with Low Moisture Sensitivity*. In: Natural Fibers, Plastics and Composites. Dordrecht, Netherlands: Kluwer Academic Publishers, 2004, p. 105–122.

[175] Ebringerová, A.: Structural Diversity and Application Potential of Hemicelluloses. *Macromolecular Symposia*, **232** (1), 2005, p. 1–12.

[176] Kalia, S., Kaith, B.S. and Kaur, I.: Pre-Treatments of Natural Fibers and their Application as Reinforcing Material in Polymer Composites-A Review. *Polymer Engineering and Science*, **49** (7), 2009, p. 1253–1272.

[177] Claramunt, J., Ardunay, M. and García-Hortal, J.A.: Effect of Drying and Rewetting Cycles on the Structure and Physicochemical Characteristics of Softwood Fibres for Reinforcement of Cementitious Composites. *Carbohydrate Polymers*, **79** (1), 2010, p. 200–205.

[178] Tarbuk, A., Grancaric, A.M. and Leskovac, M.: Novel Cotton Cellulose by Cationisation during the Mercerisation Process—part 1: Chemical and Morphological Changes. *Cellulose*, **21** (3), 2014, p. 2167–2179.

[179] Poletto, M., Ornaghi, H.L. and Zattera, A.J.: Native Cellulose: Structure, Characterization and Thermal Properties. *Materials*, **7** (9), 2014, p. 6105–6119.

[180] Zugenmaier, P.: *Crystalline Cellulose and Cellulose Derivatives - Characterization and Structures*. Berlin, Germany: Library of Congress, 2008.

[181] Calado, V., Barreto, D.W. and Doalmeida, J.R.M.: The Effect of a Chemical Treatment on the Structure and Morphology of Coir Fibers. *Journal of Materials Science Letters*, **19** (23), 2000, p. 2151–2153.

[182] Gan˜an, P., Garbizu, S., Llano-Ponte, R. and Mondragon, I.: Surface Modification of Sisal Fibers: Effects on the Mechanical and Thermal Properties of their Epoxy Composites. *Polymer Composites*, **26** (2), 2005, p. 121–127.

[183] Okano, T. and Sarko, A.: Mercerization of Cellulose. 11. Alkali Cellulose Intermediates and a Possible Mercerization Mechanism. *Journal of Applied Polymer Science*, **30** (1), 1985, p. 325–332.

[184] Chen, J.-C. and Chen, C.-C.: Crosslinking of Cotton Fabrics Premercerized with Different Alkalis Part IV: Crosslinking of Normal Length Mercerized Fabrics. *Textile Research Journal*, **64** (3), 1994, p. 142–148.

[185] Hedrick, J.L., Yilgor, I., Jurek, M., Hedrick, J.C., Wilkes, G.L. and McGrath, J.E.: Chemical Modification of Matrix Resin Networks with Engineering Thermoplastics: 1. Synthesis, Morphology, Physical Behaviour and Toughening Mechanisms of Poly (Arylene Ether Sulphone) Modified Epoxy networks. *Polymer*, **32** (11), 1991, p. 1–13.

[186] Stevulova, N., Estokova, A., Cigasova, J., Schwarzova, I., Kacik, F. and Greffert, A.: Thermal Degradation of Natural and Treated Hemp Hurds under Air and Nitrogen Atmosphere. *Journal of Thermal Analysis and Calorimetry*, **128** (3), 2017, p. 1649–1660.

[187] Santos, S.F., Tonoli, G.H.D., Mejia, J.E.B., Fiorelli, J. and Savastano, H.: Non-Conventional Cement-Based Composites Reinforced with Vegetable Fibers: A Review

of Strategies to Improve Durability. *Materiales de Construcción*, **65** (317), 2015, p. 1–20.

[188] Kurdowski, W.: *Cement and Concrete Chemistry*. New York, USA: Springer Dordrecht Heidelberg, 2014.

[189] Majumdar, A.J. and Nurse, R.W.: Glass Fibre Reinforced Cement. *Materials Science and Engineering*, **15** (2–3), 1974, p. 107–127.

[190] Florea, M.V.A. and Brouwers, H.J.H.: Chloride Binding Related to Hydration Products. *Cement and Concrete Research*, **42** (2), 2012, p. 282–290.

[191] Scheirs, J. and Long, T.: *Modern Polyesters: Chemistry and Technology of Polyesters and Copolyesters*. West Sussex, England: John Wiley & Sons. Inc, 2003.

[192] Saleh, H.E.-D.M.: *Polyester*. Rijeka, Croatia: InTech, 2012.

[193] Jensen, J.: *SPI Composites Institute's 45th Annual Conference*. In: Technical Sessions of the 45th Annual Conference Composites Instititute. New York, USA, 1990.

[194] Pasdar, H. and Mohseni, M.: Mechanical Properties of Unsaturated Polyester Resin. *International Journal of ChemTech Research*, **2** (4), 2010, p. 2113–2117.

[195] Atkins, K.: *Low Profile Additives: Shrinkage Control Mechanisms and Applications*. Munich, Germany: Hanser Publishers, 1993.

[196] Ghafaar, M.A., Mazen, A.A. and El-Mahallawy, N.A.: Application of the Rule of Mixtures and Halpin-Tsai Equations to Woven Fabric Reinforced Epoxy Composites. *Journal of Engineering Sciences, Assiut University*, **34** (1), 2006, p. 227–236.

[197] Rangaraj, S.S. and Bhaduri, S.B.: A Modified Rule-of-Mixtures for Prediction of Tensile Strengths of Unidirectional Fibre-Reinforced Composite Materials. *Journal of Materials Science*, **29** (10), 1994, p. 2795–2800.

[198] Stang, H., Li, V.C. and Krenchel, V.: Design and Structural Applications of Stress-Crack Width Relations in Fibre Reinforced Concrete. *Materials and Structures*, **28** (4), 1995, p. 210–219.

[199] Jacob, M., Thomas, S. and Varughese, K.T.: Mechanical Properties of Sisal/Oil Palm Hybrid Fiber Reinforced Natural Rubber Composites. *Composites Science and Technology*, **64** (7–8), 2004, p. 955–965.

[200] Chand, N. and Jain, D.: Effect of Sisal Fiber Orientation on Electric Properties of Sisal Fiber Reinforced Epoxy Composites. *Composites Part A: applied science and manufacturing*, **36** (5), 2005, p. 594–602.

[201] Amor, I.B., Rekik, H., Kaddami, H., Raihane, M., Arous, M. and Kallel, A.: Effect of Palm Tree Fiber Orientation on Electrical Properties of Palm Tree Fiber-reinforced Polyester Composites. *Journal of Composite Materials*, **44** (13), 2010, p. 1553–1568.

[202] Atiqah, A., Jawaid, M., Ishak, M.R. and Sapuan, S.M.: Effect of Alkali and Silane Treatments on Mechanical and Interfacial Bonding Strength of Sugar Palm Fibers with Thermoplastic Polyurethane. *Journal of Natural Fibers*, **15** (2), 2018, p. 251–261.

[203] Silva, F. de A., Mobasher, B., Soranakom, C. and Filho, T.D.R.: Effect of Fiber Shape and Morphology on Interfacial Bond and Cracking Behaviors of Sisal Fiber Cement Based Composites. *Cement and Concrete Composites*, **33**, 2011, p. 814–823.

[204] Dyczek, J.R.L. and Petri, M.A.: *27 POLYPROPYLENE FRC: FIBER-MATRIX BOND STRENGTH*. In: Fibre Reinforced Cement and Concrete: Proceedings of the Fourth International Symposium Held by RILEM (the International Union of Testing and Research Laboratories for Materials and Structures) and Organized by the Department of Mechanical and Process Engineering, University of Sheffield, UK, Sheffield, July 20-23, 1992. Taylor & Francis, 1992, p. 324.

[205] Azeez, T.O., Onukwuli, D.O., Nwabanne, J.T. and Banigo, A.T.: Cissus Populnea Fiber - Unsaturated Polyester Composites: Mechanical Properties and Interfacial Adhesion. *Journal of Natural Fibers*, **17** (9), 2020, p. 1281–1294.

[206] Proctor, B.A.: Tensile Stress-Strain Behaviour of Glass Fibre Reinforced Cement Composites. *Journal of Materials Science*, **21** (7), 1986, p. 2441–2448.

[207] Laws, V. and Ali, M.A.: *Paper 13. The Tensile Stress/Strain Curve of Brittle Matrices Reinforced with Glass Fibre*. In: FIBRE REINFORCED MATERIALS: design & engineering applications. Garston, Liverpool, United Kingdom: Thomas Telford Publishing, 1977, p. 115–123.

[208] Gray, R.J.: *Fiber-Matrix Bonding in Steel Fiber-Reinforced Cement-Based Composites*. In: Fracture Mechanics of Ceramics (Editors: R. C. Bradt A. G. Evans D. P. H. Hasselman and F. F. Lange). Boston, MA: Springer US, 1986, p. 143–155.

[209] Aveston, J.: Single and Multiple Fracture. *The properties of fiber composites*, 1972, p. 15–26.

[210] Mwaikambo, Y.L. and Ansell, P.M.: Chemical Modification of Hemp, Sisal, Jute, and, Kapok Fibers by Alkalization. *Journal of Applied Polymer Science*, **84** (12), 2002, p. 2222–2234.

[211] C27.40: *ASTM C948-81 Standard Test Method for Dry and Wet Bulk Density, Water Absorption, and Apparent Porosity of Thin Sections of Glass-Fiber Reinforced Concrete*. 100 Barr Harbor Dr., West Conshohocken, PA 19428, 1994.

[212] Inacio, W.P., Lopes, F.P.D. and Monteiro, S.N.: Diameter Dependence of Tensile Strength by Weibull Analysis: Part III Sisal Fiber. *Revista Matéria*, **15** (2), 2010, p. 124–130.

[213] Poudel, K.P. and Cao, Q.V.: Evaluation of Methods to Predict Weibull Parameters for Characterizing Diameter Distributions. *Forest Science*, **59** (2), 2013, p. 243–252.

[214] Soykeabkaew, N., Supaphol, P. and Rujiravanit, R.: Preparation and Characterisation of Jute and Flax-Reinforced Starch-Based Composite Foams. *Carbohydrate Polymers*, **58** (1), 2004, p. 53–63.

[215] Kiruthika, A.V. and Veluraja, K.: Physical Properties of Plant Fibers (Sisal, Coir) and its Composite Material with Tamarind Seed Gum as Low-Cost Housing Material. *Journal of Natural Fibers*, 2017, p. 1–13.

[216] Denise, C. de O.N.F., Ailton da Silva, F. and Sergio, N.M.: Weibull Analysis of Tensile Tested Piassava Fibers with Different Diameters. *Revista Matéria*, **23** (4), 2018, p. 1–8.

[217] Jouannot-Chesney, P., Jernot, J.-P., Bréard, J. and Gomina, M.: *Young's Modulus of Plant Fibers*. In: Natural Fibres: Advances in Science and Technology Towards Industrial Applications. Dordrecht, Netherlands: SpringerNature, 2016, p. 61–69.

[218] Monteiro, S.N., Satyanarayana, K.G. and Lopes, F.P.D.: High Strength Natural Fibers for Improved Polymer Matrix Composites. *Materials Science Forum*, **638–642**, 2010, p. 961–966.

[219] Chand, N. and Hashmi, S.A.R.: Mechanical Properties of Sisal Fibre at Elevated Temperatures. *Journal of Materials Science*, **28** (24), 1993, p. 6724–6728.

[220] *Hounsfield Tensometer (Type W)*. CR9 6HG. Croydon, United Kingdom: Tensometer Ltd, Machine Manual.

[221] *FCE 245 - Materials Science for Civil Engineers. Tensile Test using a Hounsfield Tensometer*. Department of Civil and Construction Engineering, University of Nairobi, Laboratory Procedure.

[222] Masudur, R.A., Kashif, S.M. and Razzak, A.: Tensile and Statistical Analysis of Sisal Fibers for Natural Fiber Composite Manufacture. *Advanced Materials Research*, **1115**, 2015, p. 349–352.

[223] Lingyan, S., Dongfang, W. and Yongdan, L.: Optimal Probability Estimators for Determining Weibull Parameters. *Journal of Materials Science Letters*, **22** (23), 2003, p. 1651–1653.

[224] Nwobi, F.N. and Ugomma, C.A.: A Comparison of Methods for the Estimation of Weibull Distribution Parameters. *Metodološki zvezki*, **11** (1), 2014, p. 65–78.

[225] *BS 882:1992 British Standard Specification for Aggregates from Natural Sources for Concrete*. 389 Chiswick High Road, London, W4 4AL, 1992, p. 4–5.

[226] Johansen, I.: *Graph, Plotting of Mathematical Functions*. Open Source: GNU, General Public License (GPL), 2012.

[227] *BS 181-122:2011 Testing Concrete. Method for Determination of Water Absorption*. 389 Chiswick High Road, London, W4 4AL, 2011, p. 3.

[228] C09.66: *ASTM C 642-13 Standard Test Method for Density, Absorption and Voids in Hardened Concrete*. West Conshohocken, PA, 2013, p. 3.

[229] C09: *ASTM C 293-02 Standard Test Method for Flexural Strength of Concrete (Using Simple Beam with Centre-Point Loading)*. West Conshohocken, PA, 2002, p. 3.

[230] *BS 2782-3: Methods 320A to 320F:1976 Methods of Testing Plastics Mechanical Properties, Tensile Strength, Elongation and Elastic Modulus (AMD 8057)*. 389 Chiswick High Road, London, W4 4AL, 1976, p. 18.

[231] Weibull, W.: A statistical Distribution function of Wide Applicability. *Journal of Applied Mechanics*, **18** (3), 1951, p. 293–297.

[232] Hertzberg, R., Vinci, R. and Hertzberg, J.: *Deformation and Fracture Mechanics of Engineering Materials*. New York, USA: John Wiley & Sons. Inc, 2020.

[233] Mukherjee, R.R. and Radhakrishnan, T.: Long Vegetable Fibres. *Textile Progress*, **4** (4), 1972, p. 1–75.

[234] Marwa, A.A.E.-B., Mona, M., Hend, H.E.-S. and Amal, E.A.: Mechanical Properties Evaluation of Sugarcane Bagasse-Glass/Polyester Composites. *Journal of Natural Fibers*, 2019.

[235] Seshan, S., Guruprasad, A., Prabha, M. and Sudhakar, A.: Fibre-reinforced Metal Matrix Composites - a review. *Journal of the Indian Institute of Science*, **76** (1), 2013, p. 1–1.

[236] Swift, D.G. and Smith, R.B.L.: The Flexural Strength of Cement Based Composites using Low Modulus (Sisal) Fibes. *Composites*, **10** (3), 1979, p. 145–148.

[237] Kirima, C.C.M.: *The Mechanical Properties of Sisal Fibre reinforced Mortar*. Nairobi: University of Nairobi, 1995.

[238] Satyanarayana, K.G., Sukumaran, A.G., Kulkarni, S.G.K. and Rohatgi, P.K.: Fabrication and Properties of Natural Fibre-Reinforced Polyester Composites. *Composites*, **17** (4), 1986, p. 329–333.

[239] Melkamu, A., Mulu, B.K. and Abrha, G.T.: Mechanical and Water-Absorption Properties of Sisal Fiber (Agave Sisalana)-Reinforced Polyester Composite. *Journal of Natural Fibers*, **16** (6), 2019, p. 877–885.

[240] Marom, G., Fischer, S., Tuler, F. and Wagner, D.: Hybrid Effects in Composites: Conditions for Positive or Negative Effects versus Rule-of-Mixtures Behaviour. *Journal of Materials Science*, **13** (7), 1978, p. 1419–1426.

[241] Kinkellar, M.R.: *Dilatometric Study of Low Profile Unsaturated Polyester Resins*. Ohio, USA: The Ohio State University, 1993.

[242] C03: *ASTM 1505-03 Standard Test Methods for Density of Plastics by the Density-Gradient Technique*. West Conshohocken, PA, 2005.

[243] Rude, T.J., Strait, L.H. and Ruhala, L.A.: Measurement of Fibre Density by Helium Pycnometry. *Journal of Composite Materials*, **34** (22), 2000, p. 1948–1958.

[244] Abd El-Baky, M.A., Megahed, M., El-Saqqa, H.H. and Alshorbagy, A.E.: Mechanical Properties Evaluation of Sugarcane Bagasse-Glass/ Polyester Composites. *Journal of Natural Fibers*, **18** (8), 2019, p. 1–18.

APPENDICES

APPENDIX A – SISAL FIBRE

Table A1: Absorbency test results for untreated fibres, mercerised fibres and cornified sisal fibres

	Untreated sisal fibres mass (grams)			**Mercerized sisal fibres mass (grams)**			**Cornified Sisal fibres mass (grams)**		
Dry sample mass	49.1	50.2	49.98	51	50.5	49.9	49.8	49.6	51.2
Wet mass	128.1	131	130	142.4	140.3	138.1	138.5	138.2	141.9
Mass (after 1hr)	54.4	56.22	55.65	51.6	51.2	50.52	60	60.25	62.08
Mass (after 2 hrs)	47.1	50.2	48.02	50.95	50.9	49.8	49.25	49.4	51.83
Mass (after 3 hrs)	47.1	48.05	47.65	50.95	50.45	49.8	48.82	49	50.5
Mass (after 4 hrs)	-	48.05	47.65	-	50.45	-	48.82	49	50.5
% change in dry mass	**-4.073**	**-4.28**	**-4.66**	**-0.1**	**-0.1**	**-0.2**	**-1.97**	**-1.21**	**-1.37**
Mean % change in dry mass	**-4.34 (STDEV 0.298)**			**-0.13 (STDEV 0.058)**			**-1.52 (STDEV 0.401)**		
% moisture absorption	**171.8**	**172.63**	**172.82**	**179.49**	**178.1**	**177.31**	**183.7**	**182.04**	**180.99**
Mean % moisture absorption	**172.48 (SDV 0.44)**			**178.3 (SDV 1.10)**			**182.24 (SDV 1.37)**		

Table A2: Butt-end and mid-span diameters of untreated sisal fibres

Butt-end Diameter (µm)	Mid-span Diameter (µm)
245.8	186.1
207.76	155.2
262.1	188.75
196.52	228.5
280.4	186.45
254.04	148.7
332.28	150.4
308.98	178.9
257.6	182.8
292.46	160.9
258.9	261.2
287.74	161.2
342.1	193.1
289	189.2
396.8	166.7
286.52	183.61
279	204.1
306.5	196.3
271.8	179.2
229.98	219.1

Table A3: Untreated sisal fibre diameter Weibull analysis.

WEIBULL ANALYSIS OF UNTREATED SISAL FIBRE DIAMETER											
RANK	DIA	F VALUE	Ln(1/(1-F))	X value	Y value	RANK	DIA	F VALUE	Ln(1/(1-F))	X value	Y value
1	148.7	0.0125	0.01257878	5.00193085	-4.3757438	22	229.98	0.5375	0.771108722	5.4379923	-0.259925901
2	150.4	0.0375	0.03822121	5.01329841	-3.2643646	23	245.8	0.5625	0.826678573	5.5045182	-0.190339326
3	155.2	0.0625	0.06453852	5.04471461	-2.740493	24	254.04	0.5875	0.885519073	5.5374917	-0.121581283
4	160.9	0.0875	0.09156719	5.08078305	-2.3906822	25	257.6	0.6125	0.94803943	5.551408	-0.053359185
5	161.2	0.1125	0.11934676	5.08264583	-2.1257221	26	258.9	0.6375	1.014730805	5.5564419	0.01462336
6	166.7	0.1375	0.14792013	5.11619579	-1.9110828	27	261.2	0.6625	1.086189769	5.5652864	0.082675947
7	178.9	0.1625	0.17733402	5.18682699	-1.7297202	28	262.1	0.6875	1.16315081	5.5687261	0.151132538
8	179.2	0.1875	0.20763936	5.1885025	-1.5719525	29	271.8	0.7125	1.246532419	5.6050665	0.220365631
9	182.8	0.2125	0.23889191	5.20839266	-1.4317441	30	279	0.7375	1.337504197	5.6312118	0.290805338
10	183.61	0.2375	0.27115277	5.21281394	-1.3050729	31	280.4	0.7625	1.437587656	5.6362172	0.36296647
11	186.1	0.2625	0.30448919	5.22628416	-1.1891197	32	286.52	0.7875	1.548813291	5.6578083	0.437489019
12	186.45	0.2875	0.33897537	5.22816311	-1.0818278	33	287.74	0.8125	1.673976434	5.6620573	0.515201894
13	188.75	0.3125	0.37469345	5.24042339	-0.9816471	34	289	0.8375	1.817077277	5.6664267	0.597229319
14	189.2	0.3375	0.41173472	5.24280466	-0.887376	35	292.46	0.8625	1.984131362	5.6783279	0.685181217
15	193.1	0.3625	0.450201	5.26320819	-0.7980611	36	306.5	0.8875	2.184802057	5.7252178	0.781525233
16	196.3	0.3875	0.49020634	5.2796441	-0.7129289	37	308.98	0.9125	2.436116486	5.7332765	0.890405167
17	196.52	0.4125	0.53187903	5.28076421	-0.6313392	38	332.28	0.9375	2.772588722	5.805978	1.019781441
18	204.1	0.4375	0.57536414	5.31861007	-0.5527521	39	342.1	0.9625	3.283414346	5.8351031	1.18888384
19	207.76	0.4625	0.62082652	5.33638357	-0.4767036	40	396.8	0.9875	4.382026635	5.9834324	1.477511319
20	219.1	0.4875	0.66845457	5.38952825	-0.4027868						
21	228.5	0.5125	0.71846499	5.43153621	-0.3306383						
	Scale(D_o)	shape(m)	mean	Variance	Stdev						
	254.45427	4.665	232.694344	3223.82803	56.7787639						
			Excel command								
Mean diameter	{=D_o*EXP(GAMMALN(1+1/m))}										
Variance	{=(D_o^2)*(EXP(GAMMALN(1+2/m))EXP(GAMMALN(1+1/m))^2)}										
Standard Dev	{=SQRT((D_o^2)*(EXP(GAMMALN(1+2/m))EXP(GAMMALN(1+1/m))^2))}										

Table A4: Density test results

No. of Fibre Strands in Bunch	Weight. of Fibre Bunch (gm)	Vol. of Fibres (cm^3)	Calculated Fibre Density (g/cm^3)
100	56.61	42.52	1.331
	57.42		1.35
	57.85		1.36
120	66.84	5.102	1.31
	62.67		1.228
	64.71		1.268
150	82.35	6.378	1.291
	87.98		1.379
	79.8		1.251
200	111.85	8.503	1.315
	105.63		1.242
	108.62		1.277

Untreated, Mercerised and Cornified Sisal Fibres Fracture Stress Analysis

Table A5: Fracture stress results - untreated sisal fibres

No. of fibre Strands	Cross-sectional Area ($x10^{-7} m^2$)	Breaking Load (N)	Fracture Stress, ($x10^6 Nm^{-2}$)	Fracture Strain (%)	Young's Modulus, ($x10^9 Nm^{-2}$)
15	6.38	65.022	101.955	2.356	4.33
		100.33	157.325	4.65	3.38
		94.71	148.45	4.15	3.58
	8.503	151.56	178.225	5.02	3.55
20		156.16	183.658	4.865	3.78
		123.517	145.263	4.346	3.34
30	12.76	169.45	132.85	2.71	4.9
		182.42	142.96	4.15	3.45
		205.89	161.416	4.95	3.26
40	17.01	340.14	200	5.71	3.5
		322.44	189.56	5.29	3.58
		197.72	116.258	3.624	3.21
90	38.27	583.41	152.446	5.25	2.9
		670.58	175.224	4.148	4.22
		652.31	170.45	4.24	3.45
120	51.02	933.31	182.93	4.922	3.72
		880.42	172.563	4.496	3.84
		858.82	168.33	5.152	3.27
	76.53	1325.7	173.226	5.368	3.23
180		1274.45	166.529	4.217	3.95
		1204.32	157.365	5.105	3.08

Table A6: Fracture stress results - mercerised sisal fibres

No. of fibre Strands	Cross-sectional Area($x10^{-7} m^2$)	Breaking Load (N)	Fracture Stress, ($x10^6 Nm^{-2}$)	Fracture Strain (%)	Young's Modulus, ($x10^9 Nm^{-2}$)
15	6.38	179.24	280.935	3.759	7.47
		169.12	265.082	5.652	4.69
		170.08	266.58	5.448	5.18
20	8.5	157.6	185.415	5.275	4.56
		239.38	281.628	5.113	5.51
		181.99	214.104	4.615	4.64
	12.76	368.45	288.753	4.944	5.84
30		373.9	293.018	5.836	5.02
		321.12	251.662	5.164	4.87
60	25.51	721.81	282.953	5.797	4.88
		688.43	269.868	7.656	3.53
		652.1	255.625	4.63	5.52
90	38.27	1300.17	339.736	5.978	5.68
		1012.4	264.54	5.21	5.08
		1117.08	291.895	6.792	4.3
120	51.02	1875	367.5	6.604	5.57
		1116	218.732	4.52	4.84
		1283.78	251.622	5.941	4.24
	76.53	2176.06	284.341	5.606	5.07
180		1933.68	252.669	5.948	4.25
		1849.85	241.716	5.072	4.77

Table A7: Fracture stress results - cornified sisal fibres

No. of fibre Strands	Cross-sectional Area ($x10^{-7} m^2$)	Breaking Load (N)	Fracture Stress, ($x10^6 Nm^{-2}$)	Fracture Strain (%)	Young's Modulus, ($x10^9 Nm^{-2}$)
15	6.38	112.54	176.401	5.278	3.34
		116.16	182.064	4.9	3.72
		119.25	186.917	4.41	4.24
20	8.5	122.17	143.734	2.083	6.9
		126	148.24	3.185	4.65
		137.73	162.028	3.516	4.61
30	12.76	232.49	182.202	4.995	3.65
		217.25	170.259	5.376	3.17
		272.42	213.483	4.879	4.38
60	25.51	437.63	171.552	5.113	3.36
		401.58	157.421	4.68	3.36
		591.52	231.878	6.552	3.54
90	38.27	1325.17	346.269	7.5	4.62
		914.48	238.955	6.362	3.76
		1041.97	272.269	6.224	4.38
120	51.02	1141.9	223.816	5.935	3.77
		1062.34	208.221	5.097	4.09
		859.52	168.467	3.937	4.23
180	76.53	1200	156.801	5.583	2.81
		1549.52	202.472	4.923	4.11
		1500	196.002	5.884	3.33

Table A8: Fracture stress Weibull analysis - untreated, mercerised and cornified sisal fibres

RANK	Stress(Native)	Stress(Merc	Stress(Corn)	X(Native)	X(mercerized)	X(Cornified)	F Value	Ln (1/(1-F))	LnLn(1/(1-F))
1	101.955	280.935	176.401	4.62453154	5.638123326	5.172759812	0.023809524	0.024097552	-3.72564504
2	116.258	185.415	143.734	4.75581186	5.222596556	4.967964369	0.071428571	0.074107972	-2.60223217
3	132.85	214.104	148.24	4.88922067	5.366461878	4.998832582	0.119047619	0.126751706	-2.06552518
4	142.96	218.732	156.801	4.96256487	5.387847236	5.054977485	0.166666667	0.182321557	-1.70198336
5	145.263	241.716	157.421	4.97854589	5.487763483	5.058923745	0.214285714	0.241162057	-1.42228614
6	148.45	251.622	162.028	5.0002482	5.527927961	5.08776916	0.261904762	0.303682414	-1.19177282
7	152.446	251.662	168.467	5.02681043	5.528086917	5.126739885	0.30952381	0.370373788	-0.99324254
8	157.325	252.669	170.259	5.05831373	5.532080332	5.137320807	0.357142857	0.441832752	-0.81682386
9	157.365	255.625	171.552	5.05856795	5.543711527	5.144886428	0.404761905	0.518793793	-0.65624879
10	161.416	264.54	182.064	5.08398488	5.577992469	5.204358274	0.452380952	0.602175402	-0.50720651
11	166.529	265.082	182.202	5.11516947	5.580039212	5.205115962	0.5	0.693147181	-0.36651292
12	168.33	266.58	186.917	5.12592634	5.585674386	5.230664668	0.547619048	0.793230639	-0.23164126
13	170.45	269.868	196.002	5.138442	5.597932951	5.278124863	0.595238095	0.904456274	-0.10042132
14	172.563	281.628	202.472	5.15076239	5.640587051	5.310601605	0.642857143	1.029619417	0.029189236
15	173.226	282.953	208.221	5.1545971	5.645280806	5.338600016	0.69047619	1.172720261	0.159326059
16	175.224	284.341	213.483	5.16606516	5.650174222	5.363557204	0.738095238	1.339774345	0.292501201
17	178.225	288.753	223.816	5.1830468	5.665571651	5.410824286	0.785714286	1.540445041	0.432071362
18	182.93	291.895	231.878	5.20910357	5.676394149	5.446211371	0.833333333	1.791759469	0.583198081
19	183.658	293.018	238.955	5.21307533	5.680234041	5.47627525	0.880952381	2.128231706	0.75529145
20	189.56	339.736	272.269	5.2447056	5.828168845	5.606790548	0.928571429	2.63905733	0.970421781
21	200	367.5	346.269	5.29831737	5.906723319	5.84721593	0.976190476	3.737669618	1.318462321

	shape(m)	scale(σ_o)	mean	Variance	Stdev
Native	7.615869903	171.4	161.024251	625.6994085	25.01398426
Mercerised	6.175115068	291.65	270.998403	2615.048551	51.13754541
Cornified	4.722865878	216.98	198.566856	2295.421086	47.91055298

	Output Commands:	
Fibre mean strength	{=σo*EXP((GAMMALN(1+1/m)))}	
Variance	{=((σo^2)*(EXP(GAMMALN(1+2/m))-EXP(GAMMALN(1+1/m))^2))}	
Fibre strength Stdev	{=SQRT((σo^2)*(EXP(GAMMALN(1+2/m))-EXP(GAMMALN(1+1/m))^2))}	

APPENDIX B – SISAL FIBRE-REINFORCED COMPOSITE RESULTS AND DATA ANALYSIS

Table B1(a): Acid method of determination of sand/cement ratio in mortar results

Filter paper weight (grams)		Sample Initial Weight (grams)	Final Weight (grams)	% fine aggregate	
1.013		100	75.421	74.415	
0.985		100	74.891	73.885	
0.996		100	76.065	75.059	
1.013				**74.453**	**Average**
1.005				**0.587921764**	**STDEV**
0.998					
1.003					
1.016					
1.004					
1.029					
1.0062	**Average**				
0.012227474	**STDEV**				

Table B1(b): Mortar moisture content results

Sample Initial Weight (grams)	Final Weight (grams)	% Moisture	
100	86.139	13.861	
100	86.008	13.992	
100	86.557	13.443	
		13.76533333	**Average**
		0.286730419	**STDEV**

Table B 1(c): Results of density and water absorption tests of continuous fibre-reinforced Mortar

	% V_f	Density (gcm^{-3})	$\%W_a$	$\%V_v$
Untreated	0	2.25	3.09	6.95
	1	2.246	3.26	7.32
	2	2.194	4.1	9
	3	2.182	4.14	9.03
	4	2.107	4.87	10.26
	5	2.083	5.34	11.12
	6	2.002	6.17	12.35
	7	1.961	8.92	17.46
Mercerised	1	2.245	3.01	6.76
	2	2.226	3.3	7.35
	3	2.208	3.81	8.42
	4	2.193	4.07	8.93
	5	2.171	4.47	9.7
	6	2.083	5.12	10.67
	7	2.001	5.84	11.69
Cornified	1	2.359	2.71	6.88
	2	2.212	3.39	7.49
	3	2.163	3.98	8.61
	4	2.11	4.47	9.44
	5	2.007	5.27	10.57
	6	2.033	5.75	11.69

Table B1(d): River sand sieve analysis

Sample Type River Sand	**FINE AGGREGATES-ROCK SAND**		
Sample source: Jamuhuri			
Client		**Project MSc.**	
Test date: 01.01.2018		**Sample No.1**	
Specification	BS882:1992 TABLE4 & 6		

Pan mass	(gm)	134.7		
Initial dry sample mass + pan	(gm)	363.1		
Initial dry sample mass	(gm)	228.4	Fine mass (gm)	21.3
Washed dry sample mass + pan	(gm)	341.8	Fine percent (%)	9.3
Washed dry sample mass	(gm)	207.1	Acceptance Criteria (%)	

Sieve size (mm)	Retained mass (gm)	% Retained (%)	Cumulative passed percentage (%)	Acceptance Criteria	
				Min(%)	Max (%)
14	0	**0.0**	**100.0**	**100**	
10	0	**0.0**	**100.0**	**100**	
4.76	2.2	**1.0**	**99.0**	**89**	**100**
2.36	1.6	**0.7**	**98.3**	**60**	**100**
1.18	5.7	**2.5**	**95.8**	**30**	**100**
0.6	28.2	**12.3**	**83.5**	**15**	**100**
0.3	80.6	**35.3**	**48.2**	**5**	**70**
0.15	69.3	**30.3**	**17.9**	**0**	**15**
0.075	16.6	**7.3**	**10.6**	**0**	**3**
	204.2				

Untreated Sisal CFRC of Mortar

Table B2: Flexural results data - untreated sisal CFRC of mortar

		Flexural Test Results for Continuous Untreated Sisal Fibre-Reinforced OPC Mortar Beams (100x100x500) mm								
Specimen ID #	Breadth (mm)	Depth (mm)	Length (mm)	Average Weight of embedded fibres (grams)	Fibre volume fraction (%)	Mean Fibre Volume fraction (%)	Ultimate Flexural Load (KN)	Ultimate Flexural Strength (MN/m^2)	Mean Flexural Strength (MN/m^2)	Standard Deviation (MN/m^2)
UNR	103	102	503				9.4	3.95		
ABC	104	101	500	0	0	0	9.8	4.17	3.99	0.164
XXX	104	105	504				9.8	3.85		
A1	106	103	500		0.451		11.2	4.48		
A1	105	101	502	32.03	0.463	0.455	11.4	4.79	4.7	0.188
A1	106	102	505		0.451		11.8	4.82		
A	104	101	500		0.954		15.8	6.7		
A	103	104	501	65.13	0.934	0.928	15.6	6.3	6.36	0.319
A	107	104	502		0.897		15.6	6.07		
B12	106	103	505		1.369		18.6	7.44		
B1	104	95	500	98.1	1.528	1.445	18.5	8.87	8.39	0.82
B1	106	98	505		1.439		20	8.85		
B	102	105	505		1.854		19.2	7.68		
B	106	104	506	130.33	1.797	1.822	20	7.85	7.66	0.196
B	106	104	501		1.815		19	7.46		
C1	105	104	505		2.267		15	5.94		
C1	106	105	505	162.5	2.224	2.26	18.6	7.16	6.9	0.86
C1	104	104	500		2.289		19	7.6		
C	104	103	506		2.77		15.6	6.36		
C	106	103	504	195.2	2.729	2.739	15.8	6.32	6.23	0.186
C	105	104	506		2.718		15.2	6.02		
D	104	105	501	261.2	3.673	3.745	14	5.5	5.59	0.12
D	101	103	506		3.817		13.5	5.67		
E	102	106	506	325.3	4.574	4.6	9.2	3.61	3.79	0.248
E	103	104	505		4.626		9.8	3.96		

Table B3: Polynomial regression analysis (flexural) results - untreated sisal CFRC of mortar (100 x 100 x 500 mm)

SUMMARY OUTPUT								
Regression Statistics								
Multiple R	0.99029383							
R Square	0.98068188							
Adjusted R Square	0.9227275							
Standard Error	0.44199585							
Observations	9							
ANOVA								
	df	*SS*	*MS*	*F*	*Significance F*			
Regression	6	19.83487934	3.305813	16.92162	0.056842013			
Residual	2	0.39072066	0.19536					
Total	8	20.2256						
	Coefficients	*Standard Error*	*t Stat*	*P-value*	*Lower 95%*	*Upper 95%*	*Lower 95.0%*	*Upper 95.0%*
Intercept	4.01798318	0.441434416	9.102107	0.011856	2.118644181	5.91732217	2.11864418	5.91732217
% VF	-3.96801638	4.39387073	-0.90308	0.461799	-22.87331627	14.9372835	-22.8733163	14.9372835
Vf^2	16.5208254	11.43491542	1.44477	0.285377	-32.67964461	65.7212955	-32.6796446	65.7212955
VF^3	-13.5114781	11.18382363	-1.20813	0.350467	-61.63158737	34.6086312	-61.6315874	34.6086312
VF^4	4.59308386	4.983995259	0.921567	0.454043	-16.85131695	26.0374847	-16.8513169	26.0374847
VF^5	-0.70574668	1.021635935	-0.6908	0.561094	-5.101491324	3.68999797	-5.10149132	3.68999797
VF^6	0.040176	0.078016581	0.514967	0.657842	-0.295502255	0.37585425	-0.29550226	0.37585425

Regression equation:

$$y = 0.0402x^6 - 0.7057x^5 + 4.5931x^4 - 13.511x^3 + 16.521x^2 - 3.968x + 4.018$$

$$R^2 = 0.9807$$

Table B4: Tensile and interfacial bond strength results – untreated sisal CFRC of mortar

Tensile and Interfacial Bond Test Results for Continuous Untreated Sisal Fibre-Reinforced OPC Mortar Beams (50x50x400) mm

Specimen ID #	Breadth (mm)	Depth (mm)	Length (mm)	Average Weight of embedded fibres (grams)	Fibre V_f (%)	Mean Fibre V_f (%)	Mean crack spacing for V_f	Ultimate tensile load (N)	Ultimate tensile stress (MN/m^2)	Mean Ultimate Tensile stress (MN/m^2)	Interfacial bond strength (IBS) (MN/m^2)	Mean IBS (MN/m^2)	IBS Standard deviation (MN/m^2)
1	53	55	402					7719	2.648				
2	53	52	402	0	0	0	-	6821	2.475	2.554	-	-	-
3	52	55	403					7262	2.539				
A1	52	55	402		0.436		84.5675	7553	2.641		0.401		
A2	52	51	407	6.51	0.464	0.484	74.715	7170	2.703	2.655	0.4266	0.4086	0.0156
A3	54	54	404		0.553		67.075	7762	2.622		0.3983		
B1	53	52	404		0.924		68.235	8009	2.906		0.2334		
B2	53	52	404	13.38	0.924	0.9223	50.6275	7753	2.813	2.871	0.3147	0.2745	0.0407
B3	52	53	405		0.922		57.935	7973	2.893		0.2755		
C1	56	55	407		1.194		62.7625	8991	2.919		0.1959		
C2	55	50	407	19.46	1.337	1.269	57.3725	8671	3.153	3.045	0.1911	0.2	0.0116
C3	53	55	402		1.277		53.9025	8932	3.064		0.2131		
D1	52	53	404		1.802		27.765	8017	2.909		0.2916		
D2	55	53	404	26.08	1.704	1.702	31.52	9109	3.125	2.997	0.2719	0.2794	0.0107
D3	56	55	407		1.6		33.2525	9111	2.958		0.2748		
E1	54	51	404		2.255		MMF	7020	2.549		MMF		
E2	51	52	406	32.61	2.33	2.29	20.19	6983	2.633	2.657	0.3085		
E3	53	51	406		2.286		MMF	7539	2.789		MMF		

Table B5: Polynomial regression analysis (tensile) results - untreated sisal CFRC of mortar (50 x 50 x 400 mm)

SUMMARY OUTPUT								
Regression Statistics								
Multiple R	0.999883242							
R Square	0.999766497							
Adjusted R Square	0.998832483							
Standard Error	0.006801334							
Observations	6							
ANOVA								
	df	*SS*	*MS*	*F*	*Significance F*			
Regression	4	0.198058575	0.049514644	1070.398554	0.022919439			
Residual	1	4.62581E-05	4.62581E-05					
Total	5	0.198104833						
	Coefficients	*Standard Error*	*t Stat*	*P-value*	*Lower 95%*	*Upper 95%*	*Lower 95.0%*	*Upper 95.0%*
Intercept	2.554451504	0.006786331	376.4113006	0.001691284	2.468222999	2.640680009	2.468222999	2.640680009
VF%	-0.089353989	0.056538444	-1.58041118	0.359149433	-0.807743032	0.629035054	-0.807743032	0.629035054
VF^2	0.940957106	0.122962065	7.652417896	0.082723224	-0.621424065	2.503338277	-0.621424065	2.503338277
VF^3	-0.512974101	0.088875881	-5.771803265	0.109214074	-1.642249242	0.616301041	-1.642249242	0.616301041
VF^4	0.049639519	0.020331377	2.441522707	0.247478307	-0.20869512	0.307974158	-0.20869512	0.307974158

Regression Equation:

$$y = 0.0496x^4 - 0.5130x^3 + 0.9410x^2 - 0.08940x + 2.555$$

$$(R^2 = 0.99977)$$

Mercerised Sisal CFRC of Mortar

Table B6: Flexural results data - Mercerised sisal CFRC of mortar

		Flexural Test Results for Continuous Mercerised Sisal Fibre-Reinforced OPC Mortar Beams (100x100x500) mm								
Specimen ID #	Breadth (mm)	Depth (mm)	Length (mm)	Average Weight of embedded fibres (grams)	Fibre volume fraction (%)	Mean Fibre Volume fraction (%)	Ultimate Flexural Load (KN)	Ultimate Flexural Strength (MN/m^2)	Mean Flexural Strength (MN/m^2)	Standard Deviation (MN/m^2)
UNR-M	106	104	501	0	0	0	9.6	3.77	3.74	0.023
ABC-M	103	105	504				9.4	3.73		
XXX-M	105	105	505				9.6	3.73		
A1-M	105	103	503	32.6	0.461	0.465	12	4.85	5.41	0.603
A1-M	101	103	501		0.481		14.4	6.05		
A1-M	106	104	501		0.454		13.6	5.34		
A-M	105	106	503	65.2	0.896	0.902	20	7.63	7.68	0.087
A-M	101	107	504		0.921		19.6	7.63		
A-M	106	106	503		0.888		20.6	7.78		
B1-M	103	106	500	98	1.373	1.372	21	8.17	7.96	0.349
B1-M	102	105	502		1.402		20.4	8.16		
B1-M	104	107	505		1.341		20	7.56		
B-M	105	106	502	130.6	1.798	1.827	24.4	9.31	9.35	0.491
B-M	103	105	504		1.843		22.4	8.88		
B-M	105	103	505		1.839		24.4	9.86		
C1-M	103	104	502	162.8	2.329	2.304	25.6	10.34	9.39	0.831
C1-M	106	103	501		2.29		22	8.8		
C1-M	102	106	505		2.294		23	9.03		
C-M	105	103	503	195.4	2.763	2.718	19.2	7.76	8.44	1.286
C-M	103	107	504		2.706		20	7.63		
C-M	105	106	503		2.685		26	9.92		
D-M	101	105	503	261.2	3.767	3.655	16.4	6.63	6.25	0.545
D-M	106	107	500		3.543		15.8	5.86		
E-M	102	102	507	325.6	4.748	4.735	12.2	5.17	5.16	0.021
E-M	102	104	500		4.722		12.6	5.14		
F-M	102	104	506	390.5	5.596	5.575	9.2	3.75	3.65	0.149
F-M	105	102	505		5.554		8.6	3.54		
G-M	103	105	500	455.9	6.485	-	7.8	3.09	-	-

Table B7: Polynomial regression analysis (flexural) - mercerised sisal CFRC of mortar

SUMMARY OUTPUT								
Regression Statistics								
Multiple R	0.992093							
R Square	0.984248							
Adjusted R Square	0.952743							
Standard Error	0.47037							
Observations	10							
ANOVA								
	df	*SS*	*MS*	*F*	*Significance F*			
Regression	6	41.47266663	6.912111	31.24149	0.008486942			
Residual	3	0.663743374	0.221248					
Total	9	42.13641						
	Coefficients	*Standard Error*	*t Stat*	*P-value*	*Lower 95%*	*Upper 95%*	*Lower 95.0%*	*Upper 95.0%*
Intercept	3.702908	0.468012513	7.911985	0.004209	2.213483106	5.192332492	2.213483106	5.19233249
% VF	4.703532	3.226256058	1.457892	0.240938	-5.563854721	14.97091863	-5.563854721	14.9709186
VF^2	-1.63225	6.354741825	-0.25686	0.813899	-21.85587492	18.59137437	-21.85587492	18.5913744
VF^3	1.3668	4.850182676	0.281804	0.796415	-14.06864559	16.80224629	-14.06864559	16.8022463
VF^4	-0.832392	1.706307543	-0.48783	0.659098	-6.262624495	4.597839774	-6.262624495	4.59783977
VF^5	0.186835	0.278506518	0.670845	0.550348	-0.699497273	1.073166803	-0.699497273	1.0731668
VF^6	-0.013806	0.017060429	-0.80923	0.477607	-0.068099764	0.040488037	-0.068099764	0.04048804

Regression equation:

$$y = -0.0138x^6 + 0.1868x^5 - 0.8324x^4 + 1.3668x^3 - 1.6323x^2 + 4.7035x + 3.7029$$

$$R^2 = 0.9842$$

Table B8: Tensile and interfacial bond strength results - mercerised sisal CFRC of mortar

Tensile and Interfacial Bond Test Results for Continuous Mercerised Sisal Fibre-Reinforced OPC Mortar Beams (50x50x400) mm													
Specimen ID #	Breadth (mm)	Depth (mm)	Length (mm)	Average Weight of embedded fibres (grams)	Fibre V_f (%)	Mean Fibre V_f (%)	Mean crack spacing for V_f	Ultimate tensile load (N)	Ultimate tensile stress (MN/m^2)	Mean Ultimate Tensile stress (MN/m^2)	Interfacial bond strength (IBS) (MN/m^2)	Mean IBS (MN/m^2)	IBS Standard deviation (MN/m^2)
11	57	55	407					7584	2.419				
22	52	50	408	0	0	0	-	7666	2.949	2.712	-	-	-
33	51	55	403					7761	2.767				
A11	55	52	407		0.428		75.71	8011	2.801		0.4848		
A22	51	51	402	6.48	0.477	0.434	76.1475	7590	2.918	2.851	0.4323	0.4703	0.0332
A33	57	54	407		0.398		79.9575	8726	2.835		0.4938		
B11	57	54	406		0.814		59.9625	9200	2.989		0.3206		
B22	56	55	404	13.22	0.817	0.862	64.615	9730	3.159	3.086	0.2964	0.2993	0.0194
B33	51	52	402		0.954		58.1875	8250	3.111		0.2815		
C11	56	53	402		1.26		43.9	9744	3.283		0.2816		
C22	52	54	407	19.54	1.315	1.288	46.595	9584	3.413	3.229	0.2541	0.2573	0.0228
C33	55	52	408		1.288		51.1675	8557	2.992		0.2363		
D11	51	51	406		1.907		MMF	8703	3.346		MMF		
D22	56	54	403	26.18	1.652	1.786	37.305	8791	2.907	3.15	0.2518		
D33	52	53	406		1.8		MMF	8811	3.197		MMF		
E11	55	55	407		2.034		MMF	7968	2.634		MMF		
E22	54	50	402	32.56	2.308	2.165	MMF	7304	2.705	2.595	MMF		
E33	57	50	408		2.154		MMF	6971	2.446		MMF		

Table B9: Polynomial regression analysis (tensile) - mercerised sisal CFRC of mortar (50 x 50 x 400 mm)

SUMMARY OUTPUT								
Regression Statistics								
Multiple R	0.999174945							
R Square	0.99835057							
Adjusted R Square	0.991752849							
Standard Error	0.023253264							
Observations	6							
ANOVA								
	df	*SS*	*MS*	*F*	*Significance F*			
Regression	4	0.327278119	0.08182	151.3175	0.060886272			
Residual	1	0.000540714	0.000541					
Total	5	0.327818833						
	Coefficients	*Standard Error*	*t Stat*	*P-value*	*Lower 95%*	*Upper 95%*	*Lower 95.0%*	*Upper 95.0%*
Intercept	2.710456342	0.02320197	116.8201	0.005449	2.415647364	3.005265319	2.415647364	3.005265319
VF	0.231108568	0.193300821	1.19559	0.443437	-2.225011236	2.687228372	-2.22501124	2.687228372
VF^2	0.254703028	0.420398342	0.605861	0.653222	-5.086964377	5.596370434	-5.08696438	5.596370434
VF^3	0.044893445	0.303860163	0.147744	0.906619	-3.816015996	3.905802886	-3.816016	3.905802886
VF^4	-0.103024503	0.069511497	-1.48212	0.377865	-0.986251814	0.780202809	-0.98625181	0.780202809

Regression equation:

$$y = -0.103x^4 + 0.0449x^3 + 0.2547x^2 + 0.2311x + 2.7105$$
$$R^2 = 0.9984$$

Cornified Sisal CFRC of Mortar

Table B10: Flexural results data - Cornified sisal CFRC of mortar

		Flexural Test Results for Continuous Cornified Sisal Fibre-Reinforced OPC Mortar Beams (100x100x500) mm								
Specimen ID #	Breadth (mm)	Depth (mm)	Length (mm)	Average Weight of embedded fibres (grams)	Fibre volume fraction (%)	Mean Fibre Volume Fraction (%)	Ultimate Flexural Load (KN)	Ultimate Flexural Strength (MN/m^2)	Mean Flexural Strength (MN/m^2)	Standard Deviation (MN/m^2)
O	103	107	508				9.6	3.66		
O	104	108	503	0	0	0	9.4	3.49	3.62	0.112
O	100	107	507				9.4	3.7		
A	101	103	503		0.478		11.4	4.79		
A	104	102	507	32.5	0.465	0.47	12.2	5.07	4.92	0.141
A	104	102	505		0.467		11.8	4.91		
B	102	102	505		0.961		15.8	6.7		
B	100	102	504	65.6	0.982	0.967	16.4	7.09	6.86	0.203
B	101	103	506		0.959		16.2	6.8		
C	102	103	504		1.427		18.2	7.57		
C	100	103	508	98.2	1.444	1.423	19.6	8.31	7.87	0.397
C	101	106	505		1.397		19.4	7.69		
D	102	104	507		1.865		19.8	8.08		
D	102	106	507	130.4	1.83	1.861	19.6	7.7	8.09	0.39
D	103	102	506		1.887		20.2	8.48		
E	103	102	503		2.364		17.6	7.39		
E	101	108	503	162.4	2.277	2.336	18.2	6.95	7.21	0.231
E	102	102	507		2.368		17.2	7.29		
F	104	103	503		2.792		16.3	6.64		
F	102	103	506	195.6	2.83	2.833	17.1	7.11	6.97	0.29
F	100	103	508		2.876		16.9	7.17		

Table B11: Polynomial regression analysis (flexural) - Cornified sisal CFRC of mortar

SUMMARY OUTPUT								
Regression Statistics								
Multiple R	0.999589284							
R Square	0.999178737							
Adjusted R Square	0.995072423							
Standard Error	0.114810318							
Observations	7							
ANOVA								
	df	*SS*	*MS*	*F*	*Significance F*			
Regression	5	16.03699002	3.207398004	243.3274016	0.048630819			
Residual	1	0.013181409	0.013181409					
Total	6	16.05017143						
	Coefficients	*Standard Error*	*t Stat*	*P-value*	*Lower 95%*	*Upper 95%*	*Lower 95.0%*	*Upper 95.0%*
Intercept	3.616598178	0.114759909	31.5144742	0.020194093	2.158435284	5.074761073	2.158435284	5.074761073
% VF	1.558417149	1.270957391	1.226175764	0.435541665	-14.59062767	17.70746196	-14.59062767	17.70746196
VF^2	3.461993555	3.455320038	1.001931374	0.499385818	-40.44201028	47.36599739	-40.44201028	47.36599739
VF^3	-1.570316007	3.359741615	-0.467391897	0.721655492	-44.25988082	41.11924881	-44.25988082	41.11924881
VF^4	-0.289668176	1.349150998	-0.214704045	0.865359207	-17.43225697	16.85292062	-17.43225697	16.85292062
VF^5	0.139809135	0.1905232	0.733816856	0.596979455	-2.281017649	2.56063592	-2.281017649	2.56063592

Regression equation:

$$y = 0.140x^5 - 0.290x^4 - 1.570x^3 + 3.462x^2 + 1.558x + 3.6167$$

$$R^2 = 0.999$$

Table B12: Tensile and interfacial bond strength results - cornified sisal CFRC of mortar

Tensile and Interfacial Bond Test Results for Continuous Cornified Sisal Fibre-Reinforced OPC Mortar Beams (50x50x400) mm

Specimen ID #	Breadth (mm)	Depth (mm)	Length (mm)	Average Weight of embedded fibres (grams)	Fibre V_f (%)	Mean Fibre V_f (%)	Mean crack spacing for V_f	Ultimate tensile load (N)	Ultimate tensile stress (MN/m^2)	Mean Ultimate Tensile stress (MN/m^2)	Interfacial bond strength (IBS) (MN/m^2)	Mean IBS (MN/m^2)	IBS Standard deviation (MN/m^2)
111	52	55	404					7940	2.776		-		
222	51	53	408	0	0	-	-	7805	2.889	2.785	-		
333	55	53	405					7838	2.689		-		
A111	50	53	408		0.487		77.545	7139	2.694		0.427		
A222	50	54	407	6.72	0.47	0.473	63.4275	7557	2.799	2.693	0.5409	0.465	0.0649
A333	52	53	405		0.463		81.365	7130	2.587		0.4281		
B111	54	55	407		0.869		63.27	8750	2.946		0.2921		
B222	53	52	405	13.65	0.941	0.906		8307	3.014	2.985	0.2741	0.2852	0.0097
B333	52	55	405		0.907		61.1625	8569	2.996		0.2894		
C111	53	54	407		1.296		63.7225	8841	3.089		0.1936		
C222	52	53	405	19.63	1.353	1.325	54.775	7990	2.899	3.058	0.2157	0.2121	0.017
C333	53	53	405		1.327		53.0125	8950	3.186		0.2273		
D111	53	54	408		1.721		45.415	9390	3.281		0.2037		
D222	50	53	407	26.12	1.863	1.795	MMF	8075	3.047	3.111	MMF	0.2025	0.0018
D333	53	52	405		1.8		43.94	8286	3.006		0.2012		
E111	51	52	406		2.328		MMF	6561	2.474		MMF		
E222	50	53	405	32.58	2.335	2.303	MMF	6305	2.379	2.421	MMF		
E333	53	52	405		2.245		MMF	6645	2.411		MMF		

Table B13: Polynomial regression analysis (tensile) - cornified sisal CFRC of mortar (50 x 50 x 400 mm)

SUMMARY OUTPUT								
Regression Statistics								
Multiple R	0.987079124							
R Square	0.974325196							
Adjusted R Square	0.871625981							
Standard Error	0.093727315							
Observations	6							
ANOVA								
	df	*SS*	*MS*	*F*	*Significance F*			
Regression	4	0.333372024	0.08334301	9.487173	0.2382934			
Residual	1	0.00878481	0.00878481					
Total	5	0.342156833						
	Coefficients	*Standard Error*	*t Stat*	*P-value*	*Lower 95%*	*Upper 95%*	*Lower 95.0%*	*Upper 95.0%*
Intercept	2.779547701	0.093568595	29.7059895	0.021423	1.59064598	3.968449427	1.590645975	3.96844943
VF	-0.640594011	0.757835991	-0.8452937	0.553249	-10.2698133	8.988625245	-10.2698133	8.98862524
VF^2	1.352935165	1.575707115	0.85862097	0.548332	-18.668322	21.37419237	-18.668322	21.3741924
VF^3	-0.539126873	1.077132683	-0.5005204	0.704568	-14.2253953	13.14714152	-14.2253953	13.1471415
VF^4	0.020784906	0.231022445	0.08996921	0.942878	-2.91463357	2.956203385	-2.91463357	2.95620338

Regression equation:

$$y = 0.0208x^4 - 0.5391x^3 + 1.3529x^2 - 0.6406x + 2.7795$$
$$R^2 = 0.9743$$

Untreated Sisal DFRC of Mortar

Table B14: Flexural results data - Untreated sisal DFRC of mortar

			Flexural Test Results for Discontinuous Untreated Sisal Fibre-Reinforced OPC Mortar Beams (100x100x500) mm							
Specimen ID #	Breadth (mm)	Depth (mm)	Length (mm)	Average Weight of embedded fibres (grams)	Fibre volume fraction (%)	Mean Fibre Volume Fraction (%)	Ultimate Flexural Load (KN)	Ultimate Flexural Strength (MN/m^2)	Mean Flexural Strength (MN/m^2)	Standard Deviation (MN/m^2)
UNR	101	99	508	0	0	0	9.8	4.46	4.23	0.248
UNR	101	102	509				9.6	4.11		
F1	102	105	503	32.2	0.46	0.484	10.6	4.24	4.48	0.211
F2	98	98	503		0.513		9.6	4.59		
F3	99	104	501		0.48		11	4.62		
G1	104	103	501	65	0.931	0.956	9.4	3.83	3.93	0.141
G2	97	104	506		0.98		9.4	4.03		
H1	105	100	502	98.1	1.432	1.449	11	4.71	4.9	0.262
H2	103	99	505		1.465		11.4	5.08		
J1	102	104	509	131.4	1.872	1.891	11	4.49	4.7	0.297
J2	100	104	509		1.909		11.8	4.91		
K1	103	99	508	162.8	2.418	2.409	12.2	5.44	5.22	0.318
K2	105	99	502		2.4		11.4	4.99		
L1	101	104	502	195.2	2.848	2.839	10.8	4.45	4.66	0.297
L2	103	102	505		2.83		11.6	4.87		
M1	102	103	507	260.4	3.761	3.941	10.6	4.41	4.62	0.297
M2	99	98	501		4.121		10.2	4.83		
N1	102	100	502	325.4	4.889	4.88	8.6	3.79	4.01	0.311
N2	102	99	509		4.87		9.4	4.23		
P1	102	105	509	390.2	5.506	5.459	9.2	3.68	3.51	0.248
P2	105	104	508		5.411		8.4	3.33		
S1	97	98	509	455	7.234	-	8	3.87	-	-

Table B15: Polynomial regression analysis results - untreated sisal DFRC of mortar

Standard Error	0.4142048							
Observations	10							
ANOVA								
	df	*SS*	*MS*	*F*	*Significance F*			
Regression	6	1.80734321	0.301224	1.755736	0.344736073			
Residual	3	0.51469679	0.171566					
Total	9	2.32204						
	Coefficients	*Standard Error*	*t Stat*	*P-value*	*Lower 95%*	*Upper 95%*	*Lower 95.0%*	*Upper 95.0%*
Intercept	4.2816989	0.412170215	10.38818	0.001903	2.969989333	5.593408	2.96998933	5.5934085
%Vf	-0.3257	2.750309864	-0.11842	0.913217	-9.078413554	8.427013	-9.07841355	8.4270134
VF^2	0.4018097	5.244067045	0.076622	0.943748	-16.28715209	17.09077	-16.2871521	17.090771
VF^3	0.1435378	3.9056433	0.036751	0.972992	-12.28596229	12.57304	-12.2859623	12.573038
VF^4	-0.156156	1.35172546	-0.11552	0.915329	-4.457949733	4.145638	-4.45794973	4.1456377
VF^5	0.0355119	0.218719958	0.162363	0.88134	-0.6605526	0.731576	-0.6605526	0.7315764
VF^6	-0.002562	0.013371034	-0.19164	0.860262	-0.045115018	0.03999	-0.04511502	0.0399902

Regression equation:

$$y = -0.0026x^6 + 0.0355x^5 - 0.1562x^4 + 0.1435x^3 + 0.4018x^2 - 0.3257x + 4.2817$$

$$R^2 = 0.7783$$

Mercerised Sisal DFRC of Mortar

Table B16: Flexural results data - Mercerised sisal DFRC of mortar

		Flexural Test Results for Discontinuous Mercerised Sisal Fibre-Reinforced OPC Mortar Beams (100x100x500) mm								
Specimen ID #	Breadth (mm)	Depth (mm)	Length (mm)	Average Weight of embedded fibres (grams)	Fibre volume fraction (%)	Mean Fibre Volume Fraction (%)	Ultimate Flexural Load (KN)	Ultimate Flexural Strength (MN/m^2)	Mean Flexural Strength (MN/m^2)	Standard Deviation (MN/m^2)
UNR-M	107	105	506	0	0	0	9.8	3.74	3.72	0.092
UNR-M	104	106	505				9.4	3.62		
UNR-M	105	103	505				9.4	3.8		
F1-M	104	102	503	32.2	0.464	0.46	10.8	4.49	4.31	0.238
F2-M	103	103	502		0.465		9.8	4.04		
F3-M	104	105	505		0.449		11.2	4.4		
G1-M	107	105	501	65	0.888	0.91	11.2	4.27	4.39	0.163
G2-M	106	101	501		0.932		10.8	4.5		
H1-M	104	104	507	98.1	1.376	1.414	11	4.4	4.67	0.375
H2-M	102	101	505		1.451		11.4	4.93		
J1-M	106	104	506	131.4	1.812	1.82	11.4	4.45	4.42	0.042
J2-M	104	106	502		1.827		11.4	4.39		
K1-M	103	104	506	162.8	2.31	2.259	11.6	4.69	4.6	0.134
K2-M	107	105	505		2.207		11.8	4.5		
L1-M	105	101	505	195.2	2.804	2.78	13	5.46	5.36	0.149
L2-M	105	103	504		2.755		13	5.25		
M1-M	100	102	506	260.4	3.881	3.844	12.8	5.54	5.48	0.092
M2-M	102	103	501		3.806		13	5.41		
N1-M	103	106	505	325.4	4.54	4.596	12.6	4.9	4.88	0.035
N2-M	103	104	503		4.646		12	4.85		
P1-M	100	104	503	390.2	5.738	5.607	11.6	4.83	4.74	0.134
P2-M	106	103	502		5.476		11.6	4.64		
S1-M	104	104	507	455	7	-	9.4	3.76	-	-

Table B17: Polynomial regression analysis results - Mercerised sisal DFRC of mortar

Standard Error	0.211005082							
Observations	10							
ANOVA								
	df	*SS*	*MS*	*F*	*Significance F*			
Regression	6	2.223840567	0.37064	8.324661	0.055073999			
Residual	3	0.133569433	0.044523					
Total	9	2.35741						
	Coefficients	*Standard Error*	*t Stat*	*P-value*	*Lower 95%*	*Upper 95%*	*Lower 95.0%*	*Upper 95.0%*
Intercept	3.710850874	0.20981898	17.68596	0.000394	3.043113238	4.3785885	3.04311324	4.37858851
%VF	2.197283414	1.427347898	1.539417	0.221333	-2.34517463	6.7397415	-2.34517463	6.73974146
Vf^2	-2.27556578	2.79976005	-0.81277	0.475857	-11.1856518	6.6345202	-11.1856518	6.63452025
VF^3	0.916967652	2.145567222	0.427378	0.697924	-5.911184826	7.7451201	-5.91118483	7.74512013
VF^4	-0.07719021	0.76074505	-0.10147	0.925582	-2.498220484	2.3438401	-2.49822048	2.34384006
VF^5	-0.02124686	0.125436506	-0.16938	0.876272	-0.420441806	0.3779481	-0.42044181	0.37794808
VF^6	0.002981758	0.00776693	0.383904	0.726642	-0.021736079	0.0276996	-0.02173608	0.0276996

Regression equation:

$$y = 0.003x^6 - 0.0212x^5 - 0.0772x^4 + 0.917x^3 - 2.2756x^2 + 2.1973x + 3.7109$$

$$R^2 = 0.9433$$

Cornified Sisal DFRC of Mortar

Table B18: Flexural results data - Cornified sisal DFRC of mortar

		Flexural Test Results for Discontinuous Cornified Sisal Fibre-Reinforced OPC Mortar Beams (100x100x500) mm								
Specimen ID #	Breadth (mm)	Depth (mm)	Length (mm)	Average Weight of embedded fibres (grams)	Fibre volume fraction (%)	Mean Fibre Volume Fraction (%)	Ultimate Flexural Load (KN)	Ultimate Flexural Strength (MN/m^2)	Mean Flexural Strength (MN/m^2)	Standard Deviation (MN/m^2)
O	105	100	502	0	0	0	9.4	4.03	3.94	0.28
O	104	107	503				9.6	3.63		
O	99	99	504				9	4.17		
A-1	102	99	502	32.4	0.492	0.492	10.2	4.59	4.39	0.272
A-1	98	104	505		0.484		9.6	4.08		
A-1	100	99	503		0.501		9.8	4.5		
B-1	100	101	504	65.8	0.994	0.955	10.2	4.5	4.33	0.24
B-1	106	104	502		0.915		10.6	4.16		
C-1	100	104	507	98.6	1.438	1.42	10.4	4.33	4.43	0.134
C-1	103	104	505		1.402		11.2	4.52		
D-1	103	101	504	132.2	1.94	1.907	10.8	4.63	4.58	0.078
D-1	105	103	502		1.873		11.2	4.52		
E-1	103	99	506	195.6	2.916	2.9	12.6	5.62	5.16	0.651
E-1	99	105	502		2.883		11.4	4.7		
F-1	102	103	501	261.1	3.816	3.781	11.6	4.83	4.8	0.05
F-1	106	100	506		3.745		11.2	4.76		
G-1	100	101	509	325.8	4.875	4.853	11.6	5.12	4.83	0.41
G-1	99	104	504		4.83		10.8	4.54		
H-1	99	99	506	391.4	6.071	5.952	10.2	4.73	4.62	0.163
H-1	102	101	501		5.833		10.4	4.5		

Table B19: Polynomial regression analysis results - Cornified sisal DFRC of mortar

Standard Error	0.07156786							
Observations	9							
ANOVA								
	df	*SS*	*MS*	*F*	*Significance F*			
Regression	6	0.967178304	0.16119638	31.47163	0.031113261			
Residual	2	0.010243918	0.00512196					
Total	8	0.977422222						
	Coefficients	*Standard Error*	*t Stat*	*P-value*	*Lower 95%*	*Upper 95%*	*Lower 95.0%*	*Upper 95.0%*
Intercept	3.93479698	0.071231095	55.2398778	0.000328	3.628314316	4.24127965	3.6283143	4.24127965
%VF	2.54850128	0.478815962	5.32250694	0.033534	0.488322474	4.60868009	0.4883225	4.60868009
Vf^2	-4.7279765	0.923094466	-5.1218773	0.036069	-8.699731473	-0.7562216	-8.6997315	-0.75622162
VF^3	3.62776541	0.691455162	5.24656638	0.034462	0.652673966	6.60285685	0.652674	6.60285685
VF^4	-1.2451509	0.237580238	-5.2409701	0.034532	-2.267376172	-0.2229257	-2.2673762	-0.22292565
VF^5	0.19422917	0.037607686	5.16461376	0.035506	0.03241636	0.35604199	0.0324164	0.35604199
VF^6	-0.0112483	0.002219142	-5.0687553	0.036788	-0.020796484	-0.0017001	-0.0207965	-0.00170009

Regression equation:

$$y = -0.0112x^6 + 0.1942x^5 - 1.2452x^4 + 3.6278x^3 - 4.728x^2 + 2.5485x + 3.9348$$

$$R^2 = 0.9895$$

Tensile Test Results - Sisal CFRC of Polyester Resin

Table B20 (a): Tensile test results for uniaxially aligned untreated, mercerised and cornified sisal fibre-reinforced polyester resin

Tensile test results for uniaxially aligned untreated sisal fibre-reinforced polyester resin								
	Cross-sectional area (x $10^{-5}m^2$)	Ultimate Tensile Load (KN)	*Fracture Stress (MN/m^2)	% **Fracture Strain	Secant Modulus (GN/m^2)	Mean Fracture Stress (MN/m^2)	Mean % Fracture Strain	Mean Secant Modulus (GN/m^2)
0	10	6.23	62.3	10.2	0.611	62.33	10.86	0.576
	10	6.12	61.2	11.42	536			
	10	6.35	63.5	10.95	0.58			
0.472	12	3.8	31.67	7.94	0.399	35.34	9.67	0.3713
	12	3.69	30.75	8.13	0.378			
	10	4.36	43.6	12.95	0.337			
0.916	12	3.64	30.33	9.44	0.322	32.3	8.847	0.367
	11.4	3.8	33.33	8.17	0.408			
	12	3.99	33.25	8.93	0.372			
1.436	9.75	2.57	26.36	7.6	0.347	26.76	8.19	0.327
	10	2.93	29.3	8.93	0.328			
	9.75	2.4	24.62	8.04	0.306			
Tensile test results for uniaxially aligned Mercerised sisal fibre-reinforced polyester resin								
Mean Fibre $\%V_f$	Cross-sectional area (x $10^{-5}m^2$)	Ultimate Tensile Load (KN)	*Fracture Stress (MN/m^2)	% **Fracture Strain	Secant Modulus (GN/m^2)	Mean Fracture Stress (MN/m^2)	Mean % Fracture Strain	Mean Secant Modulus (GN/m^2)
0.467	11.4	4	35.11	9.12	0.385	33.87	8.52	0.398
	11.4	3.59	31.53	7.77	0.406			
	11.4	3.99	34.97	8.66	0.404			
0.931	12	3.71	30.93	7.89	0.392	29.92	7.42	0.405
	11.8	3.19	27.04	6.33	0.427			
	11.8	3.75	31.79	8.05	0.395			
1.397	12	2.74	22.79	5.81	0.392	22.45	5.58	0.403
	9.75	2.1	21.49	5.15	0.417			
	11.4	2.63	23.07	5.78	0.399			
Tensile test results for uniaxially aligned Cornified sisal fibre-reinforced polyester resin								
Mean Fibre $\%V_f$	Cross-sectional area (x $10^{-5}m^2$)	Ultimate Tensile Load (KN)	*Fracture Stress (MN/m^2)	% **Fracture Strain	Secant Modulus (GN/m^2)	Mean Fracture Stress (MN/m^2)	Mean % Fracture Strain	Mean Secant Modulus (GN/m^2)
0.479	12	4	33.33	8.48	0.393	35.22	9.03	0.39
	11.8	4.41	37.36	9.6	0.389			
	11.8	4.13	34.97	9.01	0.388			
0.901	12.2	3.73	30.54	7.87	0.388	31.18	7.99	0.39
	12	3.9	32.49	8.31	0.391			
	12	3.66	30.51	7.78	0.392			
1.476	11.8	2.94	24.91	5.96	0.418	23.14	5.71	0.405
	11.8	2.46	20.83	5.14	0.405			
	11.8	2.79	23.68	6.03	0.393			
*-Engineering Stress **- Engineering strain								

Table B20 (b): Polynomial regression analysis (tensile) results - untreated sisal CFRC of polyester resin

SUMMARY OUTPUT								
Regression Statistics								
Multiple R	0.968331439							
R Square	0.937665776							
Adjusted R Square	0.812997328							
Standard Error	6.847734892							
Observations	4							
ANOVA								
	df	*SS*	*MS*	*F*	*Significance F*			
Regression	2	705.3674018	352.6837	7.521275771	0.249668228			
Residual	1	46.89147315	46.89147					
Total	3	752.258875						
	Coefficients	*Standard Error*	*t Stat*	*P-value*	*Lower 95%*	*Upper 95%*	*ower 95.0%*	*Upper 95.0%*
Intercept	60.53031945	6.607013173	9.161525	0.069214393	-23.41974263	144.4803815	-23.4197	144.4803815
%Vf	-58.41137441	22.67530339	-2.57599	0.235735766	-346.5284218	229.705673	-346.528	229.705673
%Vf^2	24.95035049	15.06237736	1.656468	0.345768102	-166.4353	216.336001	-166.435	216.336001

Regression equation:

$$24.95x^2 - 58.41x + 60.53$$

$$R^2 = 0.94$$

Table B20 (c): Polynomial regression analysis (tensile) results - Mercerised sisal CFRC of polyester resin

SUMMARY OUTPUT								
Regression Statistics								
Multiple R	0.978513697							
R Square	0.957489056							
Adjusted R Square	0.872467167							
Standard Error	6.230490871							
Observations	4							
ANOVA								
	df	*SS*	*MS*	*F*	*Significance F*			
Regression	2	874.3344585	437.1672293	11.2616771	0.206181823			
Residual	1	38.8190165	38.8190165					
Total	3	913.153475						
	Coefficients	*Standard Error*	*t Stat*	*P-value*	*Lower 95%*	*Upper 95%*	*Lower 95.0%*	*Upper 95.0%*
Intercept	60.94354353	6.074269911	10.03306478	0.063243302	-16.23737358	138.1244606	-16.23737358	138.1244606
%Vf	-60.30664995	20.92464523	-2.882087093	0.21261422	-326.1794763	205.5661764	-326.1794763	205.5661764
%Vf^2	24.15738612	14.35338643	1.683044363	0.341301635	-158.2196805	206.5344527	-158.2196805	206.5344527

Regression equation:

$$24.16x^2 - 60.31x + 60.94$$

$$R^2 = 0.96$$

Table B20 (d): Polynomial regression analysis (tensile) results - Cornified sisal CFRC of polyester resin

SUMMARY OUTPUT								
Regression Statistics								
Multiple R	0.982676993							
R Square	0.965654074							
Adjusted R Square	0.896962221							
Standard Error	5.456930691							
Observations	4							
ANOVA								
	df	*SS*	*MS*	*F*	*Significance F*			
Regression	2	837.2269824	418.6134912	14.05776714	0.18532654			
Residual	1	29.77809257	29.77809257					
Total	3	867.005075						
	Coefficients	*Standard Error*	*t Stat*	*P-value*	*Lower 95%*	*Upper 95%*	*Lower 95.0%*	*Upper 95.0%*
Intercept	61.11123145	5.319087871	11.48904341	0.055271738	-6.474188051	128.6966509	-6.474188051	128.6966509
%Vf	-56.05434976	17.05759097	-3.286182079	0.188058235	-272.7915929	160.6828934	-272.7915929	160.6828934
%Vf^2	20.96897934	10.94796561	1.915331129	0.306324372	-118.1381132	160.0760719	-118.1381132	160.0760719

Regression equation:

$$20.97x^2 - 56.06x + 61.11$$

$$R^2 = 0.97$$

Flexural Test Results - Sisal CFRC of Polyester Resin

Table B21 (a): Flexural test results for uniaxially aligned untreated, mercerised and cornified sisal fibre-reinforced polyester resin

Flexural test results for uniaxially aligned Untreated sisal fibre-reinforced polyester resin					
Mean Fibre $\%V_f$	B x D (mm)	Ultimate Flexural Load (N)	MOR (MN/m^2)	Mean MOR (MN/m^2)	Deflection (m)
0	20 x 8.25	94.8	29.25	28.93	0.0335
		92.45	28.53		0.0428
		93.99	29		0.0415
1	20 x 8.00	109.33	35.87	35.78	0.0488
		114.57	37.59		0.0592
		103.25	33.88		0.0574
1.445	20 x 8.15	139.22	44.02	42.53	0.0311
		130.57	41.28		0.0466
		133.76	42.29		0.0418
1.933	20 x 8.00	96.83	31.77	33.34	0.0229
		105.42	34.59		0.0533
	19 x 8.00	97.48	33.67		0.0471
Flexural test results for uniaxially aligned Mercerised sisal fibre-reinforced polyester resin					
Mean Fibre $\%V_f$	B x D (mm)	Ultimate Flexural Load (N)	MOR (MN/m^2)	Mean MOR (MN/m^2)	Deflection (m)
0.915	20 x 8.00	103.19	33.86	35.49	0.0493
		110.05	36.11		0.0569
		111.21	36.49		0.0522
1.513	20 x 8.15	146.22	46.23	48.29	0.0453
		157.9	49.92		0.0441
		154.07	48.71		0.0466
1.987	20 x 8.15	122.63	38.77	35.07	0.0439
	19.25 x 8.15	100.22	32.92		0.0628
	19.00 x 8.15	100.69	33.51		0.0609
Flexural test results for uniaxially aligned Cornified sisal fibre-reinforced polyester resin					
0.873	20 x 8.25	110.81	34.19	35.39	0.045
		118.37	36.52		0.0593
	19.15 x 8.25	110.08	35.47		0.05
1.433	20 x 8.15	140.41	44.39	44.01	0.0485
		144.61	45.72		0.0582
	20.15 x 8.15	133.62	41.93		0.0544
1.896	20 x 8.15	103.84	32.83	34.07	0.0561
		109.79	34.71		0.0464
	20.5 x 8.15	112.4	34.67		0.042

Table B21 (b): Polynomial regression analysis results - untreated sisal CFRC of polyester resin (3-point-bending test, MOR)

	0							
Observations	4							
ANOVA								
	df	*SS*	*MS*	*F*	*Significance F*			
Regression	3	96.8257	32.27523333	#NUM!	#NUM!			
Residual	0	0	65535					
Total	3	96.8257						
	Coefficients	*Standard Error*	*t Stat*	*P-value*	*Lower 95%*	*Upper 95%*	*Lower 95.0%*	*Upper 95.0%*
Intercept	28.93	0	65535	#NUM!	28.93	28.93	28.93	28.93
%Vf	-30.45225626	0	65535	#NUM!	-30.45225626	-30.45225626	-30.45225626	-30.45225626
%Vf^2	59.1330394	0	65535	#NUM!	59.1330394	59.1330394	59.1330394	59.1330394
%Vf^3	-21.83078314	0	65535	#NUM!	-21.83078314	-21.83078314	-21.83078314	-21.83078314

Regression equation:

$$-21.83x^3 + 59.13x^2 - 30.54x + 28.93$$

$$R^2 = 1$$

Table B21 (c): Polynomial regression analysis results - Mercerised sisal CFRC of polyester resin (3-point-bending test, MOR)

SUMMARY OUTPUT								
Regression Statistics								
Multiple R	1							
R Square	1							
Adjusted R Square	65535							
Standard Error	0							
Observations	4							
ANOVA								
	df	*SS*	*MS*	*F*	*Significance F*			
Regression	3	198.5819	66.19396667	#NUM!	#NUM!			
Residual	0	0	65535					
Total	3	198.5819						
	Coefficients	*Standard Error*	*t Stat*	*P-value*	*Lower 95%*	*Upper 95%*	*Lower 95.0%*	*Upper 95.0%*
Intercept	28.93	0	65535	#NUM!	28.93	28.93	28.93	28.93
%Vf	-40.03310742	0	65535	#NUM!	-40.03310742	-40.03310742	-40.03310742	-40.03310742
%Vf^2	77.09543203	0	65535	#NUM!	77.09543203	77.09543203	77.09543203	77.09543203
%Vf^3	-27.87758844	0	65535	#NUM!	-27.87758844	-27.87758844	-27.87758844	-27.87758844

Regression equation:

$$-27.88x^3 + 77.10x^2 - 40.03x + 28.93$$

$$R^2 = 1$$

Table B21 (d): Polynomial regression analysis results - Cornified sisal CFRC of polyester resin (3-point-bending test, MOR)

SUMMARY OUTPUT								
Regression Statistics								
Multiple R	1							
R Square	1							
Adjusted R Square	65535							
Standard Error	0							
Observations	4							
ANOVA								
	df	*SS*	*MS*	*F*	*Significance F*			
Regression	3	117.602	39.20066667	#NUM!	#NUM!			
Residual	0	0	65535					
Total	3	117.602						
	Coefficients	*Standard Error*	*t Stat*	*P-value*	*Lower 95%*	*Upper 95%*	*Lower 95.0%*	*Upper 95.0%*
Intercept	28.93	0	65535	#NUM!	28.93	28.93	28.93	28.93
%Vf	2.526605566	0	65535	#NUM!	2.526605566	2.526605566	2.526605566	2.526605566
%Vf^2	5.584662911	0	65535	#NUM!	5.584662911	5.584662911	5.584662911	5.584662911
%Vf^3	-0.002946199	0	65535	#NUM!	-0.002946199	-0.002946199	-0.002946199	-0.002946199

Regression equation:

$$-0.003x^3 + 5.585x^2 + 2.527x + 28.93$$

$$R^2 = 1$$

Tensile Test Results - Sisal CFRC of Epoxy Resin

Table B22 (a): Tensile test results for uniaxially aligned untreated, mercerised and cornified sisal fibre-reinforced epoxy resin

Tensile test results for uniaxially aligned untreated sisal fibre-reinforced epoxy resin

	Cross-sectional area (x 10^{-5} m^2)	Ultimate Tensile Load (KN)	*Fracture Stress (MN/m^2)	%**Fracture Strain	Secant Modulus (GN/m^2)	Mean Fracture Stress (MN/m^2)	Mean % Fracture Strain	Mean Secant Modulus (GN/m^2)
0	11.45	5.692	49.71	5.548	0.896	46.48 ± 2.944	5.105 ± 0.426	0.912 ± 0.055
	10.15	4.461	43.95	5.069	0.867			
	10.15	4.646	45.77	4.699	0.974			
0.481	10	6.2	62	5.86	1.058	64.99 ± 2.595	5.773 ± 0.139	1.126 ± 0.062
	10.2	6.749	66.17	5.612	1.179			
	10.15	6.776	66.76	5.846	1.142			
0.977	11.15	7.706	69.11	6.149	1.124	73.33 ± 3.752	5.929 ± 0.210	1.239 ± 0.106
	10	7.629	76.29	5.732	1.331			
	10.25	7.646	74.59	5.906	1.263			
1.495	10.25	8.684	84.72	6.996	1.211	82.77 ± 4.017	6.161 ± 0.747	1.353 ± 0.124
	10.15	7.932	78.15	5.558	1.406			
	11.25	9.612	85.44	5.929	1.441			
1.892	11.15	9.045	81.12	5.376	1.509	75.93 ± 4.524	5.248 ± 0.163	1.446 ± 0.064
	10.5	7.694	73.28	5.302	1.382			
	11.25	8.245	73.29	5.065	1.447			
2.315	10.15	5.188	51.11	3.666	1.394	47.39 ± 4.134	3.324 ± 0.377	1.429 ± 0.039
	10.75	4.616	42.94	2.919	1.471			
	11.25	5.414	48.12	3.386	1.421			

* - Engineering stress; ** - Engineering strain; ± - Standard deviation

Tensile test results for uniaxially aligned Mercerised sisal fibre-reinforced epoxy resin

Mean Fibre $\%V_f$	Cross-sectional area (x 10^{-5} m^2)	Ultimate Tensile Load (KN)	*Fracture Stress (MN/m^2)	%**Fracture Strain	Secant Modulus (GN/m^2)	Mean Fracture Stress (MN/m^2)	Mean % Fracture Strain	Mean Secant Modulus (GN/m^2)
0.462	11.15	9.955	89.28	10.15	0.88	75.75 ± 10.413	8.331 ± 1.623	0.940 ± 0.054
	10.75	7.421	69.03	7.03	0.982			
	10.25	7.681	74.94	7.814	0.959			
0.934	10.15	8.072	79.53	8.017	0.992	84.06 ± 4.876	8.109 ± 0.691	1.039 ± 0.068
	10.15	9.056	89.22	8.842	1.009			
	11	9.177	83.43	7.469	1.117			
1.381	10.25	9.656	94.2	7.702	1.223	92.21 ± 8.228	7.474 ± 0.899	1.237 ± 0.041
	10.15	8.442	83.17	6.482	1.283			
	10.15	10.075	99.26	8.237	1.205			
1.755	11.25	11.237	99.88	6.917	1.444	101.57 ± 4.557	7.112 ± 0.202	1.428 ± 0.041
	11.2	10.987	98.1	7.098	1.382			
	11.15	11.9	106.73	7.32	1.458			
2.252	11.2	9.28	82.86	5.811	1.426	83.21 ± 2.921	5.643 ± 0.336	1.476 ± 0.053
	11	8.853	80.48	5.257	1.531			
	11.2	9.665	86.29	5.862	1.472			

* - Engineering stress; ** - Engineering strain; ± - Standard deviation

Tensile test results for uniaxially aligned Cornified sisal fibre-reinforced epoxy resin

Mean Fibre $\%V_f$	Cross-sectional area (x 10^{-5} m^2)	Ultimate Tensile Load (KN)	*Fracture Stress (MN/m^2)	%**Fracture Strain	Secant Modulus (GN/m^2)	Mean Fracture Stress (MN/m^2)	Mean % Fracture Strain	Mean Secant Modulus (GN/m^2)
0.438	11.15	7.239	64.92	7.003	0.927	70.7 ± 5.405	7.042 ± 0.035	1.004 ± 0.072
	11.2	8.471	75.63	7.068	1.07			
	10.25	7.334	71.55	7.056	1.014			
1.056	10.15	7.812	76.97	6.681	1.152	79.38 ± 5.010	6.807 ± 0.693	1.169 ± 0.053
	10.15	7.717	76.03	6.186	1.229			
	10.25	8.727	85.14	7.555	1.127			
1.639	11.25	8.597	76.42	5.947	1.285	84.13 ± 7.849	6.588 ± 0.578	1.277 ± 0.031
	11	9.225	83.86	6.747	1.243			
	10.75	9.902	92.11	7.069	1.303			
1.917	10.15	7.894	77.77	5.219	1.49	85.24 ± 6.628	5.913 ± 0.601	1.444 ± 0.048
	10.25	9.267	90.41	6.244	1.448			
	11	9.631	87.55	6.276	1.395			
2.338	11.25	7.797	69.31	4.871	1.423	67.65 ± 6.005	4.730 ± 0.238	1.429 ± 0.063
	11.2	6.831	60.99	4.455	1.369			
	11.15	8.1	72.65	4.863	1.494			

* - Engineering stress; ** - Engineering strain; ± - Standard deviation

Table B22 (b): Polynomial regression analysis results - untreated sisal CFRC of epoxy resin (Tensile test)

SUMMARY OUTPUT								
Regression Statistics								
Multiple R	0.989409621							
R Square	0.978931399							
Adjusted R Square	0.947328497							
Standard Error	3.492059237							
Observations	6							
ANOVA								
	df	*SS*	*MS*	*F*	*Significance F*			
Regression	3	1133.208328	377.7361093	30.97599734	0.031435855			
Residual	2	24.38895543	12.19447771					
Total	5	1157.597283						
	Coefficients	*Standard Error*	*t Stat*	*P-value*	*Lower 95%*	*Upper 95%*	*Lower 95.0%*	*Upper 95.0%*
Intercept	47.39082039	3.430646637	13.81396145	0.005199553	32.62993927	62.15170151	32.62993927	62.15170151
%Vf	24.90981272	14.37116386	1.733319093	0.225176602	-36.92431471	86.74394015	-36.92431471	86.74394015
%Vf^2	16.66692798	15.27074995	1.091428256	0.389033895	-49.03780597	82.37166193	-49.03780597	82.37166193
%Vf^3	-11.78928182	4.313699985	-2.732986034	0.111861949	-30.34963483	6.7710712	-30.34963483	6.7710712

Regression equation:

$$-11.79x^3 + 16.67\,x^2 + 24.91 + 47.39$$

$$R^2 = 0.98$$

Table B22 (c): Polynomial regression analysis results - Mercerised sisal CFRC of epoxy resin (Tensile test)

SUMMARY OUTPUT								
Regression Statistics								
Multiple R	0.981105356							
R Square	0.96256772							
Adjusted R Square	0.906419299							
Standard Error	5.773506792							
Observations	6							
ANOVA								
	df	*SS*	*MS*	*F*	*Significance F*			
Regression	3	1714.329772	571.4432573	17.14327337	0.055619655			
Residual	2	66.66676135	33.33338068					
Total	5	1780.996533						
	Coefficients	*Standard Error*	*t Stat*	*P-value*	*Lower 95%*	*Upper 95%*	*Lower 95.0%*	*Upper 95.0%*
Intercept	48.11243732	5.645454226	8.522332376	0.013490406	23.82200829	72.40286636	23.82200829	72.40286636
%Vf	56.36389817	22.56403126	2.497953381	0.129784618	-40.72129253	153.4490889	-40.72129253	153.4490889
%Vf^2	-14.79811881	22.50077917	-0.657671394	0.578323206	-111.6111577	82.01492011	-111.6111577	82.01492011
%Vf^3	-0.756000551	5.818100971	-0.1299394	0.908504366	-25.78926858	24.27726747	-25.78926858	24.27726747

Regression equation:

$$-0.76x^3 - 14.80x^2 + 56.36x + 48.11$$

$$R^2 = 0.96$$

Table B22 (d): Polynomial regression analysis results - Cornified sisal CFRC of epoxy resin (Tensile test)

SUMMARY OUTPUT								
Regression Statistics								
Multiple R	0.977011348							
R Square	0.954551173							
Adjusted R Square	0.886377933							
Standard Error	4.880931912							
Observations	6							
ANOVA								
	df	*SS*	*MS*	*F*	*Significance F*			
Regression	3	1000.718741	333.5729136	14.00184544	0.067392672			
Residual	2	47.64699267	23.82349633					
Total	5	1048.365733						
	Coefficients	*Standard Error*	*t Stat*	*P-value*	*Lower 95%*	*Upper 95%*	*Lower 95.0%*	*Upper 95.0%*
Intercept	47.88632414	4.764248901	10.05118018	0.009753835	27.3874156	68.38523268	27.3874156	68.38523268
%Vf	50.15003875	20.5796896	2.436870513	0.135096484	-38.3972189	138.6972964	-38.3972189	138.6972964
%Vf^2	-14.62983578	21.21744463	-0.689519216	0.561751481	-105.9211318	76.66146026	-105.9211318	76.66146026
%Vf^3	-1.259029407	5.855534659	-0.215015277	0.849688597	-26.45336159	23.93530278	-26.45336159	23.93530278

Regression equation:

$$-1.26x^3 - 14.62x^2 + 50.15\,x + 47.89$$

$$R^2 = 0.96$$

Temperature Variation during Curing of Polyester Resin

Table B23(a): Temperature variation data during curing of unreinforced and reinforced polyester resin

	time (minutes)	Unreinforced (°C)	Fibre reinforced (°C)	
	0	21.6	21.6	
	10	68.3	113.8	
	18	85.6	101.2	
	23	94.6	85.5	
	28	83.2	77.1	
	33	70.6	69.5	

Table B23(b): Polynomial regression analysis results - temperature variation during curing of unreinforced polyester resin

SUMMARY OUTPUT								
Regression Statistics								
Multiple R	0.996439821							
R Square	0.992892317							
Adjusted R Square	0.982230793							
Standard Error	3.458663723							
Observations	6							
ANOVA								
	df	*SS*	*MS*	*F*	*Significance F*			
Regression	3	3342.11029	1114.037	93.128551	0.010642557			
Residual	2	23.9247095	11.96235					
Total	5	3366.035						
	Coefficients	*Standard Error*	*t Stat*	*P-value*	*Lower 95%*	*Upper 95%*	*Lower 95.0%*	*Upper 95.0%*
Intercept	21.65709664	3.446044256	6.284625	0.024396	6.829964918	36.484228	6.829964918	36.48422836
time	5.511037484	1.043449828	5.281555	0.0340296	1.021435232	10.00064	1.021435232	10.00063974
tSQ	-0.07620943	0.078866155	-0.96631	0.4358357	-0.415543107	0.2631242	-0.41554311	0.263124247
tCBD	-0.001403482	0.00155595	-0.90201	0.4622526	-0.008098195	0.0052912	-0.0080982	0.005291231
Regression equation:y= -0.0014x^3-0.0762x^2+5.5110x+21.657								

Table B23(c): Polynomial regression analysis results - temperature variation during curing of sisal fibre-reinforced polyester resin

SUMMARY OUTPUT								
Regression Statistics								
Multiple R	0.995412152							
R Square	0.990845353							
Adjusted R Square	0.977113382							
Standard Error	4.845821191							
Observations	6							
ANOVA								
	df	*SS*	*MS*	*F*	*Significance F*			
Regression	3	5083.104367	1694.36812	72.156092	0.013700495			
Residual	2	46.96396602	23.481983					
Total	5	5130.068333						
	Coefficients	*Standard Error*	*t Stat*	*P-value*	*Lower 95%*	*Upper 95%*	*Lower 95.0%*	*Upper*
Intercept	22.14675471	4.828140465	4.58701541	0.0443865	1.372942957	42.9205665	1.372942957	42.92
t	16.92663363	1.461943598	11.5781714	0.0073772	10.63639801	23.2168692	10.63639801	23.21
tSQ	-0.947932106	0.110496803	-8.5788193	0.0133169	-1.423361478	-0.4725027	-1.423361478	-0.47
tCBD	0.01455224	0.002179991	6.67536651	0.0217132	0.005172495	0.02393199	0.005172495	0.023
Regression Equation: y=0.0145x^3-0.948x^2+16.927x+22.147								

APPENDIX C – LIST OF PUBLICATIONS FROM THE STUDY

From the findings of the current study, the following two (2) papers were published in *Taylor & Francis'* **Journal of Natural Fibers** (ISSN:1544-046X), a peer-reviewed scientific journal listed in the SCImago Scopus® database (Elsevier B.V.):

1) Mengo W. Kithiia, Munyasi. M. David and Mutuli. M. Stephen: **Strength Properties of Surface Modified Kenyan Sisal Fibers**. *Journal of Natural Fibers*, **19** (6), 2022, p. 2277–2287. https://doi.org/10.1080/15440478.2020.1807446 Link to full article: https://www.tandfonline.com/eprint/BXPRCH8TAHSYNVB6BPQN/full?target=10.1080/15440478.2020.1807446
2) Mengo W. Kithiia, Munyasi. M. David, Mutuli. M. Stephen and Mumenya W. Siphila: **Flexural Properties of Surface-Modified Sisal Fiber-Reinforced Polyester Resin.** *Journal of Natural Fibers,* 2021, p. 1-14. https://doi.org/10.1080/15440478.2021.1993471 Link to full article: https://www.tandfonline.com/eprint/2FZF6XAEZRKQITZS9HBE/full?target=10.1080/15440478.2021.1993471